Rheology of Pastes:
Effects of Fibrillation, Thixotropy and Structure

by

Hesam Anvari Ardakani

BSc. Tehran University Iran, 2007

MSc. King's College London UK, 2008

A THESIS SUBMITTED IN PARTIAL FULFILLMENT OF
THE REQUIREMENTS FOR THE DEGREE OF

DOCTOR OF PHILOSOPHY

in

The Faculty of Graduate and Postdoctoral Studies
(Chemical and Biological Engineering)

THE UNIVERSITY OF BRITISH COLUMBIA
(Vancouver)

June 2014

Abstract

Three different pastes (toothpaste, PTFE paste that is mixture of polytetrafluoroethylene of submicron size particles with a liquid lubricant, and chocolate) are investigated in this thesis as model paste systems to study their processing characteristics in capillary flow using various dies. The rheological behaviour of toothpaste and melt chocolate paste is identified as that of a yield-stress, thixotropic material with a time-dependent behaviour. The rheological data obtained from a parallel-disk were used to formulate a constitutive equation with a structural parameter which obeys a kinetic equation, typically used to model thixotropy. For semi-solid paste extrusion (PTFE paste and solid chocolate), a simple phenomenological mathematical model is developed. The model takes into account the elastic-plastic (strain hardening) and viscous nature of the material in its non-melt state. In addition, it takes into account the slip boundary condition at the paste/wall interface. To study scale-up possibilities, the rheology of non-melt processible polytetrafluoroethylene (PTFE) pastes is studied using three capillary rheometers having barrels of different diameter and equipped with capillary dies of various designs. The effects of process conditions on fibrillation and mechanical properties of polytetrafluoroethylene (PTFE) paste extrudates are also studied. To describe the effects of die design on the quality of the final product, a basic phenomenological mathematical model is developed. The model consists of a simple equation that explains fibril formation, due to the compression of PTFE resins, plus a kinetic equation, which is coupled with the "radial-flow" hypothesis to predict the structure and the tensile strength of extrudates. Model predictions for structural parameter compared with the tensile strength measurements, have shown a good qualitative agreement. For all paste systems, the pressure drop is measured as a function of apparent shear rate (flow rate), reduction ratio (cross sectional area of barrel to that of die), contraction angle, length-to-diameter ratio, and diameter of the barrel (scale-up). In all cases, model shown to have coefficient of determination (R^2) above 0.84. Finally, extrusion pressure predictions based on the proposed models are compared with the experimental data obtained from macroscopic pressure drop measurements and are found to be consistent.

Preface

The work of this thesis consists of four different manuscripts.

Chapter 5 is based on manuscript that has been published. H. Anvari Ardakani, E. Mitsoulis, S.G. Hatzikiriakos, Thixotropic flow of toothpaste through extrusion dies, J. Non-Newtonian Fluid Mech. 166 (2011) 1262-1271.

Chapter 6 is based on two published manuscripts; H. Anvari Ardakani, E.Mitsoulis, S.G. Hatzikiriakos, A simple improved mathematical model for polytetrafluoroethylene (PTFE) paste extrusion, Chem. Eng. Sci. 99 (2013) 216-222; and H. Anvari Ardakani, E. Mitsoulis, S.G. Hatzikiriakos, Polytetraflouroethylene paste extrusion: A fibrillation Model and its relation to mechanical properties, Int. Polym. Proc. 28 (2013) 306-313.

Chapter 7 is based on a submitted manuscript. H. Anvari Ardakani, Evan Mitsoulis, S.G. Hatzikiriakos, Capillary flow of chocolate, 2014.

All the experiments and data analysis have been performed by myself. The manuscripts were a collaborative effort between my supervisors Prof. Savvas G. Hatzikiriakos and Prof. Evan Mitsoulis and myself.

The initial and final drafts of this thesis were prepared by Hesam Anvari Ardakani, with revisions edited and approved by Prof. Savvas G. Hatzikiriakos and Prof. Evan Mitsoulis.

Table of Contents

List of Tables

List of Figures

Nomenclature

A	constant in the fibril formation kinetic equation (Eq. 6.7)
B	model parameter defined as $B = f \sin\alpha / [2(1-\cos\alpha)]$ (Eq. 2.18)
C	consistency constant for the elastic term (Eq. 2.14)
D_a	die exit diameter
D_b	barrel diameter
f	Coulomb's friction coefficient between paste and die wall
G'	elastic modulus
G''	visous modulus
G^*	complex modulus
H	gap size (parallel-disk geometry)
K	viscous consistency index
K_1	structure break-down coefficient
K_2	structure build-up coefficient
L	die length
m	power-law index for the viscous term
M	constant in the fibril formation kinetic equation (Eq. 6.7)
m_p	stress-growth exponent
n	power-law index for the elastic term
P	pressure
Q	volumetric flow rate
R	die radius
R_i	bob radius (cup-and-bob geometry)
R_o	cup radius (cup-and-bob geometry)
RR	reduction ratio defined as $(D_b/D_a)^2$
r	distance from die apex
r_p	distance from centre in parallel-disk geometry
t	time
T	torque
V_p	piston velocity
V_s	slip velocity

U flow velocity at die entrance

Greek Letters

α half die entrance angle

α_1 model coefficient (Eq. 2.12)

β slip coefficient (Eq. 5.3)

β_1 model coefficient (Eq. 2.12)

$\overline{\overline{\gamma}}$ shear strain

γ_0 shear strain amplitude

$\overline{\overline{\dot{\gamma}}}$ rate of deformation or shear rate tensor

$\dot{\gamma}_A$ apparent shear rate

$\dot{\gamma}_{A,S}$ apparent shear rate corrected for the effect of slip

δ phase angle

ε Hencky strain

η viscosity

η^* complex viscosity

η_∞ viscosity at very high shear rates ($\xi = 0$)

ξ structural parameter

$\Pi_{\dot{\gamma},t}$ flow regime

σ stress

σ_{rb} stress at the entrance of the die (Eq. 6.3)

σ_{ra} stress at the entrance of die land (end of the conical zone) (Eq. 6.4)

σ_{oa} stress at the entrance of die land (Eq. 6.5)

σ_{zo} stress at the entrance of die land (origin of the conical zone) (Eq. 6.5)

σ_{ZL} shear stress imposed at the die exit (Eq. 6.5)

$\overline{\overline{\tau}}$ stress tensor

τ_y yield stress

$\tau_{y,0}$ initial yield stress

ω angular frequency

Acknowledgements

Foremost, I would like to express my sincere gratitude to my supervisor, Prof. Savvas G. Hatzikiriakos. You have been a great mentor for me. Thank you for your encouragement, and support. My deepest appreciation goes to my co-supervisor, Prof. Evan. Mitsoulis for his influential guidance and patience. I would never forget their tremendous concern for the success of this research work.

Additionally, I would like to thank my committee members, Prof. Ian A. Frigaard and Professor Fariborz Taghipour for their brilliant comments and suggestions. I had good and bad days working in our rheology lab but it was always a blessing working with helpful, caring and professional labmates. I would like to thank you all and wish you all the best in your research and career.

I would like to gratefully acknowledge NSERC for the financial support of this research project.

Most importantly, my heartfelt gratitude to those who matter to me the most, my parents, my sister, my friends Saleh, Sina, Zahra, Niki, Arya, and Milad.

"The sea of being has emerged from hidden depths

But how, that's a pearl of scholarship no one has pierced

Each scholar has conjectured idly on the subject,

But none can describe how the matter actually rests."

(khayam)

To my wonderful parents,

Simin and Keramat,

And my lovely sister,

Yasaman

1. Introduction

A paste can be defined as a mixture of a solid and a liquid phase or as a dense suspension which is shown to demonstrate properties between liquid and solid (Coussot, 2005). Knowledge of using pastes goes back to ancient civilizations when they used pastes to make pottery, tiles, bricks, bread dough, and many others. Nowadays, many products ranging from traditional goods, ceramics, and pharmaceuticals to more advanced materials, such as honeycomb panels and catalysts, are manufactured in the form of paste. Despite the tremendous diversity of pastes, they have shown to have similar rheological behaviour. Different parameters, like solid concentration, temperature, and applied shear rate, play a significant role in paste rheological behaviour. Many pastes are able to retain their shapes against gravity like solids (Barnes, 2000). At higher values of shear stress they start to flow, which implies the existence of a yield stress, that is, a critical stress for transition from solid-like to fluid-like behaviour (Bingham, 1924; Blair, 1933; Barnes, 1998; Coussot, 2005). Moreover most of these pasty materials have shown to exhibit thixotropic behaviour, i.e., their viscosity decreases with time, which implies structure breakup (Coussot, 2005). Pastes with higher solid concentration might show solid-like behaviour. This can be described by the elastic behaviour before yielding and plastic deformation afterwards.

The rheological behaviour of pastes is determined by the interactions between phases. These include solid-solid and solid-liquid interactions (Coussot, 2005). In the absence of solid particles, liquid molecules interact with each other by van der Waals (1873) forces. At low solid concentration, hydrodynamic interaction between solid and liquid phase play a role. Drag force between liquid and solid particle gives rise to apparent viscosity as liquid has been replaced by solid particles (Larson, 1999). Colloidal interactions appear for small particles generally with characteristic length below 1 μm. For higher solid concentrations, the solid-solid contacts become a significant factor. For moderate concentrations, the solid particle interactions are mostly lubricated contacts, while for higher concentrations solid particles interact through collision and friction (Coussot, 2005).

Particles and interactions among them create a potential field. Each particle interacts with its neighbouring particles and can be assumed that the particle is trapped inside a potential well. A certain amount of energy is needed to overcome the potential barrier. The nature of interaction among system elements defines the characteristics of the network potential field.

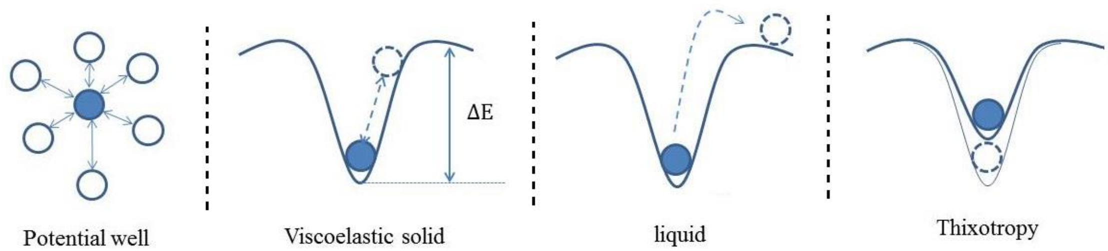

Figure 1.1: *Potential well for different regimes: solid regime when the applied energy on the system is lower than the energy barrier, liquid when particle leaves the potential well, and thixotropy for the case when the depth of potential well changes with time.*

1.1. Solid Regime

As mentioned before, paste can be considered as a complex network of interactions which results in a potential field. At rest, a particle tends to locate in the way that they have the minimum potential energy. Applied force or stress changes the network configuration and the system starts to deform. Work that has been done by applied force is stored in particles in the form of potential energy. If the given energy to the system is lower than the energy barrier, the system stores that energy and it will be released as soon as the force is removed. In other words, the deformation under stress is not permanent.

Robert Hooke (1678) has stated that "The power of any spring is in the same proportion with the tension thereof". This statement may be considered as the basis for first constitutive equation for ideal elastic materials or Hookes's law:

$$\overline{\overline{\tau}} = G\overline{\overline{\gamma}} \tag{1.1}$$

In this $\overline{\overline{\tau}}$ is stress tensor, G is modulus, and $\overline{\overline{\gamma}}$ is strain. Hooke's law has shown to be valid for most metals at low strain. In pasty systems, due to the presence of liquid phase, hydrodynamic dissipation is inevitable. Therefore, a viscous effect should be considered. The Kelvin-Voigt is one of the simplest models for a visco-elastic solid:

$$\overline{\overline{\tau}} = G\overline{\overline{\gamma}} + \mu\overline{\overline{\dot{\gamma}}} \tag{1.2}$$

The second term in the right hand side of equation (1.2) represents viscous dissipation, where μ is the viscosity and $\dot{\gamma}$ is the shear rate. The linear relation between stress, shear strain, and rate is a simple approximation of the solid-paste rheological behaviour. In general, for a solid-like paste system, stress comes from both elastic and viscous contributions as:

$$\overline{\overline{\tau}} = f(\overline{\overline{\gamma}}) + g(\overline{\overline{\dot{\gamma}}}) \tag{1.3}$$

Paste system deforms elastically until a certain limit, where the exerted work on the system exceeds the energy barrier. At this point one or more particles in the system jump out of the potential well and new configurations would form. Despite the elastic deformation, this deformation is irreversible and called plastic deformation or yielding.

1.2. Yielding

Below yield stress, the material shows solid-like behaviour. By increasing the stress, the material starts to flow in some point. As it was discussed, a certain amount of work is needed to overcome the energy barrier in the system. For each material, yield stress is associated to a strain value which is defined as the critical deformation (γ_c), above which deformation is not reversible.

The yield stress behaviour of materials might be the first reported deviation from Newtonian behaviour. However, it turns out to be a controversial subject, and there is still ongoing discussion on its concept and definition (Barnes, 1998). According to Blair (1933), yield stress is the stress below which no flow can be observed under the condition of experimentation. It has been claimed by many authors that the appearance of yield stress indicates existence of structure that requires initial energy to decay and let the material flow.

Yield stress has been first modeled by Bingham (1924). A more sophisticated model has been suggested by Herschel and Bulkley (1926) in which the material shows power-law behaviour after yielding. For one dimensional flow yielding starts when stress equals to the yield stress. However, for three-dimensional regimes the definition of yield criterion becomes more complicated. Tresca (1864) and von Mises (1913) proposed models for plastic fractions criterion in a three-dimensional stress field. Based on Tresca's work, yielding happens when the maximum shear stress in the system reaches the value of yield stress. On the other hand, the von Mises model suggests that the material starts to yield when the stored energy in the system is equal to the yield energy for one dimensional system. The von Mises model has shown to be a more accurate yield criterion for pasty materials.

1.3. Thixotropy and Structural Parameter

The term thixotropy was first suggested by Freundlich and Juliusburger (1935) for some gels that transform from gel-like to fluid-like by shaking or stirring. At that time, they did not consider time dependency for those gels. Pryce-Jones (1934), based on his work on paints, suggested that the thixotropic behaviour of materials can be defined as an increase of viscosity in the state of rest and a decrease of viscosity when submitted to a constant shearing stress. Like yield stress phenomena, it is believed that the origin of thixotropic behaviour is caused by the presence of structure within the material. As shear stress (strain) applies on these kinds of materials, it takes time for the structure to decompose and as the shear stress (strain) release, again it requires time to reform its initial structure. Because of these similarities, many authors considered thixotropy and yield stress as two inseparable phenomena with the same origin.

The first idea of using a structure parameter for modelling thixotropy was initiated by Goodeve (1938). He proposed a general theory for thixotropy and viscosity. According to his work, the rheological behaviour of some suspensions can be defined by the number of links between suspension particles. It has been also discussed that formation and breakage of these links are functions of shear rate and thermal conditions. Mooney (1946) published his work on thixotropic behaviour of compounded latex. He correlated the thixotropic behaviour and recovery of the material with the degree of aggregation.

Structural parameter is either a dimensionless number that represents some physical aspects of structure like number on links between particles or can be a phenomenological number that helps define the rheological behaviour of material. In the first case, it is referred to as a direct structural parameter and in the latter is referred to as an indirect structural parameter. Aside from being direct or indirect, the definition of the structural parameter is arbitrary. Most researchers define it as a scalar in the range between zero and one. The value of one for the structural parameter means that the material is fully structured. On the other hand, the value of zero of the structural parameter represents a totally destroyed structure. In general, the relationship between the shear stress and the structural parameter can be defined as (Goodeve, 1938):

$$\overline{\overline{\sigma}}(t) = f(\xi_t, \Pi_{\dot{\gamma},t}), \tag{1.4a}$$

$$\xi(t) = g(\xi_t, \Pi_{\dot{\gamma},t}), \tag{1.4b}$$

where the stress at each moment is a function of structural parameter at that point of time (ξ_t) and flow regime ($\Pi_{\dot{\gamma},t}$). Meanwhile, the structural parameter at each point is determined by its previous values and history of flow regime that applied on the material. Basically, the majority of models are based on the work by Herschel-Bulkley and consist of yield stress and changing viscosity. However, yield stress and viscosity are themselves functions of the structural parameter.

Worral and Tuliani (1964) based on their work on clay-water suspensions suggested that the yield stress is independent of the structural parameter and it remains constant during the flow. However, Tiu and Boger (1974), Nguyen and Boger (1985), and Toorman (1997) believed that the yield stress, τ_y, is a linear function of the structural parameter and an initial yield stress, $\tau_{y,0}$ ($\tau_y = \xi\tau_{y,0}$). There are also some models (Coussot et al., 2002) that do not consider any yield stress, and the behaviour of the material at very low shear rates is explained by a large value of the instantaneous viscosity.

Introduction of the structural parameter increases the number of unknowns that need to be determined from experiments. Therefore, it is necessary to introduce a kinetic equation to define the evolution of the structural parameter and close the system of equations. A general observation is that the rate of structure breakdown due to shear forces is a function of shear rate and the degree of structure at the moment. Worral and Tuliani (1964), Mujumbar et al. (2002), and Coussot et al. (2002) suggested that the rate of structure breakdown due to an applied shear rate is equal to $K_1\xi\dot{\gamma}$. Lee and Brodkey (1971), and Yziquel et al. (1999) considered a shear-stress dependency as well as a shear-rate dependency for the rate of structural breakdown, suggesting more complicated functions. The choice of functions might be dependent on the specific system under study.

Brownian motion compensates for structural breakdown and helps the material to rebuild its structure. Most authors assumed that the rate of structural build-up due to Brownian motion is proportional to (1-ξ). Meanwhile, Pinder (1964) and Coussot et al. (2002) suggested that the rate of structural build-up is independent of the structural parameter and is always constant. A few researchers also consider build-up due to shear rate (Worral and Tuliani, 1964; Lee and Brodkey, 1971; Dullaert and Mewis, 2005).

As mentioned above, there are many existing models to predict thixotropic behaviour of materials under simple viscometric regimes. Each of these models could be suitable for a different class of materials. More information could be found in the review articles by Mewis (1987), Barnes (1997), and Mewis and Wagner (2008). In this thesis some of these models will be adopted to develop a thixotropic model for the flow of toothpaste, chocolate and polytetrafluoroethylene (PTFE).

1.4. Fibrillation

For some pastes like PTFE paste, the rheology of the material continuously changes as it flows through contractions. Similar changes happen to most thixotropic materials with the difference that the structure of PTFE is not reversible. Paste starts as a two-phase fluid-like system, an oversaturated suspension and it ends as a highly fibrillated solid-like system. Thus, fibril formation during PTFE paste flow has to be considered as an important parameter in modeling the paste flow dynamics.

During the extrusion process, compacted resin particles entering the die conical zone are highly compressed due to the reduction in the flow cross-sectional area. PTFE crystallites in adjacent particles begin to mechanically interlock, as the particles rub against one another under the application of high pressure. This results into the interconnection of adjacent particles. As these particles flow towards the exit of the die, they experience an accelerated flow, during which the mechanically locked crystallites are unwound, creating fibrils (Ariawan et al., 2002a; Ariawan et al., 2002b). Therefore, fibrillation should be taken into account in the modelling of PTFE paste flow.

In this thesis, the rheology of three different pastes is studied. First, a commercial toothpaste is considered. Its rheology is studied by means of a parallel-disk rheometer while its processing is assessed by means of a capillary rheometer using a variety of capillary dies. The modelling considers the formulation of a rheological constitutive law and subsequent CFD simulations in capillary flow as an indirect proof of the suitability of the formulated constitutive law in the prediction of experimental data from capillary rheometry. A similar study was performed for a commercially manufactured chocolate in both its solid and viscoelastic fluid state. A study of the paste extrusion of polytetrafluoroethylene (PTFE) is performed. While in the case of toothpaste and melt chocolate the materials are modelled by using concepts of thixotropy (reversible structural models), the fibrillation model for the case of PTFE is a non-reversible model as will be exp;ained below.

2. Literature Review

2.1. Rheological Analysis

Rheology is the study of flow and deformation of matter. A constitutive rheological equation defines the mathematical relation between stress field and deformation. In this chapter the basic rheological behaviour of pasty materials is discussed as it is important in several fabrication processes for quality control of the final product. The rheological methods and rheometers used in these studies are also discussed in this chapter.

2.1.1. Parallel-disk Rheometry

Consider a fluid (i.e. a paste) placed between two parallel disks of radius R and separated by an adjustable distance H (Figure 2.1). The upper plate is capable of rotating along their common axis with an angular velocity of ω. The shear rate is proportional to the angular velocity. Therefore, it varies from zero in the center to $R\,\omega / H$ at the edge of plates (Larson, 1999). The torque required to rotate the upper plate can be written as:

$$T = \int_0^R 2\pi r^2 \tau(r)\,dr \tag{2.1}$$

Then the viscosity can be calculated by measuring the torque at any specific shear rate. Finding the flow curve (shear stress versus shear rate) is one of the basic rheological experiments for any material. The flow curve can be used to calculate the viscosity of the material at different shear rate values.

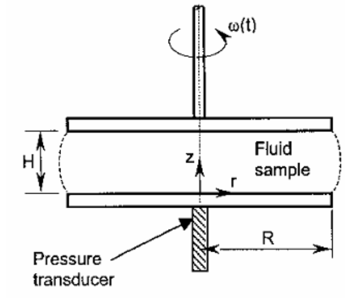

Figure 2.1*: Schematic view of the parallel-disk rheometer*

Some materials show both solid and liquid behaviour, known as viscoelastic fluids. To study their rheological behaviour, small-amplitude oscillatory shear (SAOS) tests can be used. For such a test the upper plate is moving in a sinusoidal manner. Specifically, the strain and strain rates imposed by the rotational angular velocity of the upper plate can be written as:

$$\gamma(t) = \gamma_0 \sin(\omega t) \quad (2.2a)$$

$$\dot{\gamma}(t) = \gamma_0 \omega \cos(\omega t) \quad (2.2b)$$

where $\gamma(t)$ is the strain , $\dot{\gamma}(t)$ is strain the rate, γ_0 is the strain ampliture and ω is the frequency. For an elastic material, the stress is in phase with strain, while, for a viscous material it is in phase with the strain rate. For very small strain it can be proven that the shear stress for viscoelastic material is:

$$\sigma(\mathrm{t}) = \sigma_0 \sin(\omega t + \delta) \quad (2.3)$$

where δ is the phase angle. This shear stress response can be decomposed as:

$$\sigma(\mathrm{t}) = \gamma_c \left[G'(\mathrm{t}) \sin(\omega \, \mathrm{t}) + G'' \cos(\omega \, \mathrm{t}) \right] \quad (2.4)$$

where G' is the elastic modulus, which appears in the first term of right hand side of the equation and it is in-phase with strain. The second term is proportional to G'', it is called loss modulus and it is in-phase with the strain rate. When the material deforms under the application of stress, part of the applied work is stored as elastic energy and it is proportional to the elastic modulus. The other part of the work is dissipated through viscous forces and it is proportional to the loss modulus. The phase angle can be defined by $\tan\delta = G'' / G'$. For a purely viscous liquid the phase angle is $\pi / 2$ and for a purely elastic solid it is equal to zero. The complex modulus is defined by $G^* = G' + iG''$, where i is the imaginary unit. Therefore, the complex modulus magnitude is $|G^*| = \sqrt{G'^2 + G''^2}$. The complex viscosity is another important property in the study of viscoelasticity and it can be defined by $\eta^* = G^* / i\omega$; its magnitude is $|\eta^*| = |G^*| / \omega$ (Dealy and Wissbrun, 1990; Dealy and Wang, 2013; Larson, 1999) .

2.1.3. Flow between Two Coaxial Cylinders (Couette Flow)

Two coaxial cylinders can also be used in rheometry to determine rheological properties. The outer cylinder is called cup and it is fixed. The inner cylinder (bob) can rotate along their common axis with an arbitrary angular velocity, ω. In the limit of small gap to radius ratio, the flow can be considered one dimensional and the nominal shear rate can be written as:

$$\dot{\gamma} = \frac{\omega R_i}{R_o - R_i} \tag{2.5}$$

The torque needed for rotation is:

$$T = 2\pi h R_i^2 \tau(R_i) \tag{2.6}$$

where $\tau(R_i)$ is the wall shear stress on the surface of bob.

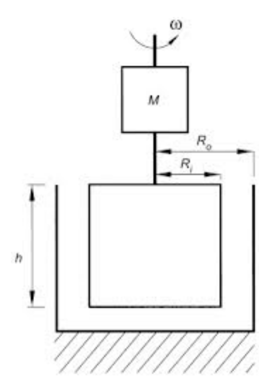

***Figure 2.2**: Schematic view of the cup-and-bob rheometer*

2.1.4. Capillary Rheometer

Capillary rheometer is the most widely used rheometer to mimic the paste extrusion process in the lab. This device consists of a reservoir, or barrel, and a plunger or piston that causes the paste to flow through the capillary die of known diameter, D_a, and length, L.

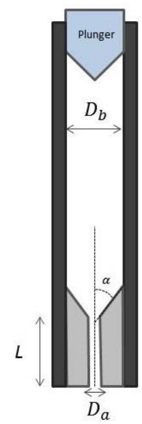

Figure 2.3*: Schematic view of the capillary rheometer*

Consider a fluid (i.e. a paste) in the barrel. As the plunger moves downwards it forces the fluid to come out of the die. Figure 2.4 shows a typical pressure profile along the capillary rheometer. Due to low apparent shear rate, the pressure drop in the reservoir is negligible. Most of the pressure drop occurs in the capillary die that consists of pressure drop in the conical part of the die and the die land. Finally, there is a small pressure drops as the fluid comes out of the die, known as exit pressure.

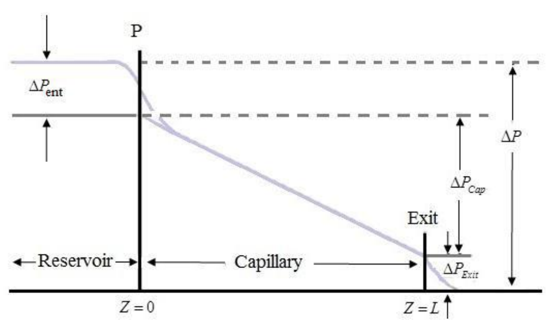

Figure 2.4*: Typical diagram of the pressure drop along the length of a capillary die, adapted from Mitsoulis and Hatzikiriakos (2003)*

The quantities normally measured in a capillary are the flow rate, Q (related to the piston speed) and the driving pressure, Δp (related to force on the piston that is measured by means of a load cell). For fully developed flow, force balance on cylindrical element of flow in die land results:

$$\sigma_w = -\frac{\Delta p D_a}{4L} \tag{2.7}$$

where σ_w is shear stress on the wall and Δp is the pressure drop over the tube length. For a Newtonian fluid, the shear rate on the wall can be written as:

$$\dot{\gamma} = \frac{32Q}{\pi D_a^3} \tag{2.8}$$

For the case of non-Newtonian fluids this quantity is called the apparent shear rate, $\dot{\gamma}_A$.

$$\dot{\gamma}_A = \frac{32Q}{\pi D_a^3} \tag{2.9}$$

As discussed, the measured pressure drop is associated with the pressure drop in reservoir, the conical part of the die, and also the end effects. To find the pressure associated with the die land, the Bagley correction procedure can be followed or simply an orifice die can be used to determine it directly. Then the pressure drop in the die land can be calculated by subtracting the pressure drop from the orifice die from the capillary die pressure drop (Macosko, 1994).

2.1.5. Wall Slip Characterization

Complex fluids typically slip at solid boundaries (Benbow and Bridgwater, 1993). In a rheological study, slip effects should be determined to correct the rheological data. There are various methods to determine slip and check for its presence. Some of these methods relevant to the present work are discussed below.

In parallel-disk rheometry a simple way to check for slip effects is to determine the flow curve of the complex fluid/paste (shear stress versus shear rate) using different gap heights. If the flow curve shows gap dependency, slip effects are present and the following expression can be used to determine slip at a specified wall shear stress value (τ_r) (Yoshimura and Prudhome, 1988):

$$V_{slip}(\tau_r) = \frac{\dot{\gamma}_{A,H_1}(\tau_r) - \dot{\gamma}_{A,H_2}(\tau_r)}{2(1/\mathrm{H}_1 - 1/\mathrm{H}_2)} \tag{2.10}$$

where H_1 and H_2 indicate gap size for different experiments. The symbol $\dot{\gamma}_A$ is the apparent shear rate and τ_r is the stress at which slip is to be determined.

In capillary flow the Mooney technique can be used (Mooney, 1931). The apparent shear rate in the presence of slip is given by:

$$\dot{\gamma}_A = \dot{\gamma}_{A,S} + \frac{8V_S}{D_a} \tag{2.11}$$

where $\dot{\gamma}_{A,S}$ is corrected apparent shear rate for the effect of slip and V_S is the slip velocity. This implies that if capillary experiments are performed for different capillary diameters, a diameter dependence of the low curve would imply the presence of slip. Then a plot of $\dot{\gamma}_A$ versus $1/D_a$ at different shear stress values would allow the determination of wall slip function experimentally. The slip velocity can be found as a function of wall shear stress.

2.2. Paste Flow - General Review

A broad range of products in industry are set in flow during processing, including bricks, tiles, catalyst pellets, drugs, dental materials, pencil leads, toothpaste, chocolate and poly-tetra-fluoro-ethylene (PTFE), among others. During paste extrusion, the paste is forced through a certain die by means of a pressure difference (pressure-driven flow). As the paste comes out of the die land it takes the shape of the die (Benbow and Bridgwater, 1993). The idea of extruding materials for the first time was offered by Bramah (1797). Since the present thesis studies the rheology and processing of toothpaste, chocolate and PTFE, a brief discussion of the previous work on the rheology of these materials will be presented.

2.2.1. Toothpaste

It is common to introduce toothpaste as an example for Bingham plastic behaviour (Tanner, 2000; Barnes et al., 1999). Barnes et al. (1989) have listed toothpaste as a shear-thinning material and assumed that its viscosity changes almost instantaneously. However, toothpaste is usually considered as a thixotropic material. There are different additives to improve the rheological properties of toothpaste like increasing its shear-thinning and shorten its thixotropy (Barrel, 2001). The thixotropic behaviour of toothpaste results in a delay between the instantaneous rheological behaviour and its equilibrium shear-thinning flow curve. The effects of toothpaste thixotropy on its flow regime in large-gap Couette geometry have been studied in a recent paper by Potanin (2010). His simulations, which are verified by the experimental data in simple shear, have shown that the calculated torque is greater for the thixotropic model compared to an equilibrium model. His work on toothpaste and similar works on thixotropic materials (Derksen and Prashant, 2009) clearly show the importance of considering thixotropy in flow analysis, and therefore the present work follows those guidelines.

In the present work, we are interested in studying first the rheological behaviour of a commercial toothpaste using simple rheological flows. Based on these experimental results, a rheological constitutive equation is developed. Furthermore, capillary extrusion experiments are performed using capillary dies of different geometrical characteristics such as die diameter, length-to-diameter ratio and contraction angle. Using the constitutive equation developed, capillary flow simulations are performed to predict the pressure drop in the various geometries.

2.2.2. Chocolate

Chocolate is rheologically complex both above and below its melting range. It shows semi-solid behaviour at room temperature (20-25^{o}C). Chocolate has a broad melting range. It melts down and turns into liquid form (in reality a dense suspension of non-colloidal particles) at temperatures very close to oral temperature that is about 30-32^{o}C. At room temperature the material typically contains about 10% liquid cocoa butter and this increases to 100% when the chocolate is fully molten above about 35^{o}C. Generally, chocolate contains around 70% fine powders (~20μm), like sugar and cocoa, which are dispersed in a continuous fat phase. Different commercially manufactured chocolate can be found and are categorized into three primary groups, namely, dark chocolate, milk chocolate, and white chocolate. They differ in content of cocoa solids, milk, and cocoa butter. Cocoa butter itself can be extracted from cocoa mass (ground cocoa beans) by pressing them during processing (Afoakwa et al., 2009; Whitefield, 2005; Awua, 2002; Becket, 2000). Cocoa butter triglyceride is mainly formed from Palmitic (P), Stearic (S), and Oleic (O) fatty acids (Whitefield, 2005; Beckett, 1999). Due to the presence of these triglycerides, cocoa butter is able to form six different crystal structures with different melting behaviours. Chocolate crystallinity is greatly influenced by temperature treatment during the process, fat content, and triglycerides type (Loisel et al., 1998; Lovegren et al., 1974; Lovegren et al., 1976; Wille and Lutton, 1966).

Usually, chocolates are made by pouring or extruding melt chocolate into a mould at temperature around 30^{o}C and cool down to retain the desired shape (Chevalley, 1999). More recently, a new method has been used, which involves cold extrusion of chocolate in temperature between 5^{o}C and 25^{o}C (Beckett, 2000). During extrusion, chocolate paste is forced through the die by a pressure difference. As the paste comes out of the die land it takes the shape of the die (Becket et al., 1994; Ovaici et al., 1998). Although cold extrusion is an isothermal thermal process, an increase in liquid fat content has been observed due to shear forces. Therefore, structural decomposition occurs during the process that results into a lower extrusion pressure (Mulji et al., 2003).

Rheologically, “liquid” chocolates have shown non-Newtonian behaviour with a yield stress and plastic viscosity (stress to keep fluid in motion) with mild shear-thinning characteristics. Different parameters affect the rheological behaviour of chocolate, such as fat content, emulsifier content, water content, conching time, crystallization, particle size, and temperature (Schants and Rohm, 2005; Vavreck, 2004; Tscheuschnerand and Wunsche, 1979). Knowing the yield stress and the thixotropic behaviour of pastes is extremely important from the rheological point of view to develop a rheological constitutive equation capable of predicting correctly their flow behaviour in well-defined flows (Coussot, 2005).

Chocolate fat content has a significant effect on yield stress. Generally, a lower amount of fat results into higher yield stress values (De Graef et al., 2011). Particle size distribution is another important parameter, which plays a role in chocolate rheological behaviour (Chevalley, 1999). Cocoa particle size varies from 15 to 30 μm (Jackson, 1999). It has been reported that a bimodal distribution with a small amount of fine and large amount of coarse particles reduces the apparent viscosity (Mongia and Ziegler, 2000). Surfactant is another determining parameter in chocolate rheology. Addition of lecithin at low concentration (below 3%) reduces both yield stress and viscosity. After around 5%, addition of more lecithin increases the yield stress while the shear viscosity of the melt continues to drop (Chevalley, 1999; De Graef et al., 2011).

Different important rheological models have been used to characterise the rheological behaviour of chocolate melts including Herschel-Bulkley, Casson, Bingham, and Carreau model (Chevalley, 1999; Beckett, 2000; Sokmen and Gunes, 2006; Taylor et al., 2009). Although the Casson is the recommended model by IOCCC (International Office of Cocoa, Chocolate, and Confectionery), it has been reported that it is not able to accurately characterise chocolate melt behaviour at low shear rates (Taylor et al., 2009; Afoakwa et al., 2007).

In the present work, we are interested in studying first experimentally the rheological behaviour of commercially manufactured at both semi-solid and melt forms. Based on these experimental results, a rheological constitutive equation is developed for “liquid” chocolate ($T>30^oC$). Furthermore, capillary extrusion experiments are performed using capillary dies of different geometrical characteristics, such as die diameter, D_a, length-to-diameter ratio, L/D_a, and contraction angle, 2α. Using the developed constitutive equation, flow simulations in capillary flow are performed to predict the pressure drop in the various geometries and examine in detail the flow behaviour inside the dies with emphasis on the structure evolution of chocolate with emphasis on the structure evolution of chocolate. Since reliable rheological data for semi-solid states are not available, a simple analytical phenomenological model is used to capture effects of different geometrical parameters of dies on this process at temperatures less than 30^{o}C.

2.2.3. Polytetrafluoroethylene (PTFE) Paste

Polytetrafluroethylene (PTFE) has a high melting point, that is 342^{o}C the first time that it is melted (Sperati, 1989), which is high for a thermoplastic polymer. A previously melted PTFE shows a lower melting point of 327^{o}C, which is the value that is often reported in the literature i.e. second melting point. PTFE melt is stable, even at 380^{o}C, however its melt viscosity is relatively high at approximately 10 GPa·s. Due to this high melting temperature and melt viscosity, it is not possible to fabricate PTFE resin using conventional polymer melt processes (Gangal, 1994; Ebnesajjad, 2000). Therefore other techniques, such as cold pressing and paste extrusion at low temperatures, are used.

This is possible because PTFE have two transition temperature points as can be seen in the phase diagram of Figure 2.5. One is about 19°C in which, PTFE molecules undergo a slight untwisting from 180° twist per 13 CF_2 groups to 180° twist per 15 CF_2 groups (molecules and particles become more flexible). The chain segments form a perfect three-dimensional order and the change in the twist results in a volume increase of about 1.3% (Domininghaus, 1993; Plunkett, 1987; Ariawan, 2001; Ebnesajjad, 2000; Blanchet, 1997; Gangal, 1994; Mazur, 1995; Ebnesajjad, 2005; DuPont, 1994).

The second transition occurs at 30°C. Above this temperature, the number of CF_2 per 180° twist remains the same at 15. However, the extent of disorder of the rotational orientation of molecules about their long axis is increased. The total volume change as temperature is increased from below 19°C to above 30°C can be as high as 1.8% (Domininghaus, 1993). Shearing below 19°C will do nothing to particles as they are undeformable. However, above 19°C, shearing will cause unwinding of crystallites that will produce fibrils interconnecting all particles together. Therefore paste extrusion happens effectively at least higher than 19°C and more preferably higher than 30°C (second transition temperature) to increase the degree of fibrillation for obtaining products of higher dimensional stability (Domininghaus, 1993; Ariawan, 2001; Separati, 1989; DuPont, 1991; Ochoa, 2006).

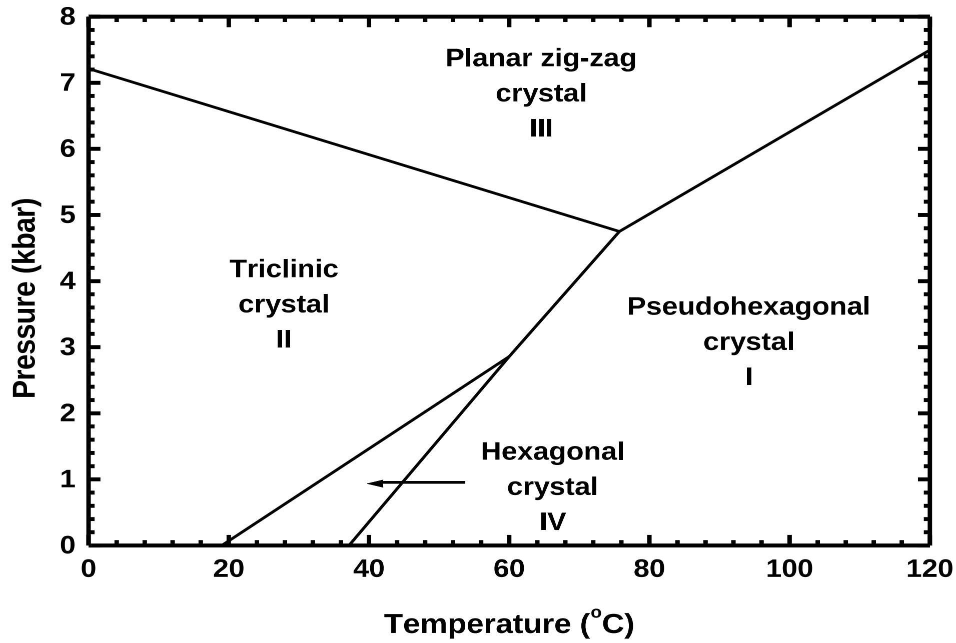

***Figure 2.5**: Partial phase diagram of PTFE (Sperati, 1989)*

Figure 2.6 represents a typical pressure transient, obtained during PTFE paste extrusion by means of a capillary rheometer (Ariawan, 2001). Three operating zones can be seen. Zones II and III correspond to the steady-state paste flow and the extrusion of a progressively drier paste at the final stages, respectively. The initial increase of pressure in zone I is due to the jamming of the paste in the die. An immobile network of PTFE particles is formed (similar to that of sand flow in a funnel) and a critical pressure (yield pressure) is needed to break this network to initiate flow.

Ariawan et al. (2002b) and Ochoa and Hatzikiriakos (2005) have performed detailed experiments to show the effect of volumetric flow rate, die entrance angle, die reduction ratio, and the physical properties of lubricants on the extrusion pressure of PTFE. A few of these effects most relevant to this work will be presented in this section. Figure 2.7 depicts the effect of lubricant concentration and volumetric flow rate on the extrusion pressure for a PTFE resin. The authors have concluded that a lower lubricant concentration results in a higher extrusion pressure due to reduction in lubrication. A lower lubricant concentration causes fibril breakage, and the extrusion frequently is discontinuous. On the other hand, a higher lubricant concentration results in an overlubricated flow that does not create enough pressure for fibril formation. Therefore, there exists an optimum lubricant concentration for optimization of mechanical properties. Similar results have been reported by Mazur (1995) based on industrial experience.

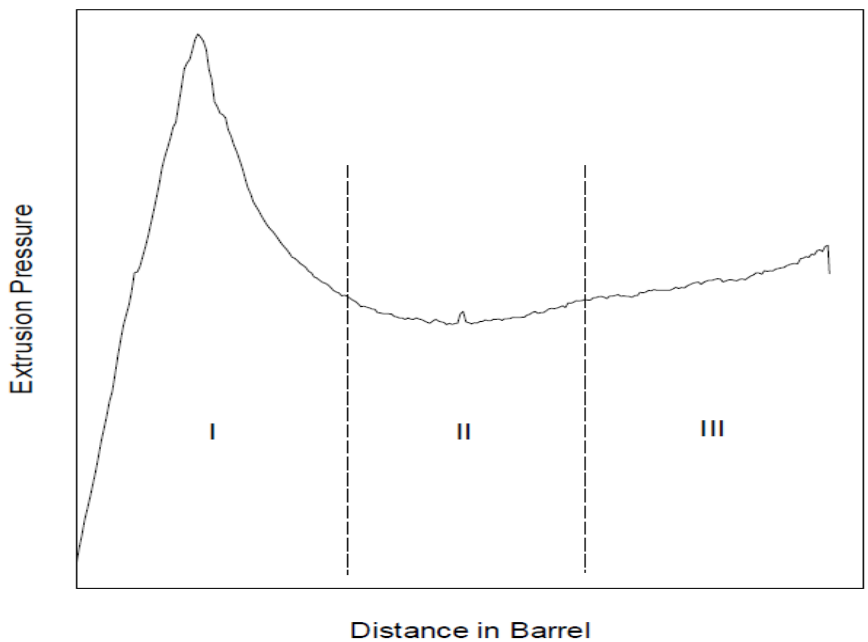

Figure2.6: *Typical behaviour of pressure transient during PTFE paste extrusion (Ariawan et al., 2001)*

The reduction ratio of the die is another important geometrical parameter. It is defined as the ratio of cross sectional area of barrel to cross sectional area of die at the exit or $RR \equiv D_b^2 / D_a^2$, where D_b is the barrel diameter and D_a is the die land diameter. Figure 2.8 shows its effect on the extrusion pressure of a PTFE paste. An increase in reduction ratio results in an increase of extrusion pressure with a concavity downwards.

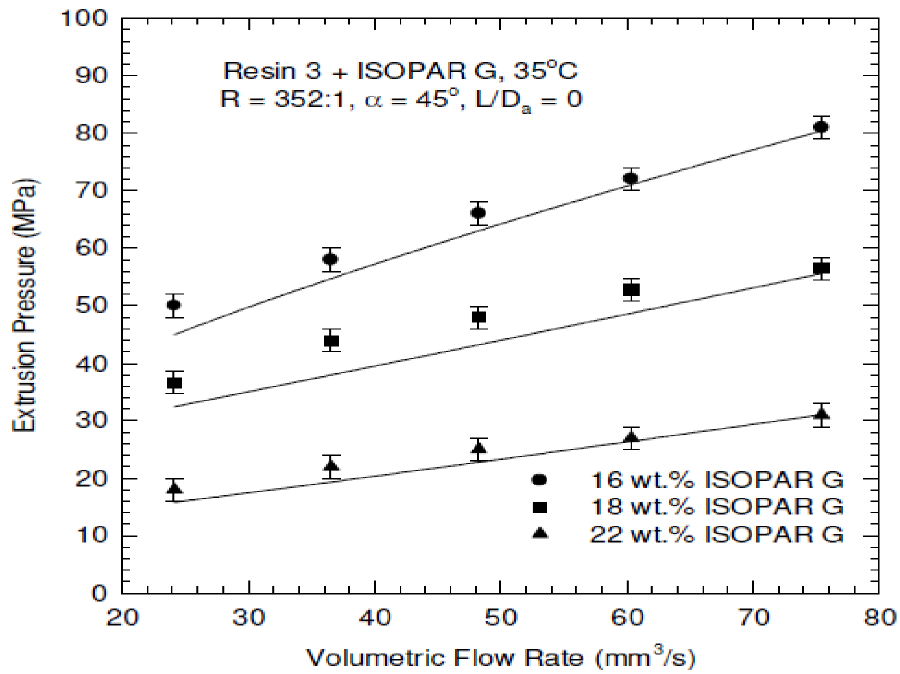

Figure 2.7: *The effect of lubricant (ISOPAR G) concentration on the steady-state extrusion pressure for resin 3 (PTFE resin). Solid lines are model predictions (Ariawan et al., 2002b)*

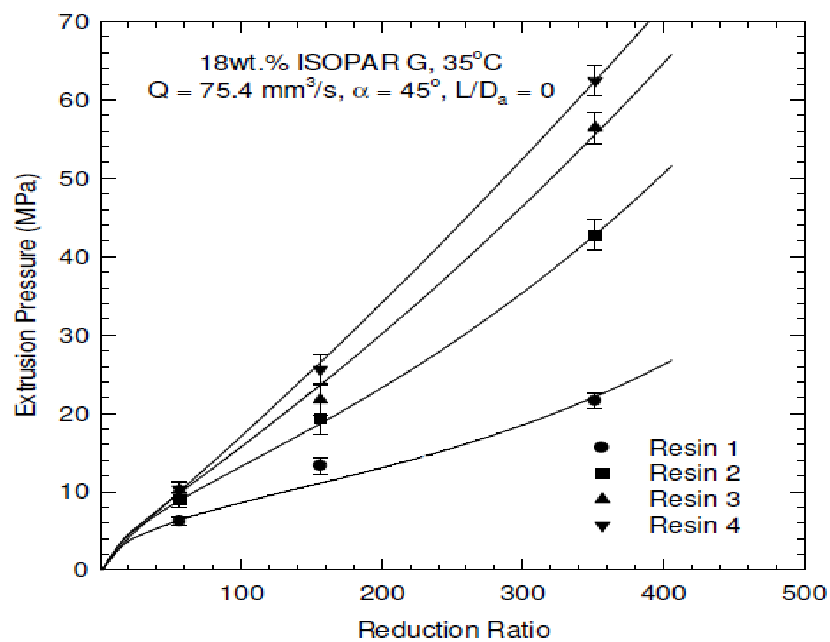

Figure 2.8. *The effect of reduction ratio on the pressure of steady-state extrusion for different PTFE resins. Solid lines are model predictions (Ariawan et al., 2002b)*

Figure 2.9 plots the effect of L/D_a on the extrusion pressure. The extrusion pressure increases with increase in the length-to diameter ratio, L/D_a, more and more as the reduction ratio increases. While the increase of extrusion pressure with increase of L/D_a is moderate, the most significant contribution to pressure comes from the contraction angle (see the pressure that corresponds to L/D_a =0), because the majority of fibrils are formed in the contraction zone where flow is mainly extensional, a requirement for fibril formation as discussed above.

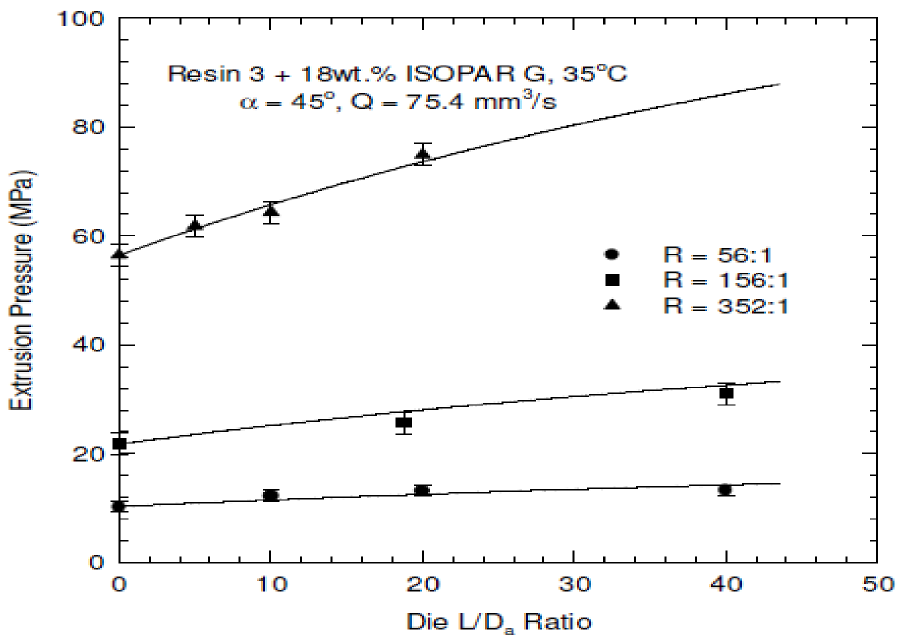

Figure 2.9. *The effect of die L/D_a ratio on the steady-state extrusion pressure at different reduction ratios for resin 3 (PTFE resin). Solid lines are model predictions (Ariawan et al., 2002b)*

In figure 2.10, the effect of entrance angle (the figure illustrates α instead 2α) of on the extrusion pressure is illustrated. The extrusion pressure varies non-monotonically with the entrance angle of the conical die; α, and it takes a minimum for an entrance angle about 20^o. It has been also recognized that the rheological behaviour of PTFE paste is strongly dependent on the number of fibrils formed between PTFE particles during the extrusion. At very small entrance angle, PTFE paste behaves mostly as a shear-thinning fluid with a little fibrillation that results in a decrease in extrusion pressure. Beyond a certain entrance angle greater than about 30^{o}, the extrusion pressure increases with increasing angle, as is commonly observed with the extrusion of elastic solids. More examples could be found in the work by Horrobin and Nedderman (1998). As fibrils are created, the paste attains significant elastic extensional properties that cause a significant increase in the extrusion pressure at high contraction angles.

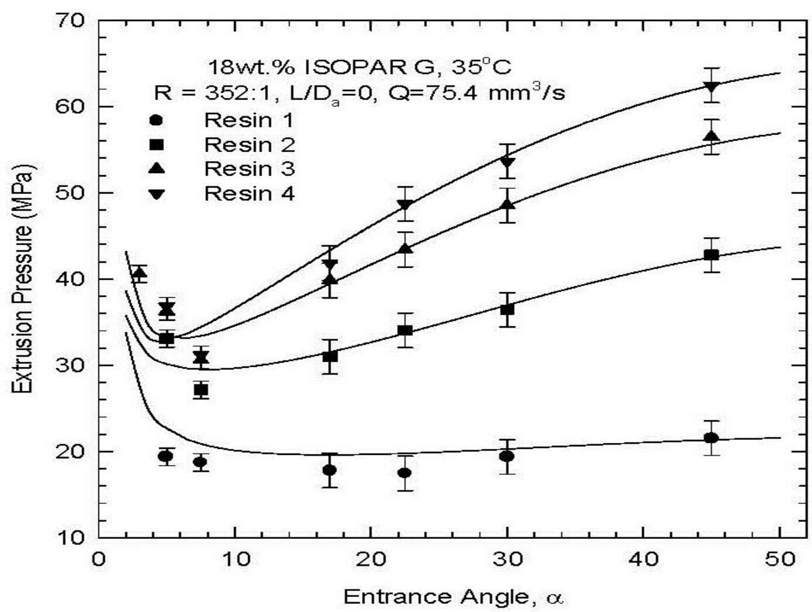

Figure 2.10. *The effect of die entrance angle on the steady-state extrusion pressure for different PTFE resins. Solid lines are model predictions (Ariawan et al., 2002b)*

Figure 2.11 depicts the steady-state extrusion pressure results as a function of apparent shear rate at different temparatures ranging from 15 to 65°C (Ochoa, 2008). At low temperatures below 19°C the extrusion pressure is low mainly due to limited fibril formation. PTFE experiences its first transition temperature at 19°C. Below this temperature, the PTFE particles are strong enough to resist the deformation and therefore very few fibrils are formed. Since the viscosity and surface tension are functions of temperature, the lubricant at low temperature can neither wet the PTFE particles nor move freely within the paste, and its distribution is expected to be very poor. Thus, even though the extrusion pressure is very low the extrudates appear very weak as confirmed by their low tensile strength. As the temperature increases going through the two transition temperature of 19°C and 30°C, the extrusion pressure and the degree of fibrillation increase accordingly, and the appearance of the extrudates in general improves. However, at temperature beyond 45°C, the extrusion pressure experiences a decrease, and there is no significant difference in the extrusion pressure at 55°C and 65°C. This is mainly due to the effect of temperature on the viscosity of the lubricant, while fibril formation remains the same.

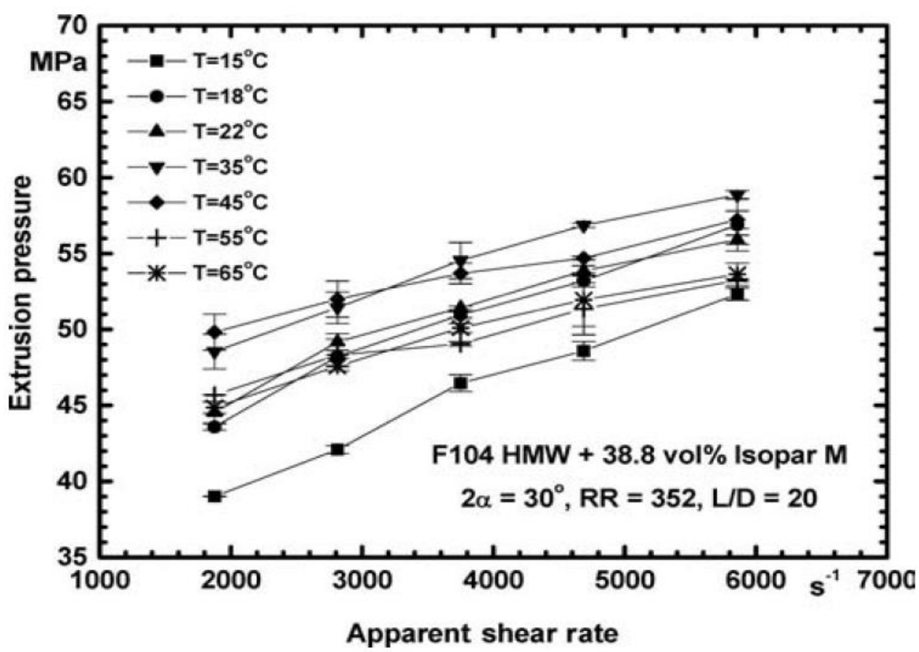

***Figure 2.11**: The effect of temperature on extrusion pressure of paste as a function of shear rate, (Ochoa, 2006)*

2.2.4. Models for Paste Extrusion

Generally, paste extrusion consists of four main stages: paste preparation, preforming, paste extrusion and sintering (see Figure 2.12). In the paste preparation, a desired amount of solid particles is blended with suitable concentration of liquid phase.

Mixing is carried out using different mixing methods like stirring or a motorized roll. Consequently the mixture should be aged for certain time to ensure absolute wetting of solid particles (Ebnesajjad, 2000; Blanchet, 1997; Mazur, 1995).

During the previous stages air might get into the mixture and would cause creation of voids in the final products. To remove air, the paste is compressed into a cylindrical billet in a cylinder that has the same dimensions with those of the extrusion barrel (Ebnesajjad, 2000; Ebnesajjad and Khaladkar, 2005). The preformed billet is consequently placed in the extrusion barrel and is forced through the extrusion die by means of a piston (plunger). This step is important from the rheological point of view and it will be studied into some detail in the present study both experimentally and theoretically though modelling.

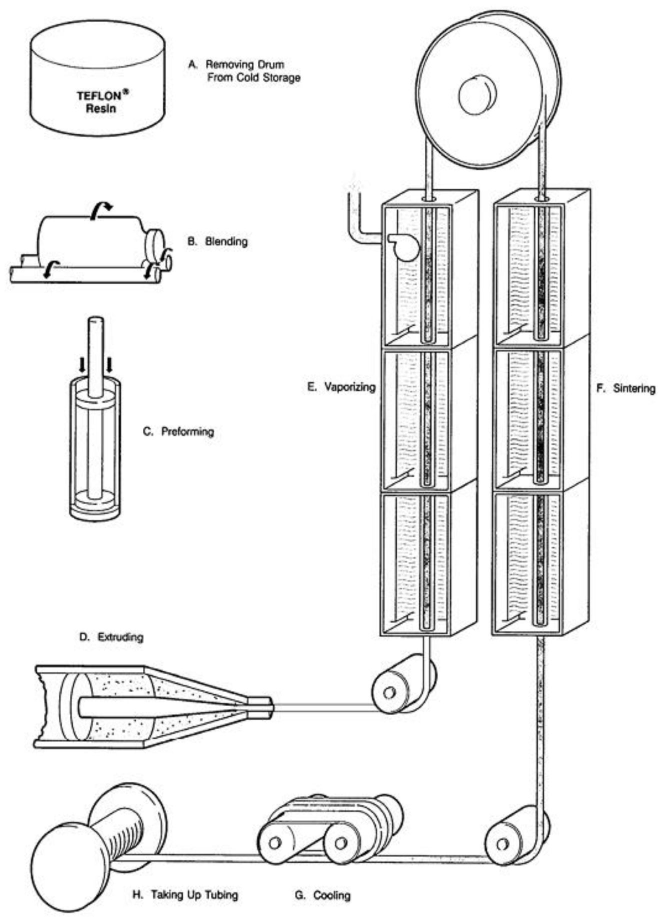

Figure 2.12*: Schematic picture of the paste extrusion process*

Various models have been developed over the years for paste flow and more specifically for PTFE paste. These are:

Benbow and Bridgwater model (1993): Benbow and Bridgwater assumed that paste behaves as visco-plastic material with severe slip on the wall. For a steady state flow through a capillary die of entry angle *2*α, the following relationship for the total pressure drop was derived:

$$\Delta p = \left\{ 2(\sigma_0 + \alpha_1 V^m + \tau_0 \cot\alpha)\ln(\mathrm{D}_b/\mathrm{D}_a) + \frac{\beta_1 Q^n}{n D_b^{2n}}(1-(D_b/D_a)^{2n})\cot\alpha \right\} + \left\{ \frac{4L}{D_a}(\tau_0 + \beta_1 V^n) \right\} \quad (2.12)$$

where σ_0, α_1, m, τ_0, β_1, n are parameters to be determined experimentally, and *V*, *Q* and D_b are the mean paste velocity, flow rate, and barrel diameter, respectively. The first term accounts for the change in cross sectional area in the conical entry (extensional and shear term), while the second term accounts for pressure drop in the die land (shear term). The rheological model used to obtain equation (2.12) was

$$\sigma = \sigma_0 + \alpha_1 V \quad (2.13)$$

Snelling and Lontz model (1960): Snelling and Lontz model assumes steady-state flow through an orifice die ($L/D_a = 0$) of conical entry angle *2*α, and using the following rheological model:

$$\tau = C\gamma^n + \eta(\frac{d\gamma}{dt})^{\mathrm{m}} \quad (2.14)$$

Based on the Snelling-Lontz assumption, paste is a visco-elastic solid with total slip on the wall. Using this expression for the stress tensor, Snelling and Lontz (1960) derived the following relationship for the total pressure drop for flow of PTFE paste in a tapered die

$$\Delta p = \frac{4C}{3(n+1)}\left[3\ln(\frac{D_b}{D_a})\right]^{n+1} + \frac{4\eta}{3m}\left[\frac{12Q\sin^3\alpha}{\pi(1-\cos\alpha)D_a^3}\right] \quad (2.15)$$

where *C, m,* η, and *n* are constants to be evaluated experimentally, $\left(\frac{D_b}{D_a}\right)^2$ is the reduction ratio for the die, and *Q* is the volumetric flow rate. The authors approached the problem by considering a constitutive equation that includes a strain-hardening term (elastic term) and a shear-thinning one (viscous resistance). The authors had related, in this work, the flow rate, die dimensions, lubricant concentrations, and time of extrusion. Additionally, by following the redistribution of pigmented paste within the die during extrusion, the authors have managed to experimentally determine the velocity field in the die entry region. This is the "radial flow" hypothesis which assumes that paste particles at the same radial distance from the virtual apex of the conical zone of the die, move towards the die apex at the same velocity (see Figure 2.13). Thus, the velocity of a point on a spherical surface at distance *r* from the apex is (Snelling *et al.,* 1960):

$$\frac{dr}{dt} = -\frac{Q}{2\pi(1-\cos\alpha)r^2} \tag{2.16}$$

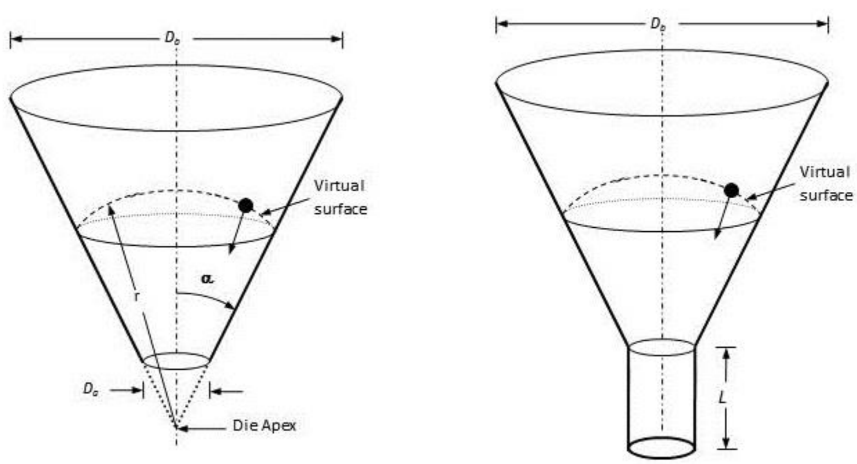

Figure 2.13: *(a) Schematic of a tapered orifice die showing the various characteristic dimensions and (b) schematic of a tapered die that includes a certain length of die land L*

Ariawan model (2002b): By following the Radial Flow Hypothesis proposed by Snelling and Lontz (1960), Ariawan et al. (2002b) had found a one-dimensional mathematical model to describe the effect of extrusion conditions for PTFE paste. This model considers the paste as visco-elastic solid, material that exhibits both strain hardening and viscous resistance effects during flow. Thus, by using a power-law modified Kelvin's stress-strain, Ariawan (2002b) used the following constitutive equation:

$$\sigma_\theta - \sigma_r = C\gamma_{\max}^n + \eta\dot{\gamma}_{\max}^m \tag{2.17}$$

where σ_θ and σ_r are the principal stresses in θ and *r* directions, respectively, and $\gamma_{\max}$ and $\dot{\gamma}_{\max}$ are the maximum values of the strain and strain rate, respectively. The extrusion pressure in the conical zone was found to be:

$$P_{extrusion} = \sigma_{rb} = \sigma_{ra} RR^B + 2(1+\mathrm{B}) \begin{Bmatrix} C\left(\frac{D_b}{2sin\alpha}\right)^{2B} \int_{r_a=\frac{D_b}{\sqrt{RR}sin\alpha}}^{r_b=\frac{D_b}{2sin\alpha}} \frac{\left(3\ln\left(\frac{r_b}{r}\right)\right)^n}{r^{2b+1}} dr + \\ \frac{\eta}{(3m+2B)}\left(\frac{12Qsin^3\alpha}{\pi(1-cos\alpha)D_b^3}\right)^q (RR^{B+\frac{3m}{2}} - 1) \end{Bmatrix} \tag{2.18}$$

where σ_{ra} is the stress at the die exit, *RR* is the reduction ratio, defined as $(\frac{D_b}{D_a})^2$, and C, η, *m*, *n* and *f* are material constants that have to be determined experimentally. This model was found to describe adequately most experimental observations. Specifically, it was found to predict quantitatively and qualitatively the effects of die entrance angle, reduction ratio, pressure, L/D_a ratio of the die, and PTFE properties. The above models, while they perform reasonably well in predicting the extrusion pressure, they provide no information on the effect of various parameters on the degree of fibrillation of the paste (structure formation). Therefore it becomes an objective of this work to improve this model (eq. (2.18) developed by Ariawan, 2002b), and in addition couple this with a kinetic equation that would predict structure formation as a function of the geometrical parameters of the die.

3. Objectives and Thesis Organization

3.1. Objectives

The main objective of this thesis is a comprehensive study (experimental and theoretical) of the rheological behaviour of different pastes that exhibit thixotropic effects reversible and non-reversible. More specifically, the main objective is to model the paste extrusion process by considering different aspects of their behaviour, such as visco-elasticity, yield stress, thixotropy, and fibrillation.

The particular objectives of this thesis are as follows:

1. Study the rheological behaviour of commercial toothpaste both in its equilibrium state and thixotropic region and develop an appropriate thixotropic constitutive equation coupled with a kinetic equation for the structural parameter to model experimental results obtained from a capillary and a parallel-disk rheometer. The experimental data from various capillaries would include the effects of different geometrical parameters, such as reduction ratio, length-to-diameter ratio, and contraction angle on extrusion pressure of toothpaste as well as chocolate and PTFE.
2. Develop a new simple phenomenological mathematical model for semi-solid extrusion of chocolate and PTFE paste. The model would take into account the elastic-plastic (strain hardening) and viscous nature of the material in its non-melt state for PTFE and solid chocolate.
3. Study the fibrillation phenomenon in PTFE paste extrusion, its origin and the critical parameter that affect it. This phenomenon is important since it produces the dimensional stability of the final product. It is expected that the tensile strength of the extrudates would be a function of the extent of fibrillation.
4. Develop a new model for fibril formation during PTFE paste extrusion. The model would take into account the effect of Hencky strain on fibrillation (an elongational characteristic) and a kinetic equation for fibril formation.
5. Study the rheological behaviour of melt chocolate both in its equilibrium state and in its thixotropic region and develop an appropriate thixotropic constitutive

equation coupled with a kinetic equation for the structural parameter to model experimental results obtained from a capillary and a parallel-disk rheometer.

3.2. Thesis Organization

This thesis is organized as follows. A brief introduction of this study is described in chapter 1. This chapter also covers the main rheological behaviours of different pastes and their origins. Chapter 2 starts with a short review of typical rheological analysis. The different rheological measurements and methods that have been used in this work are explained briefly. Also, the literature review on the rheology and properties of three different pastes (toothpaste, PTFE paste, chocolate paste) are presented in this chapter. Chapter 2 ends with a general review on PTFE paste extrusion and existing models developed in literature.

Chapter 3 presents the objectives and the organization of this thesis. In chapter 4, the materials and methodology used in this research are discussed in detail. In chapter 5, the rheology of a commercial toothpaste is investigated as a model paste system to study its processing characteristics in capillary flow using various dies. Its rheological behaviour has been determined as that of a yield-stress, thixotropic material with a time-dependent behaviour, and severe slip at the wall. The rheological data obtained from a parallel-disk rheometer were used to formulate a constitutive equation with a structural parameter, which obeys a kinetic equation, typically used to model thixotropy. The predictive capabilities of this model are tested against capillary data for a variety of capillary dies having different length-to-diameter ratios (L/D_a), contraction angles (2α), and contraction ratios $(D_b/D_a)^2$, where D_b is the diameter of the barrel of the capillary rheometer. The major trends are well captured by the thixotropic model and show that slip is the essential parameter in predicting the flow behaviour of toothpaste.

In chapter 6, the rheology of non-melt processible polytetrafluoroethylene (PTFE) pastes has been studied using three capillary rheometers having barrels of different diameter and equipped with capillary dies of various designs. The pressure drop is measured as a function of apparent shear rate (flow rate), reduction ratio (cross sectional area of barrel to that of die), contraction angle, length-to-diameter ratio, and diameter of the barrel (scale-up). To describe the effects of die design for scale-up purposes, a simple phenomenological mathematical model has been developed. The model takes into account the elastic-plastic (strain hardening) and viscous nature of the material in its non-melt state, due to the creation of fibrils and presence of lubricant, respectively. In addition, it takes into account the slip boundary condition at the paste/wall interface. The model predictions are found to be consistent with experimental results obtained from macroscopic pressure drop measurements and it can be used for scale-up purposes. The effects of process conditions on fibrillation and mechanical properties of polytetrafluoroethylene (PTFE) paste extrudates have been studied. The tensile strength of PTFE extrudates is measured as a function of apparent shear rate (flow rate), reduction ratio (cross sectional area of barrel to that of die), contraction angle, and diameter of the barrel. To describe the effects of die design on the quality of the final product, a basic phenomenological mathematical model has been developed. The model consists of a simple equation that explains fibril formation, due to the compression of PTFE resins, plus a kinetic equation, which is coupled with the "radial-flow" hypothesis to predict the structure and the tensile strength of extrudates. The model predictions are found to be consistent with tensile strength measurements and SEM micrographs of the PTFE extrudates.

In chapter 7, the rheological behaviour of a commercial milk chocolate is studied. Its rheological behaviour is distinctly different at temperatures below and above 30^{o}C. At temperatures below 30^{o}C, it behaves as a soft solid. A previously developed phenomenological mathematical model for polytetrafluoroethylene (PTFE) paste flow was used to model its rheology and capillary extrusion. At temperatures above 30^{o}C, chocolate behaves as a visco-elasto-plastic liquid. Its behaviour has been determined as a Herschel-Bulkley viscoplastic material with a small degree of thixotropy. The rheological data obtained from parallel-disk and bob-cup rheometer are used to formulate a thixotropic model using a structural parameter. The capillary data are found to be well described with the proposed models.

The conclusions and recommendations for future research are presented in the final chapter 8.

4. Materials and Methodology

4.1. Materials

In this thesis the rheological behaviours of three different pastes were studied. Namely, a commercial toothpaste, a commercial milk chocolate and a PTFE paste prepared based on accepted industrial protocol using a PTFE powder and a lubricant (DuPont, 1994).

The commercial toothpaste chosen for this study was made by Colgate (Colgate Total Whitening Paste). Because of the homogenous structure of toothpaste, it is expected that liquid migration becomes negligible compared to the case of granular materials with a liquid medium. All experiments have been carried out at room temperature (25°C). The density of this particular toothpaste has been measured and it was found to be 1300 kg/m^3 The commercial milk chocolate chosen for this study was obtained from Purdy's chocolatiers (Vancouver, BC, Canada). This particular chocolate contains 26% wt fat, 54% wt sugar, 2% wt fiber, and 6% wt protein. The density of chocolate has been measured and found to be about 1300 kg/m^3 at 25°C. We assume that chocolate will behave in a homogeneous way (at a length scale of μm). Then it is expected that liquid migration becomes negligible compared to the case of granular materials with a liquid medium.

To determine the rheological behaviour of PTFE pastes, experiments were performed using PTFE fine-powder resins supplied by Daikin. This resin has a density equal to 2140~2160 kg/m^3 at 23^{o}C and a primary particle dimension of about 2 μm. An isoparaffinic compound under the trade name of ISOPAR H® was used as the lubricant (supplied by ExxonMobil Chemicals). It is a Newtonian fluid with a viscosity of 1.36 mPa·s and a surface tension of 23 mN/m at 25^{0}C. The paste was prepared using guidelines reported by Ariawan et al. (2001) and Ochoa and Hatzikiriakos (2004).

4.2. Paste Preparation

For reproducible results, it is essential to use the same protocol for paste preparation, i.e., PTFE paste made out of PTFE resins and an isoparaffinic lubricant. To minimize any fibrillation prior to extrusion process, PTFE resins were stored in a refrigerator.

Toothpaste and chocholate were obtained from the commercial suppliers. A pre-shearing process for both cases was carried out to gurantee the same initial structure. In the case of chocolate, the same melting process (heating history) was followed to minimize structural difference.

4.2.1. PTFE Paste Preparation

Pastes were prepared by mixing PTFE fine-powder resins with the lubricant in a desired mass proportion at a temperature lower than 19^{o}C to produce pastes of 18% wt in lubricant. The resulting mixture (paste) was aged at room temperature for 24 hours before experiments, to allow more uniform wetting of the resin particles by the lubricant. Following this, the paste was preformed into the cylindrical reservoir of the capillary rheometer by using a blank die to prevent flow. A pressure of 1-2 MPa for 1 min was used to minimize lube migration and produce preforms of uniform density (Ariawan et al., 2001; Ochoa et al., 2004). Consequently, the blank die was replaced by a tapered die, and extrusion then proceeded at a constant piston speed. Typically, the extrusion pressure goes through a maximum at the beginning due to the initial filling of the die conical zone by the paste. After this transient stage, the pressure decreases and settles to a steady value (Benbow and Bridgwater, 1993; Ariawan et al., 2001).

4.2.2. Pre-shearing

The chocolate paste was prepared by grinding the solid chocolate bars and heating them at the desired temparature. A simillar heating procedure was used for toothpaste.

For both these pastes, excessive levels of shear force might decompose and alter their structure. Since the shear history for commercial toothpaste and liquid chocolate are unknown, a standard pre-shearing procedure was carried out to start all experiments from the initial structure. To obtain consistent and reproducible results, the samples are pre-sheared (a common practice for thixotropic fluids) for a certain period of time (15 min) under a certain shear rate (50 s^{-1}) using a rotational rheometer (Kinexus) and left to rest for 2 hours thereafter to recover their structure.

4.3. Rheological Measurements

The rheological properties of toothpaste and melt chocolate, such as yield stress and thixotropy, have been studied using a rotational rheometer (Kinexus) equipped with a cup-and-bob and parallel-disk geometry. First, steady shear experiments were performed to determine the equilibrium apparent viscosity. After pre-shearing, the shear rate is increased to determine the equilibrium viscosity value at this higher shear rate. This continues until enough points are obtained to determine the complete equilibrium flow curve of the toothpaste under study.

It is also necessary to characterise the time dependency and thixotropic behaviour of the toothpaste. To do so, various start-up experiments are carried out. In each experiment, the rheometer is first loaded with a sample. After pre-shearing and rest to recover the structure, the shear rate is suddenly increased from zero to a certain value. As a result the shear stress increases from zero to a high value rapidly and subsequently gradually decreases with time until it reaches its steady value. Essentially a shear stress overshoot is obtained in each case, indicating time dependency.

Even though the thixotropic behaviour is amplified in the case of sudden step shear rate from rest, similar although milder thixotropic behaviour is observed when the shear rate suddenly increases from a lower to a higher shear rate value. Therefore, experiments have been carried out using the same procedure with sudden shear-rate changes from a lower to a higher value. The same procedure has been followed to design a multistep shear-rate test for model evaluation.

A similar experimental procedure was followed for chocolate paste at three different temperatures, namely at 30°C, 32.5°C and 35°C. In addition, temperature sweep experiments from 19°C to 50°C were carried out to study the effect of temperature on complex viscosity of chocolate.

One of the objectives of this work is to study the effect of die design on paste extrusion pressure and quality of final product. Figure 2.13 shows a schematic picture of the simple capillary die geometry used in this study. Each capillary die can be defined by the barrel diameter, D_b, and the three dimensionless numbers, namely, the reduction ratio, $RR=(D_b/D_a)^2$, the length-to-diameter ratio, L/D_a, and the contraction angle, 2α.

Experiments were performed by usilizing three different barrels of various diameters, D_b. For each barrel, tapered dies of various diameter, D_a, total tapered (contraction) angle, 2α, length to diameter ratio, L/D_a, and reduction or contraction ratio, $RR=(D_b/D_a)^2$, were used to determine the effects of die design on the extrusion pressure. The dimensions of all dies for each barrel diameter are summarized in Table 3.1. To address the effect of temperature, extensive experiments were performed at different temperatures. Each experiment was repeated 2 to 3 times and the loads measured (by means of a load cell) were averaged and is reported here as the extrusion pressure defined as the load divided by the cross section of the barrel.

4.4. Characterization

4.4.1. Differential Scanning Calorimeter (DSC)

The thermal properties of chocolate have been analysed with a Shimadzu DSC-60 calorimeter with air as bath. A sample was placed in a sealed aluminum pan and heated at a rate of 5°C/min from 20°C to 50°C. For milk chocolate, a melting peak slightly above 30°C has been identified that separates solid from liquid behaviour.

4.4.2. Scanning Electron Microscopy (SEM)

During PTFE paste extrusion, fibrils form among PTFE particles. The morphological studies of the PTFE extrudates were carried out by using a scanning electron microscope (SEM), HITACHI S-3000 N. Cutting extrudates at room temperature results in breakage of old fibrils and formation of new ones due to shear forces. Therefore, PTFE extrudates were put in liquid nitrogen prior to sampling to minimize structural changes during the sampling procedure.

Table 4.1. *Reservoir and die dimensions used in the present work*

Barrel diameter, D_b=2.54 cm, Big Barrel			
D_a (mm)	*RR*	L/D_a	2α
1.397	330	10	35
2.54	100	10	35
5.08	25	10	35
Barrel diameter, D_b=1.5 cm, Medium Barrel			
D_a (mm)	*RR*	L/D_a	2α
0.85	310	20	15
0.85	310	20	30
0.85	310	20	45
0.85	310	20	60
0.85	310	20	90
0.85	310	20	180
1.24	140	20	45
2.25	45	20	45
0.85	310	10	45
0.85	310	0	45
Barrel diameter, D_b=0.952 cm, Small Barrel			
D_a (mm)	*RR*	L/D_a	2α
0.508	350	20	15
0.508	350	20	30
0.508	350	20	45
0.508	350	20	60
0.508	350	20	90
0.762	150	20	90
1.27	50	20	90
0.508	350	5	90

4.4.3. Tensile Measurements

The degree of fibrillation during the extrusion pressure is associated with the tensile strength of final extrudates. A Com-Ten, Compression & Tensile Strength was used to measure the tensile strengths of the dried PTFE extrudates collected during the extrusion process. The unit consists of a load cell moving upward at a constant speed to stretch the sample up to the point where rupture occurs. Each experiment was repeated three to five times and the average value is reported along its standard deviation shown by means of error bars.

5. Thixotropic Flow of Toothpaste

In this chapter, the rheology of a commercial toothpaste is investigated as a model paste system to study its processing characteristics in capillary flow using various dies. Its rheological behaviour is determined as that of a yield-stress, thixotropic material with a time-dependent behaviour, and severe slip at the wall. The rheological data obtained from a parallel-disk rheometer are used to formulate a constitutive equation with a structural parameter which obeys a kinetic equation, typically used to model thixotropy. The predictive capabilities of this model are tested against capillary data for a variety of capillary dies having different length-to-diameter ratios (L/D_a), contraction angles (2α), and contraction ratios $(D_b/D_a)^2$, where D_b is the diameter of the barrel of the capillary rheometer. The major trends are well captured by the thixotropic model and show that slip is the essential parameter in predicting the flow behaviour of toothpaste.

5.1. Rheological Characterisation

5.1.1. Equilibrium Flow Curve

First, steady shear experiments were performed to determine the equilibrium apparent viscosity. After pre-shearing, the shear rate is increased to determine the equilibrium viscosity value at this higher shear rate. This continues until enough points are obtained to determine the complete equilibrium flow curve. Figure 5.1 shows the steady values of the measured shear stress as a function of the shear rate. Different sets of steady-state experiments with different geometries have been carried out to observe the effects of slip. For two different cup-and-bob geometries (different gap), the results fall on the same curve, which means the effects of slip are negligible, consistent with previous reports (Potanin, 2010).

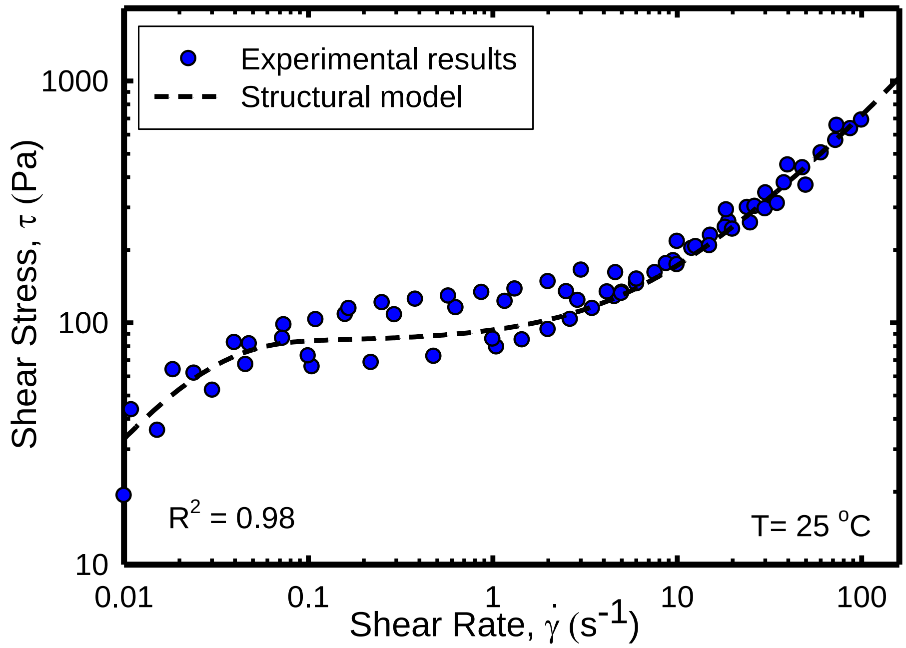

Figure 5.1. *The equilibrium flow curve and the fitted thixotropic-structural model*

For shear rates beyond about 0.1 s^{-1}, the experimental measurements were shown to be reproducible and consistent over three decades of shear rate. Below 0.1 s^{-1}, the data has shown some inconsistency, which might be due to the occurrence of shear banding. It has been reported in the literature that for many materials al low shear rates, experimental measurements are not reproducible due to occurrence of shear banding, flow bifurcation and shear rejuvenation (Coussot et al., 2009). The flow behaviour of some materials with shear banding behaviour has been studied with flow visualisation techniques. It has been shown that for the parallel-disk geometry under some critical shear rate there is no homogeneous flow, and shear rate is localized in a plane between the plates, meanwhile the rest of the material is in solid form (Coussot et al., 2009; Pignon et al., 1996). Due to shear banding the flow curve exhibits a minimum, and for each nominal shear stress there are at least two existing true shear rates. In simple words, flow below a certain shear rate (minimum of the flow curve) is always unstable. As a result of this instability it is impossible to report any equilibrium data below the critical shear rate.

To show the existence of shear banding, creep tests have been performed at different shear stress values. Figure 5.2 shows this flow bifurcation. For all shear stress values below a critical value (in this case about 20 Pa), a continuous decrease of shear rate is observed. Meanwhile, for shear stress beyond that critical stress, the shear rate attains its steady-state value. Since it takes time for the flow to develop or to reach cessation, the stability analysis is affected by the duration of the experiment. Therefore, it is not simple to define a precise value for critical stress. There is a window of shear rate values (roughly below 0.1 s^{-1}) that are shown not to be reachable by any shear stress value. For example, for a shear stress value of 20 Pa, a steady shear rate 0.001 s^{-1} does not last for more than 200 s, and flow terminates as the degree of structure is increased. Comparing these data with data obtained from shear-rate sweep experiments shows that the shear rates at the same shear stress values are not necessarily the same due to the occurrence of shear banding.

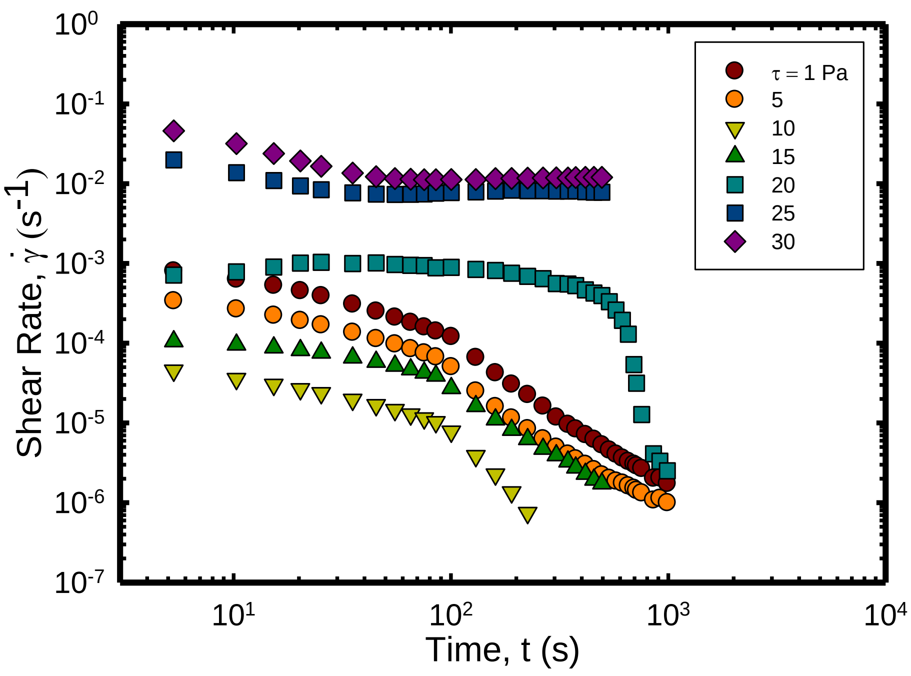

Figure 5.2. *Shear banding or flow bifurcation*

For all practical purposes, the low shear stress part of the flow curve can be described by the existence of a yield stress, τ_y. As pointed out by Papanastasiou

(Papanastasiou , 1987), the downturn of the experimental data at low shear rates can be obtained by multiplying the yield stress with the following exponential function of the shear rate $\dot{\gamma}$:

$$\tau_y \rightarrow \tau_y \left[1-\exp\left(-m_p \dot{\gamma}\right)\right], \tag{5.1}$$

where m_p is a stress-growth exponent with units of time. Choosing a suitable value for m makes a yield-stress curve pass through the low-shear-rate data (see Figure 5.1).

5.1.2. Time Dependency

It is also necessary to characterise the time dependency and thixotropic behaviour of the toothpaste. To do so, various start-up experiments are carried out. In each experiment, the rheometer is first loaded with a sample. After pre-shearing and rest to recover the structure, the shear rate is suddenly increased from zero to a certain value. As a result the shear stress increases from zero to a high value rapidly and subsequently gradually decreases with time until it reaches its steady value. Essentially a shear stress overshoot is obtained in each case, also indicating time dependency.

Even though the thixotropic behaviour is amplified in the case of sudden step shear rate from rest, similar, although milder, thixotropic behaviour is observed when the shear rate suddenly increases from a lower to a higher value. Therefore, experiments have been carried out using the same procedure with sudden shear-rate changes from a lower to a higher value. The same procedure has been followed to design a multistep shear-rate test for model evaluation.

Two main methods have been suggested in the literature to study thixotropy. The first method, referred to as the *iso-structure flow curve*, is based on the idea of measuring the flow curve of the material at a certain level of its structure (Mewis and Wagner, 2009). This method requires the determination of the flow curve with respect to a certain level of shear rate (reference rate). Each point in the flow curve is determined after the material is pre-sheared at the reference rate. Figure 5.3 shows flow curves with various levels of the reference shear rate. We observe that increasing the pre-shearing shear rate causes the flow curve to shift to small shear stress values due to the breakdown of the structure.

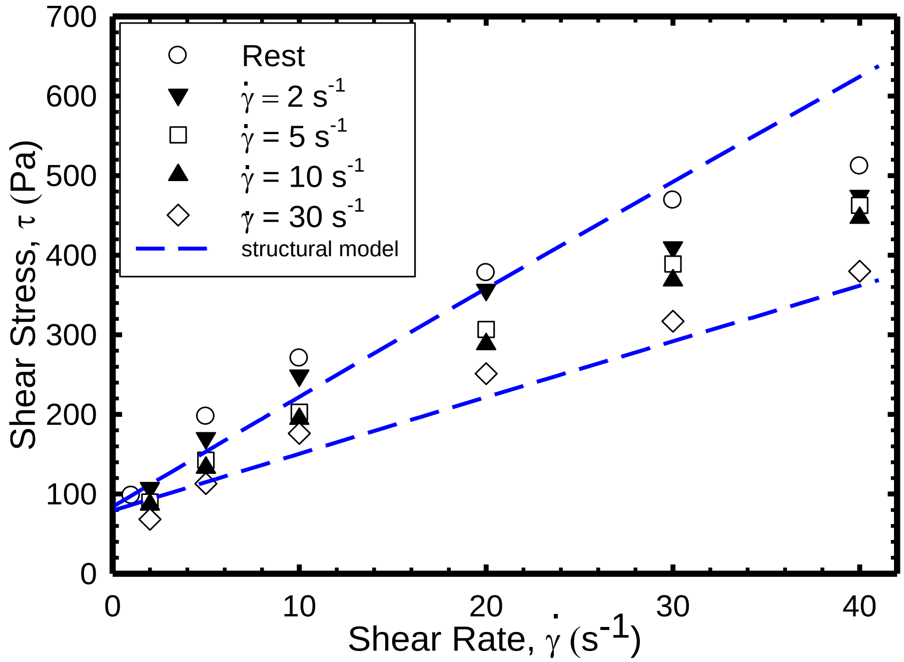

Figure 5.3. *Iso-structure flow curves*

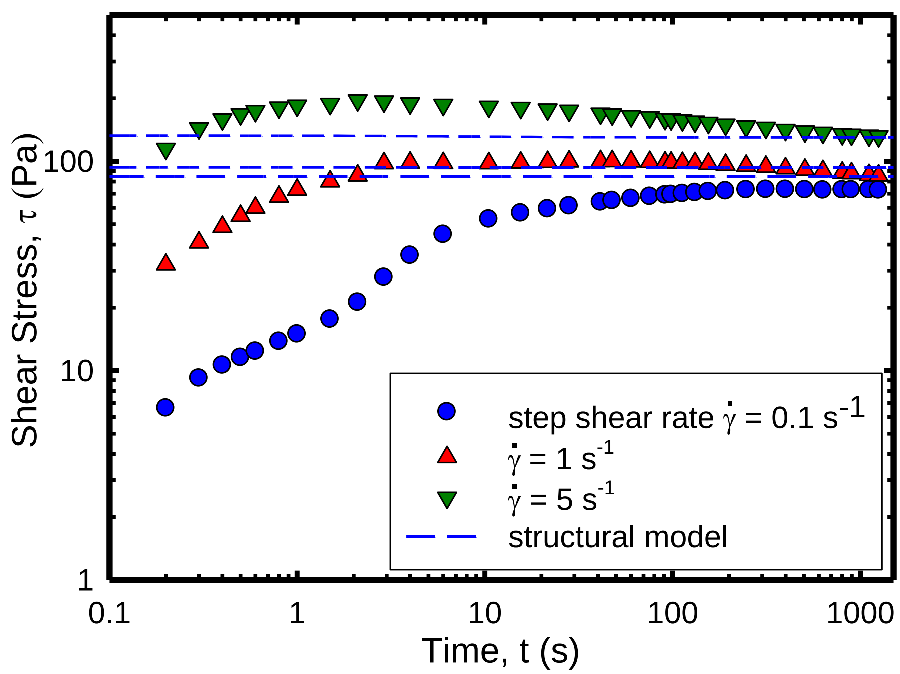

Figure 5.4. *The rheological response of toothpaste to different step shear rates*

Another method for the characterisation of thixotropy is the observation of the material's rheological response to any change in the flow regime like the shear rate. In this work, shear-rate step tests have been performed. It was observed that as the shear rate suddenly increased, the shear stress started from zero and quickly rose to a higher value. This initial part is related to the viscoelastic response of the material. After this viscoelastic response, thixotropic behaviour can be observed. Figure 5.4 shows both viscoelastic and thixotropic effects. The viscoelastic effect can only be tracked at low shear rates where the thixotropic effect is limited. Therefore for model development, the elastic response is neglected and the material is assumed to be purely thixotropic.

Figures 5.5a,b show two different sets of shear-rate jump tests; the first from a material at rest to a high shear rate and the second from an equilibrium state of shear rate at 5 s^{-1} to a new higher shear rate. As can be seen the overall description of the changes are satisfactory. Deviations at short times are related to the viscoelastic nature of the material; as such effects are neglected such deviations are expected.

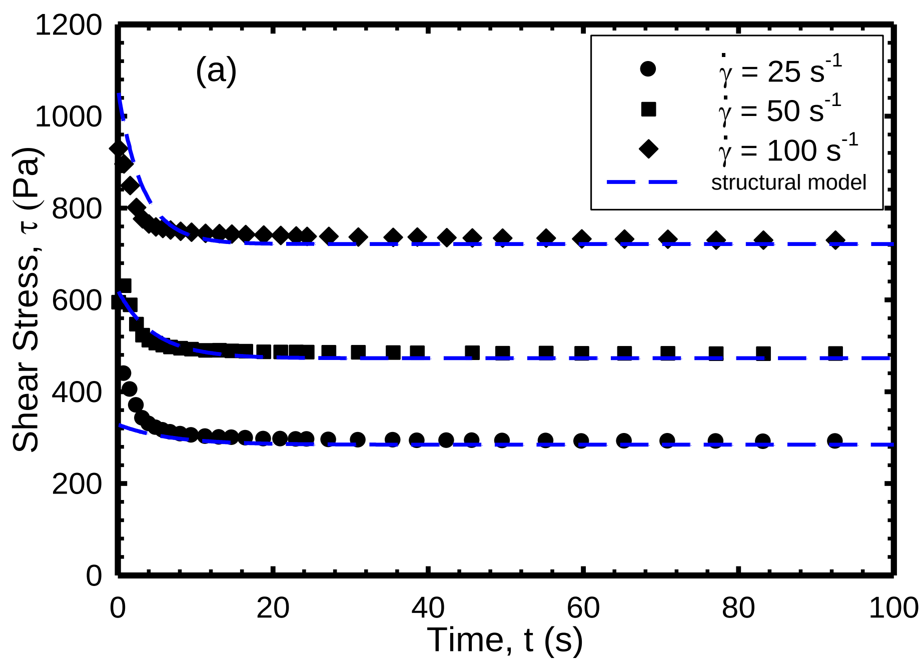

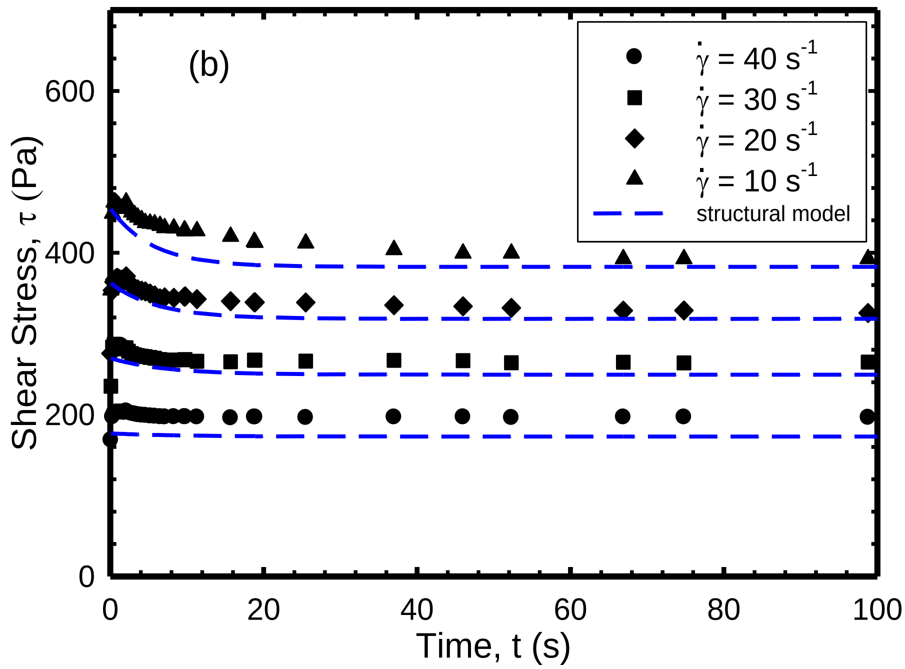

Figure 5.5. (a) *Thixotropic behaviour of paste in three start-up tests at different shear rates.* ***(b)*** *Thixotropic behaviour of toothpaste at various shear-rate jumps from an initial shear rate of 5 s^{-1}*

5.1.3. Slip at the Wall

Experiments were performed with capillary dies having different diameters to detect effects of slip. Figure 5.6 depicts the results, where a diameter dependence of the flow curve is obvious. Moreover the flow curves determined from capillary flow deviate significantly from the one obtained from the parallel-disk rheometer (data of Figure 5.1).

The Mooney analysis has been used to determine the slip velocity of toothpaste as a function of the wall shear stress (Mooney, 1931; Ramamurthy, 1986; Hatzikiriakos and Dealy, 1992). This analysis gives:

$$\dot{\gamma}_A = \dot{\gamma}_{A,s} + \frac{8V_s}{D_a}, \tag{5.2}$$

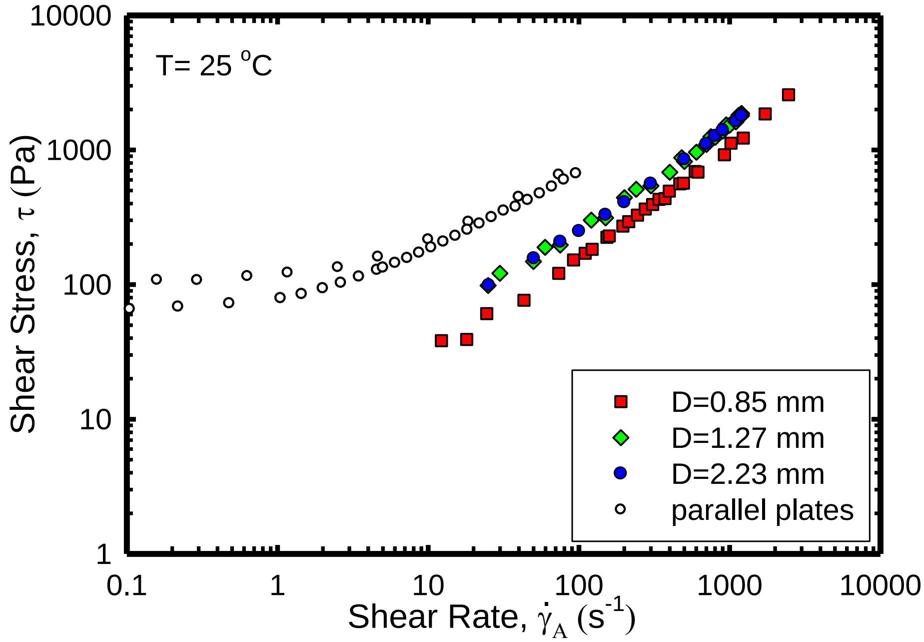

Figure 5.6. *The effect of die diameter, D_a, on the flow curve of toothpaste. Slip effects cause the diameter dependence*

where $\dot{\gamma}_A$ is the apparent shear rate, $\dot{\gamma}_{A,s}$ is the slip-corrected apparent shear rate, which corresponds to the parallel-disk flow curve of Figure 5.6, and V_s is the slip velocity.

Figure 5.7 plots the slip velocity versus the wall shear stress, τ_w. A linear relationship for slip is obtained, which can be written as:

$$V_s = \beta \tau_w, \tag{5.3}$$

where β is the slip coefficient. Its value was found to be 8x10^{-5} m/(Pa·s). For the flow conditions used in the capillary experiments and the rheological properties at hand, this value amounts to massive slip, as will become evident in the simulations further down. It should be noted that other reports on PTFE paste extrusion (Patil et al., 2006b; Mitsoulis and Hatzikiriakos, 2009a; Mitsoulis and Hatzikiriakos, 2009b) also showed severe slip occurring at the die walls, which is the norm rather than the exception for pastes in die flows.

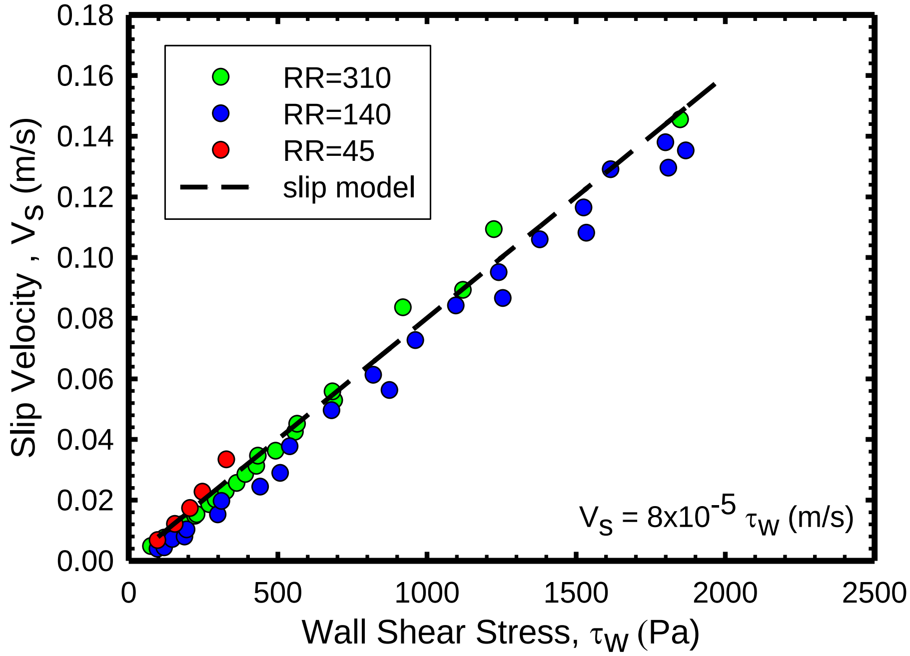

Figure 5.7. *Slip velocity of toothpaste as a function of wall shear stress at 23°C*

5.1.4. Capillary Extrusion Results

Capillary extrusion experiments were also performed using a piston-driven constant-speed capillary rheometer (Bohlin RH 2000). Various dies were used to study the effects of geometrical parameters of the die on the capillary flow (essentially pressure drop) of toothpaste. Important parameters include the die diameter, D_a, the length-to-diameter ratio, L/D_a, the reduction ratio, $RR \equiv (D_b^2 / D_a^2)$, where D_b is the barrel diameter, and the entrance contraction angle, 2α. Table 5.1 lists all capillary dies used in this study along with their geometrical characteristics. Since only one barrel was used for this study, the barrel diameter, D_b, is 15 mm for all cases. The results are presented below along with the flow simulations below.

Table 5.1. *List of capillary dies used in this chapter. The barrel diameter, D_b, is 15 mm*

Die Number	RR (-)	L/D_a (-)	2α(deg)	D(mm)
1	310	18	15	0.85
2	310	20	30	0.85
3	310	20	45	0.85
4	310	20	60	0.85
5	310	20	90	0.85
6	310	20	180	0.85
7	45	20	45	2.225
8	140	20	45	1.27
9	310	0	45	0.85
10	310	10	45	0.85

5.2. Constitutive Modeling

A constitutive model for a typical paste should possess at least two elements. First, a yield stress which is the stress below no flow is observed. Then, thixotropy should be included through an appropriate kinetic equation involving a structure parameter. It has been claimed by many authors that the existence of yield stress indicates the existence of structure that requires initial energy to decay and let the material flow, which implies that flow might alter the structure and thus thixotropy is expected (Mewis and Wagner, 2009; Krieger, 1990).

To represent toothpaste rheology, the proposed model includes two terms and can be written as follows:

$$\tau = \tau_y \left(1 - \exp\left(-m_p \dot{\gamma}\right)\right) + (1 + \xi^b)\eta_\infty \dot{\gamma} \,. \tag{5.4}$$

The first term represents the yield stress behaviour of the material. It is often assumed that the yield stress is related to the structure of the material through a structural parameter, ξ. However, in the present case the apparent yield stress shows a weak dependence on ξ, and we have neglected this dependence. Papanastasiou's exponential modification (Eq. 5.1) is applied on this term for fitting the data of Figure 1 at the lower shear-rate range.

The second term includes the viscous part of the response, and it is a function of the structural parameter ξ, which can be described by a kinetic equation. The rate of change in structure can be described by (Derksen and Prashant, 2009):

$$\frac{d\xi}{dt} = -k_1\dot{\gamma}\xi + k_2(1-\xi)\,. \tag{5.5}$$

This way the structural parameter ξ is a normalized quantity that varies between 0 and 1 and indicates the integrity of the network (ξ = 0: no network or structure; ξ = 1: fully developed network or structure). The first term on the RHS of Eq. (5.5) indicates breakdown of the network due to material deformation; the second term is responsible for build-up of the network with a time constant $1/k_2$ associated to it (here found to be equal to 10 s).

Structure formation occurs due to Brownian motion and is partially due to imposition of shear rate (Mewis and Wagner, 2009). According to the above Eq. (5.5), the shear contribution in structure build-up is neglected, and the rate of formation is set proportional to $(1-\xi)$ (Mujumdar et al., 2002). It has been assumed that the shear rate may break down structure. The rate of structural break-down is proportional to the shear rate and also to the degree of structure.

According to this kinetic equation, the structural parameter approaches a steady-state value, ξ_{eq}, at a given value of shear rate, $\dot{\gamma}$, that is:

$$\xi_{eq} = \frac{k_2}{k_1\dot{\gamma} + k_2}\,. \tag{5.6}$$

Therefore the equilibrium flow curve is given by:

$$\tau_{eq} = \tau_y\left(1-\exp\left(-m_p\dot{\gamma}\right)\right) + (1+\xi_{eq}^b)\eta_\infty\dot{\gamma}\,. \tag{5.7}$$

Then the equilibrium apparent viscosity η_{eq} is given by:

$$\eta_{eq} = \frac{\tau_y}{\dot{\gamma}}\left(1-\exp\left(-m_p\dot{\gamma}\right)\right)+(1+\xi_{eq}^b)\eta_\infty . \tag{5.8}$$

Optimized values for the proposed models are summarized in Table 5.2. The ratio k_1/k_2, m and the power b were calculated by fitting Eq. (5.7) to the data of Figure 5.1 by writing $\xi_{eq} = 1/[1+(k_1/k_2)\dot{\gamma}]$ from Eq. (5.6). Subsequently, using the data of Figures 5.5a,b, the individual values of k_1 and k_2 were calculated. Each flow curve at a given level of the structural parameter (or apparent viscosity) should look like a Bingham model and cross the equilibrium flow curve at its corresponding initial shear rate (see Figure 5.3). Figure 5.5b shows two different sets of shear-rate jump tests; the first from a material at rest and the second from an equilibrium state of shear rate at 5 s^{-1}. The thixotropic behaviour of the material has been adequately captured by the proposed model.

Table 5.2. *Fitted parameters for the structural model*

k_1 (-)	k_2 (s^{-1})	b (-)	τ_y (Pa)	η_∞ (Pa·s)	m (s)
0.003±0.0004	0.1±0.01	1.1±0.06	80±20	4.9±0.2	50±0.3

5.3. Governing Equations

We consider the conservation equations of mass and momentum for incompressible fluids under isothermal, creeping, steady flow conditions. These are written as (Tanner, 2000):

$$\nabla \cdot \bar{u} = 0 , \tag{5.9}$$

$$0 = -\nabla p + \nabla \cdot \bar{\bar{\tau}} , \tag{5.10}$$

where $\bar{u}$ is the velocity vector, p is the pressure and $\bar{\bar{\tau}}$ is the extra stress tensor.

The viscous stresses are given for inelastic incompressible fluids by the relation (Tanner, 2000):

$$\bar{\bar{\tau}} = \eta\left(\left|\dot{\gamma}\right|\right)\bar{\bar{\dot{\gamma}}}\,, \tag{5.11}$$

where $\eta\left(\left|\dot{\gamma}\right|\right)$ is the apparent viscosity of Eq. (5.8), in which the shear rate $\dot{\gamma}$ is replaced by the magnitude $\left|\dot{\gamma}\right|$ of the rate-of-strain tensor $\bar{\bar{\dot{\gamma}}} = \nabla\bar{u} + \nabla\bar{u}^{T}$, which is given by:

$$\left|\dot{\gamma}\right| = \sqrt{\frac{1}{2} II_{\dot{\gamma}}} = \left(\frac{1}{2}\left(\bar{\bar{\dot{\gamma}}} : \bar{\bar{\dot{\gamma}}}\right)\right)^{1/2}, \tag{5.12}$$

where $II_{\dot{\gamma}}$ is the second invariant of $\bar{\bar{\dot{\gamma}}}$

$$II_{\dot{\gamma}} = \left(\bar{\bar{\dot{\gamma}}} : \bar{\bar{\dot{\gamma}}}\right) = \sum_{i}\sum_{j}\dot{\gamma}_{ij}\dot{\gamma}_{ij}\,, \tag{5.13}$$

Thus, the apparent viscosity is written as:

$$\eta\left(\left|\dot{\gamma}\right|, \xi\right) = \frac{\tau_{y}}{|\dot{\gamma}|}\left(1 - \exp\left(-m\,|\,\dot{\gamma}\,|\right)\right) + (1 + \xi^{b})\eta_{\infty}\,. \tag{5.14}$$

In the above, the apparent viscosity is a function of ξ, which obeys the kinetic Eq. (5.5). In general flows, Eq. (5.5) becomes the convective-transport equation (Mitsoulis and Hatzikiriakos, 2009a; Mitsoulis and Hatzikiriakos, 2009b):

$$\frac{\partial\xi}{\partial t} + \bar{u}\cdot\nabla\xi = -k_{1}\,|\,\dot{\gamma}\,|\,\xi + k_{2}\left(1 - \xi\right). \tag{5.15}$$

For steady-state conditions, $\partial\xi / \partial t = 0$.

The above rheological model (Eqs. 5.11 and 5.14) is introduced into the conservation of momentum (Eq. 5.10) and closes the system of equations. Boundary conditions are necessary for the solution of the above system of equations. Figure 5.8 shows the solution domain and boundary conditions for the tapered contraction geometry of capillary flow. For the structural parameter, ξ, the entry boundary condition is ξ = 1 (i.e., it is assumed that the network is fully established) and $\partial\xi / \partial\bar{n} = 0$ at the walls, where $\bar{n}$ is the unit outward normal vector. The last boundary condition means that the structural parameter is free to take its values at the wall such that normal to the wall there are no changes in ξ. Because of symmetry only one half of the flow domain is considered, as was done in our previous works (Mitsoulis and Hatzikiriakos, 2009a; Mitsoulis and Hatzikiriakos, 2009b).

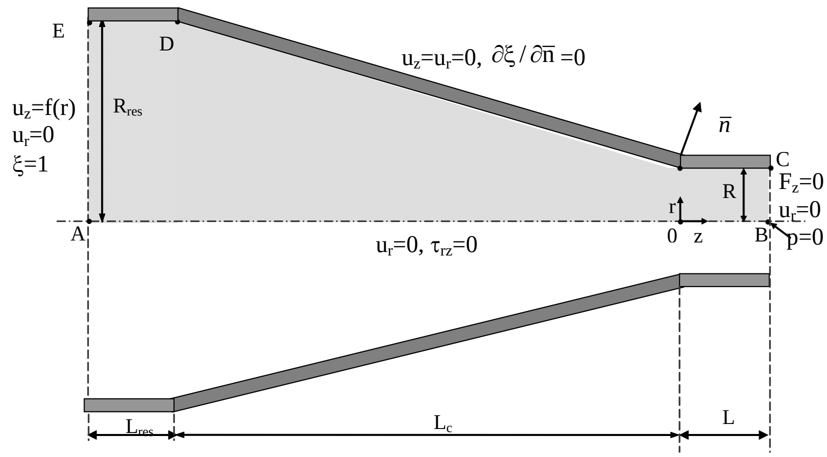

Figure 5.8. *Field domain and boundary conditions for capillary flow of toothpaste*

All lengths are scaled by the die radius R, all velocities by the average velocity U at the die exit, all pressures and stresses by $\eta_\infty \left(U/R\right)$.

5.4. Method of Solution

The numerical solution is obtained with the Finite Element Method (FEM), employing as primary variables the two velocities, pressure, and structural parameter (*u-v-p-ξ formulation*). Noting the similarity of the kinetic equation with the energy equation, we have substituted in our previous formulation the temperature, T, with the structural parameter, ξ (Mitsoulis and Hatzikiriakos, 2009a; Mitsoulis and Hatzikiriakos, 2009b). We use Lagrangian quadrilateral elements with biquadratic interpolation for the velocities and the structural parameter, and bilinear interpolation for the pressures. The solution process is similar to that employed by Mitsoulis and Hatzikiriakos (Mitsoulis and Hatzikiriakos, 2009a; Mitsoulis and Hatzikiriakos, 2009b), using the same grids as before. As in the previous results with PTFE paste modeling, the solution process was based on incrementing the apparent shear rate from low to high values. Due to the massive slip at the wall present in both cases (PTFE and toothpaste extrusion), convergence was fast and easy and could be obtained within few iterations to satisfy criteria for the norm-of-the-error and the norm-of-the-residuals below 10^{-5}. To ensure the occurrence of convergence, for any different geometry at one apparent shear rate mesh refinement analysis carried out. In this analysis, the number of mesh doubled and then quartered. Then the simulation results of those three cases (initial meshing, doubled, and quartered) compared together.

5.5. Flow Simulations

5.5.1. Flow Field

The flow simulations have been performed with the above conservation, constitutive and convective-transport equations, their boundary conditions, and the parameters of Table 2. Reference results are given for the highest apparent shear rate ($\dot{\gamma}_A = 4Q/\pi R^3 = 4U/R$ = 2560 s^{-1}) and one die design (Die #3, 2α=45°, L/D_a=20). The purpose is to find out the effect of the structural parameter ξ on the results, and how it affects the relative importance of the various forces at play in toothpaste extrusion.

Results are shown as contours of two important variables of the model, namely, the yield stress, τ_y, and the structural parameter, ξ. First, Figure 5.9 shows the yielded/unyielded (shaded) zones for different apparent shear rates. The dividing line between the two regions is the contour of the magnitude of the stress tensor $|\boldsymbol{\tau}| = \tau_y$. For the lowest apparent shear rate of 25.6 s^{-1}, the yielded region is contained in the tapered region just before the die entry. At intermediate shear rates, this region is extended inside the die, leaving a small unyielded plug in the die core. At the highest apparent shear rate, the yielded region is further extended both upstream and downstream to encompass the whole tapered region and die.

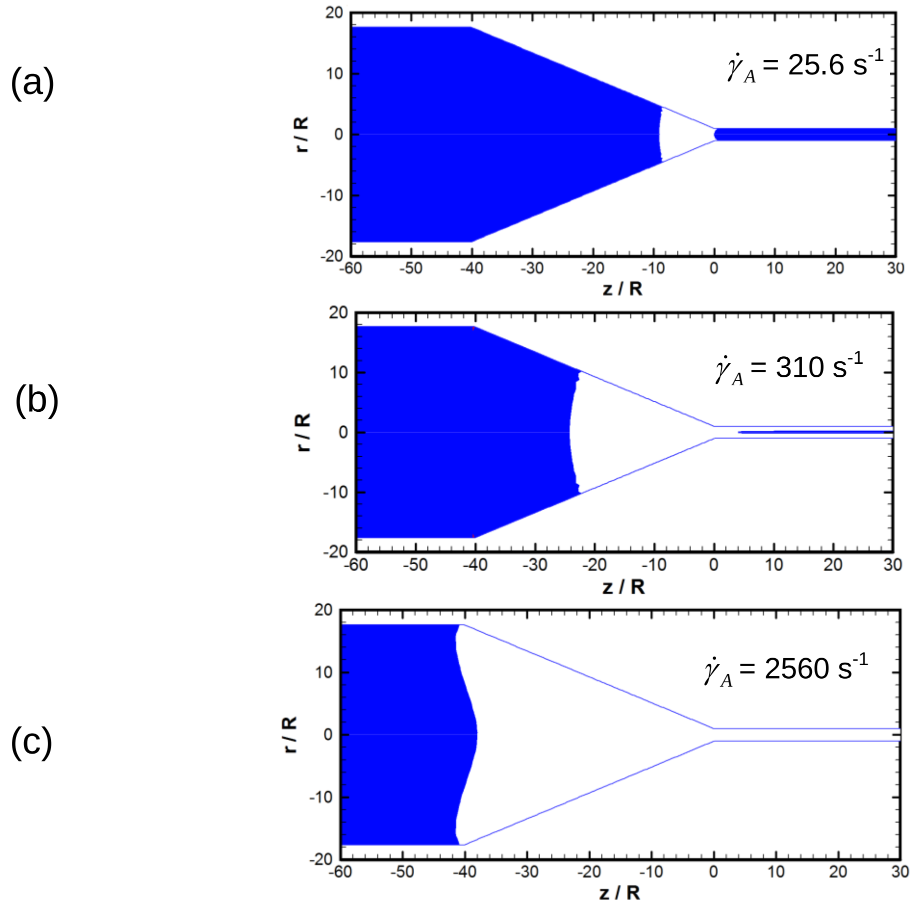

Figure 5.9. *Yielded/unyielded (shaded) regions in toothpaste extrusion at 23^{o}C for three different apparent shear rates. Incompressible flow with slip at the wall for Die #3, L/D$_a$=20, 2α=45^o, RR=311*

The corresponding results for contours of the structural parameter ξ are given in Figure 5.10. It becomes apparent that structure changes are small, and occur mainly in the die at high levels of shear rate. This is not surprising because the flow is fast as evidenced by the inverse of the apparent shear rates, and no time is given for the material to break down its structure. The ξ starts with 1 at entry (ξ not being 1 or 0 at the wall when slip is allowed), and then most of the changes occur in a cone near the die entry and inside the die.

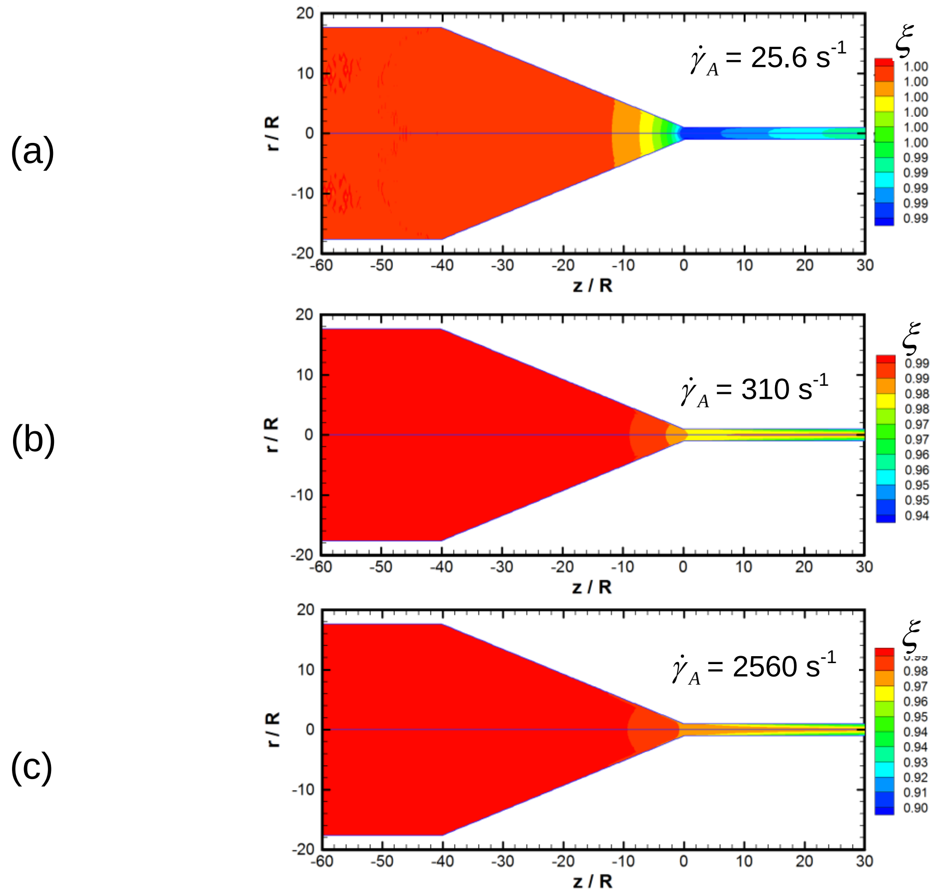

Figure 5.10. *Contours of the structural parameter ξ in toothpaste extrusion at 23^{o}C for three different apparent shear rates. Incompressible flow with slip at the wall for Die #3, L/D$_a$=20, 2α =45^o, RR=311*

5.5.2. Axial Distributions

Figure 5.11 shows the axial distribution of the axial velocity (at the centreline and the wall) for two apparent shear rates of 25.6 s^{-1} and 2560 s^{-1}. The velocity is made dimensionless by *U*, the average velocity at the die exit. Surprisingly, slip in the lower range of shear rate causes plug flow along the entire length of the die, including the contraction part, as the distribution along the wall and the centreline almost coincide (broken lines), while at the higher range of shear rates there is a clear difference between the velocity at the wall and the centreline (solid lines). The velocity rises to values of about 250U at the wall and 360U at the centreline in the die region. Thus, slip is relatively massive at lower shear rates and substantial at higher shear rates, as there is a clear difference between centreline and wall velocities.

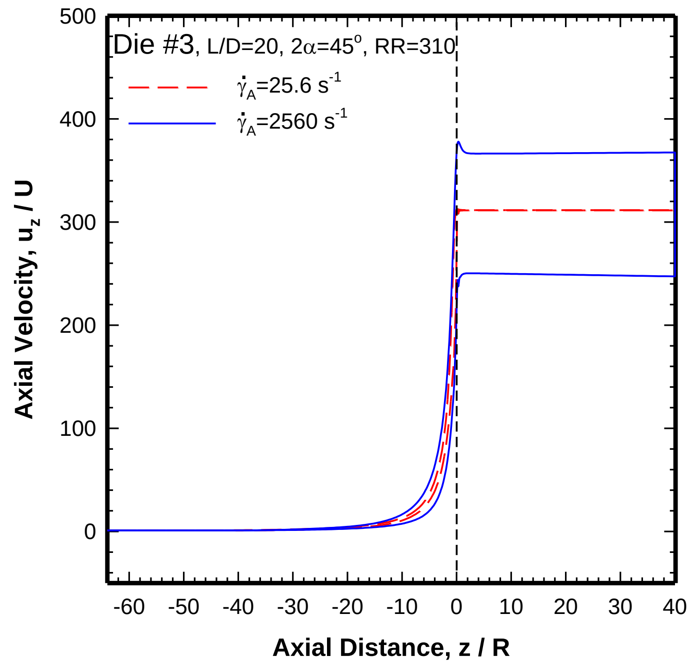

Figure 5.11. *Axial velocity distribution for toothpaste extrusion at 23°C for two different apparent shear rates. Incompressible flow with slip at the wall for L/D_a=20, 2α=45°, RR=310*

Figure 5.12 shows the axial distribution of pressure for different apparent shear rates. There are no surprises here, the pressure increases from about 3 MPa for $\dot{\gamma}_A$ = 25.6 s^{-1} to 270 MPa for $\dot{\gamma}_A$ = 2560 s^{-1}. The axial pressure drops are linear showing that the wall shear stress is constant along the die.

Figure 5.13 depicts the axial distribution of the structural parameter, ξ, at the centreline and the wall for the two apparent shear rates. We observe that for the lower shear rate, the structural parameter decreases continuously from the inlet up to the die entry where it increases slowly. However, at higher shear rates, there is a continuous decrease at the centreline, and in the die there is a linear drop, as expected from the kinetic Eq. (5.15), while at the die wall ξ remains almost constant. However, all the values are close to 1, meaning that the structure is mildly affected by the flow kinematics.

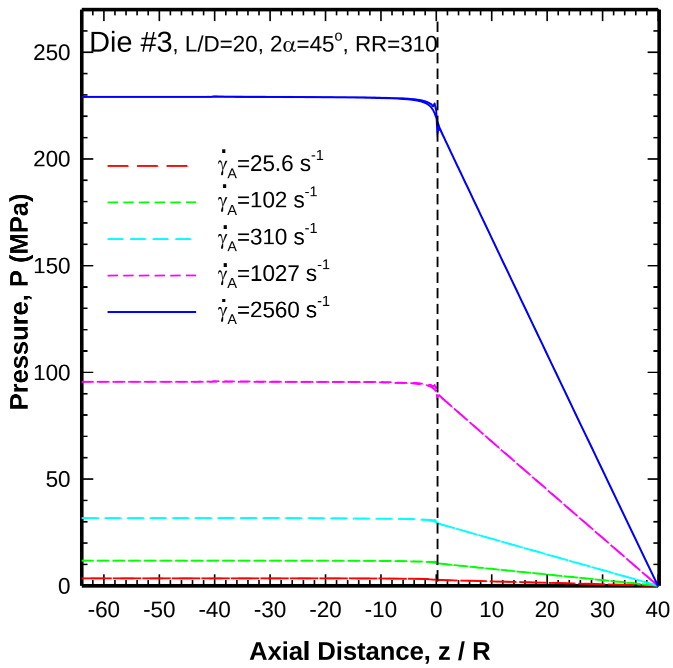

Figure 5.12. *Axial pressure distribution for toothpaste extrusion at 23°C for different apparent shear rates. Incompressible flow with slip at the wall for L/D=20, 2α=45°, RR=310*

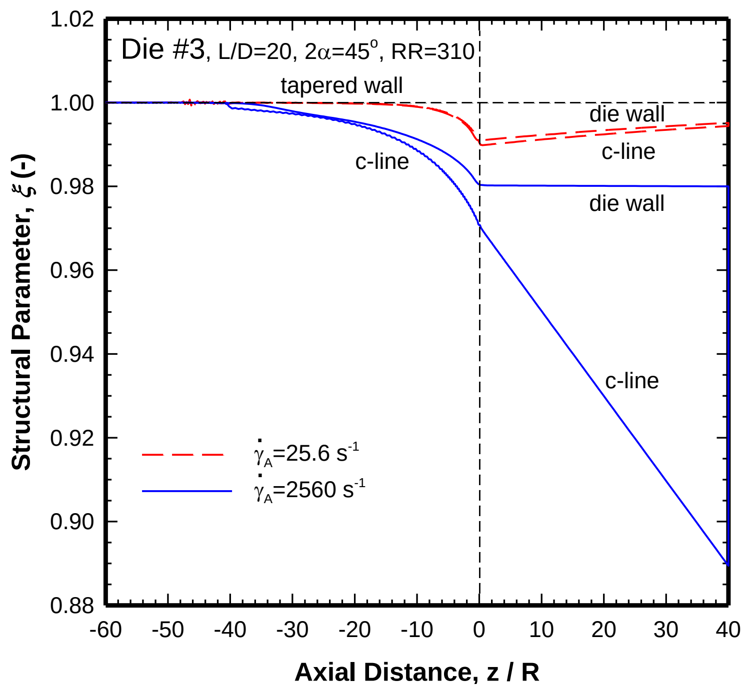

Figure 5.13. *Axial distribution for the structural parameter, ξ, along the centreline and the wall for toothpaste extrusion at 23°C for two different apparent shear rates. Incompressible flow with slip at the wall for L/D_a=20, 2α=45°, RR=310*

5.5.3. Effect of Flow and Design Parameters

The effect of the die entrance angle on the structural parameter ξ is depicted in Figure 5.14. The effect for the highest apparent shear rate of $\dot{\gamma}_A$ = 2560 s^{-1} is similar to that of Figure 5.13. The angles have a small effect on ξ. These effects originate from differences in the extensional components of the flow conditions at the entry, which are functions of the entrance angle.

The effect of the apparent shear rate for a given geometry (2α=45°) is shown in Figure 5.15. Increasing the apparent shear rate decreases the ξ–parameter, hence it leads to network breakdown, but again these changes are mild, hardly reaching ξ = 0.88. Again the effects are more significant at high shear rates and close to the centreline, where extensional components become significant.

Finally, the effect of L/D_a on the structural parameter for a given geometry (2α=45°) and apparent flow rate ($\dot{\gamma}_A$ = 2560 s^{-1}) is shown in Figure 5.16. A longer die allows the material more time to break down its network and to reach lower values of ξ.

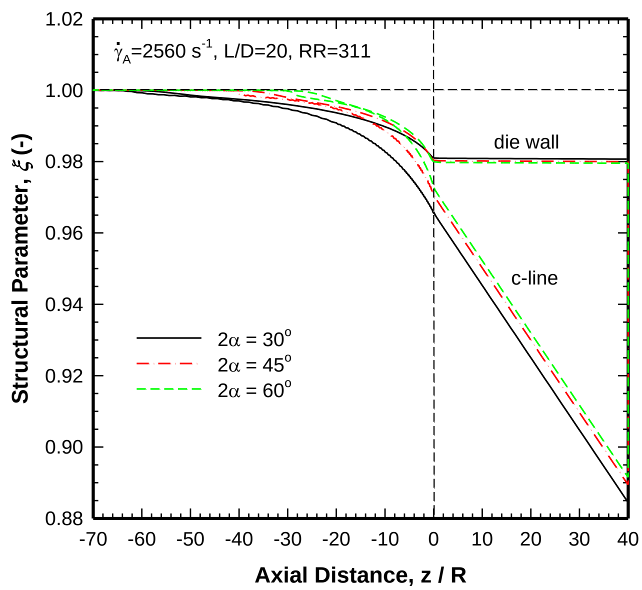

***Figure 5.14**. The effect of die entrance angle, 2α, on the structural parameter, ξ. Axial distribution of ξ along the centreline and the wall for toothpaste extrusion at 23°C. Incompressible flow with slip at the wall for $\dot{\gamma}_A$ =2560 s^{-1}, L/D_a=20, RR=310*

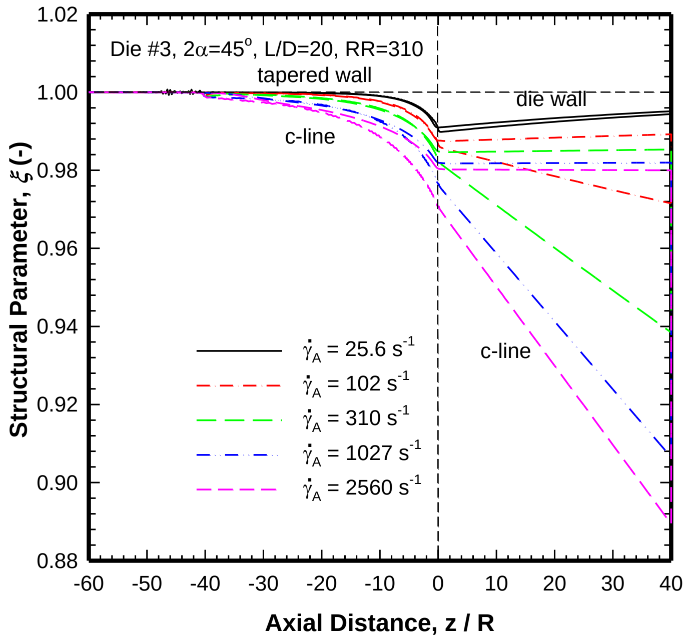

Figure 5.15. *The effect of apparent shear rate, $\dot{\gamma}_A$, on the structural parameter,??. Axial distribution of ξ along the centreline and the wall for toothpaste extrusion at 23°C. Incompressible flow with slip at the wall for 2α =45°, L/D_a=20, RR=310*

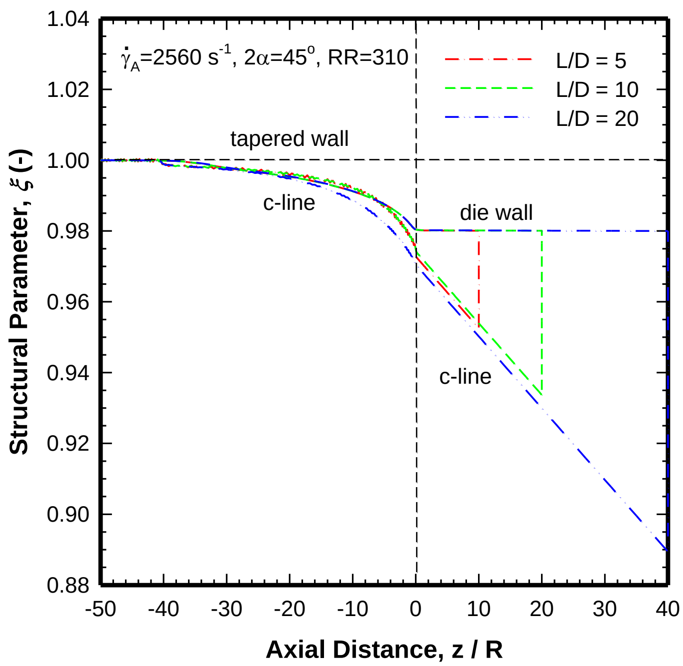

Figure 5.16. *The effect of die length, L/D_a, on the structural parameter,??. Axial distribution of ξ along the centreline and the wall for toothpaste extrusion at 23°C. Incompressible flow with slip at the wall for $\dot{\gamma}_A$ =2560 s^{-1}, 2α =45°, RR=310*

5.5.4. Comparison with Experiments

As mentioned in the experimental part, experiments were performed in capillary dies of different designs (see Table 5.1). The simulations have been carried out for all dies and shear rates and below they are compared with experimental results.

The first geometrical property studied is L/D_a, while $2\alpha = 45°$ and $RR = 311$ are kept constant. Because of the smaller diameter of the die land compared to the die entrance, it is assumed that the main pressure drop occurs in the die land. Figure 5.17 shows the extrusion pressure for three different L/D_a ratios of 0, 10, and 20 (note here that D_a=D). For the case of L/D_a = 0, we have used in the simulations a small value L/D_a = 0.2. For the other L/D_a ratios, a linear relation between L/D_a and pressure drop is expected. However, as illustrated in Figure 5.17, the pressure drop for L/D_a = 20 is much greater than the pressure drop for L/D_a =10. The origin of this phenomenon could be the formation of an unyielded area inside the die land, which grows because of structural formation as the material relaxes through the die land. The growth of the unyielded area increases the shear rate inside the yielded area. Therefore, the shear rate increases along the die land wall and causes higher shear stresses.

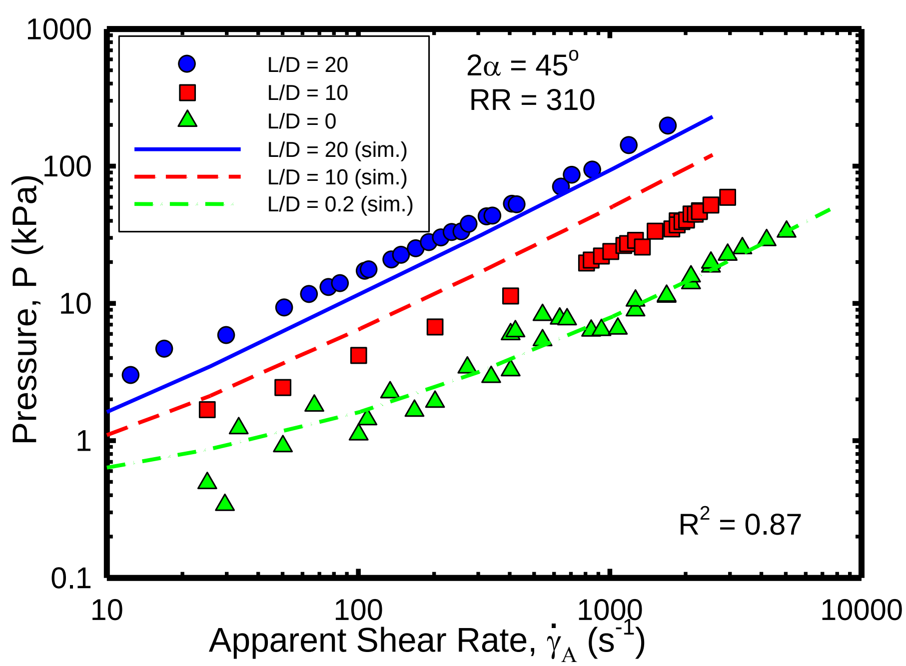

Figure 5.17. *Effect of L/D_a on extrusion pressure*

The numerical simulations with the structural parameter model show that the general trends are captured by the model, although quantitatively the L/D_a = 10 results are over-predicted. The simulations show that doubling the die length leads to doubling the pressure in the system, while experimentally there is a quadrupling effect!

The second geometrical property studied is *RR*, while 2α = 45° and L/D_a = 20 are kept constant. Typically the material would tolerate higher shear rates through the conical zone when the geometry has a high reduction ratio. As it can be seen in Figure 5.18, the pressure drop is almost the same for the two lower reduction ratios of 45 and 139, and slightly lower for the highest reduction ratio of 311. This can be explained by a greater structure break-down for this case, which results in a lower apparent viscosity. The numerical simulations are in general agreement with these findings but they distinguish more clearly among the three cases. Thus the model can adequately take into account the effect of *RR* on toothpaste extrusion.

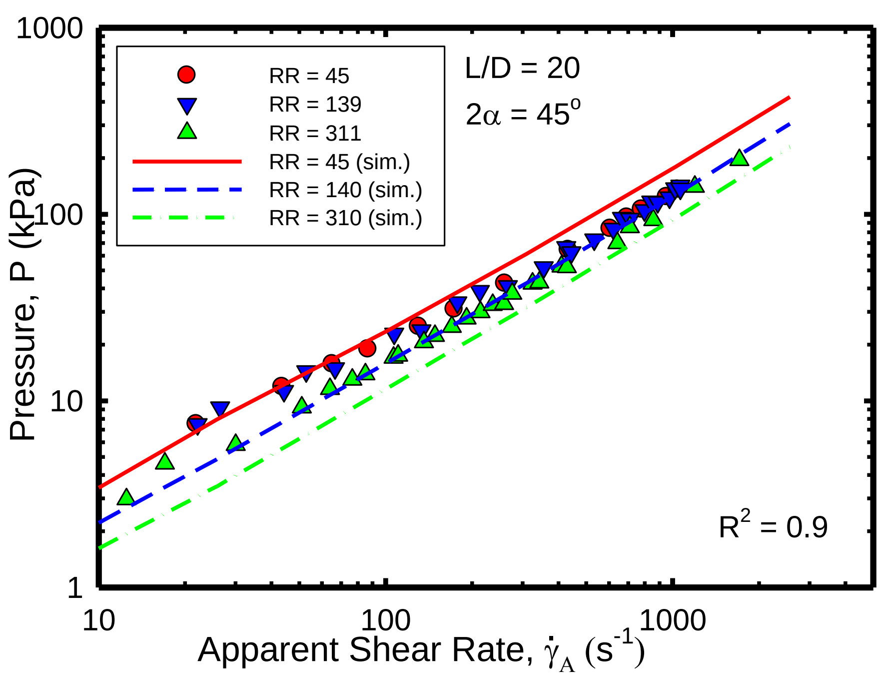

Figure 5.18. *Effect of reduction ratio RR on extrusion pressure*

The third geometrical property studied is 2α, while RR= 311 and L/D_a = 20 are kept constant. The extrusion pressure could be affected by the die entrance angle. Since most of the pressure drop occurs in the die land, and the pressure drop in the conical zone is almost negligible, it is hard to detect the effect of die contraction angle on the pressure drop. However, Figure 5.19 shows that for lower contraction angles, the extrusion pressure is slightly higher due to an increased effect of shear. In the case of polymer melts, it has been observed that the extrusion pressure is independent of the die entrance angle for angles greater than about 30^o. The same conclusion can be made for thixotropic toothpaste.

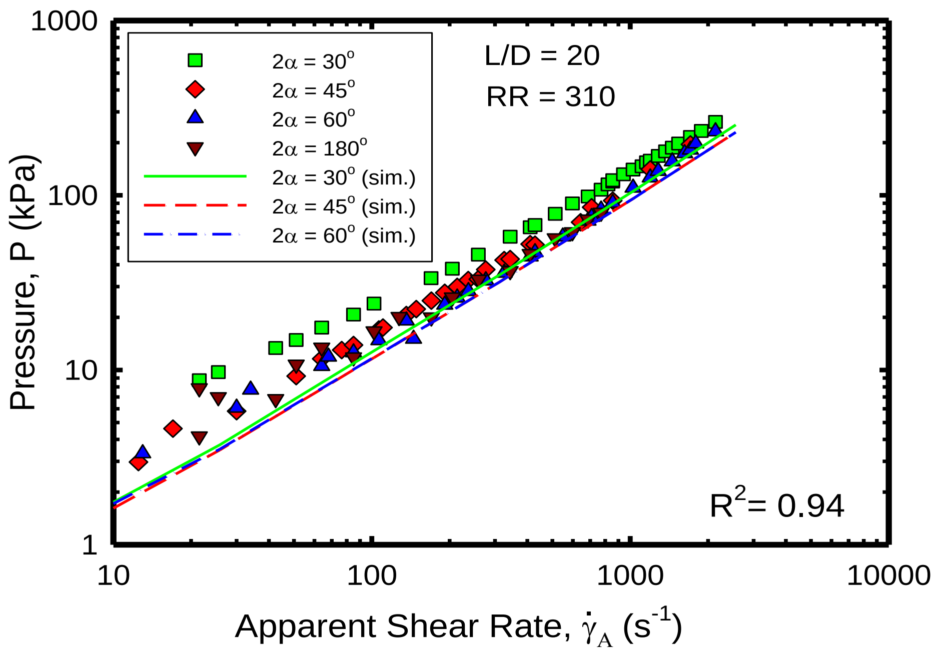

Figure 5.19. *Effect of contraction angle 2α on extrusion pressure*

The numerical simulations, in general, corroborate these findings as they show that for all cases the pressure drop is more or less the same, except for the lower angle of 30°, where the results are slightly higher. Thus the model underestimates the pressures for the lower angles, but can differentiate the effect of the contraction angle 2α on toothpaste extrusion.

5.6. Summary

Experiments and simulations were performed for a commercial toothpaste. The experiments showed the existence of a yield stress and time-dependent phenomena associated with thixotropy, hence structure. Severe slip at the wall was found to occur in capillary flow with different die designs. A simple thixotropic model was formulated and the parameters of the model were found by matching experimental data. The model accounts for yield stress and structure through a kinetic-type convective-transport equation.

Simulations based on the proposed model for capillary flow showed that the rheological model essentially captures the pressure drop in the system for the majority of the cases investigated. The simulations were found to provide details about structure evolution in the die and show that due to slip and fast flows, structure breakdown is not strong. Some discrepancies between theory and experiments may be attributed to possible viscoelastic effects not accounted for in the model.

6. Polytetrafluoroethylene (PTFE) Paste Rheology and Extrusion

6.1. Introduction to PTFE Paste Rheology and Extrusion Process

Polytetrafluoroethylene (PTFE) is a highly crystalline polymer with a high melting temperature of approximately 342^{o}C. It is not possible to process PTFE using conventional polymer melt processes due to this high melting temperature and melt viscosity (Sperati, 1989). Instead, techniques involving cold pressing, cold extrusion in the form of paste, and sintering have to be employed. This is possible because PTFE has two transition temperatures at approximately 19^{o}C and 30^{o}C (Blanchet, 1997). Below 19^{o}C, shearing will cause PTFE crystals to slide past each other, retaining their identity. However, above 19^{o}C, shearing will cause the unwinding of crystallites, creating fibrils interconnecting most of the PTFE particles in the flow direction (Mazur, 1995; Ebnesajjad, 2000; Ariawan et al., 2001; 2002a; 2002b). At temperatures greater than 30^{o}C, a higher degree of fibrillation can be achieved, which also depends on the surface tension and viscosity of the lubricant used (Ariawan et al., 2002b; Ochoa et al., 2004; 2005; 2006). This behaviour is shown in Figure 6.1 in two SEM micrographs obtained before extrusion (Figure 6.1a) and after extrusion (Figure 6.1b). The creation of fibrils is clear.

In PTFE paste extrusion, fine powder resin of individual primary particle diameter of approximately 0.2 μm is first mixed with a lubricating liquid (lube) at concentrations from 16 to 25% to form a paste (Mazur, 1995; Ochoa et al., 2004; 2005; 2006). The paste is then compacted at a typical pressure of 1-2 MPa to produce a preform that is nearly free of air void (Ariawan et al., 2001; Ochoa et al., 2004). The next step involves the extrusion of the preform using a ram extruder at a temperature slightly higher than 30^{o}C and a die, which typically includes a contraction, i.e., a cylindrical die whose surface is reduced by a factor known as the reduction ratio (Ebnesajjad, 2000). During flow in the contraction region, PTFE particles are squeezed under high pressure, and crystallites across the interface are mechanically interlocked and subsequently unwound to produce fibrils (Hatzikiriakos, 2012).

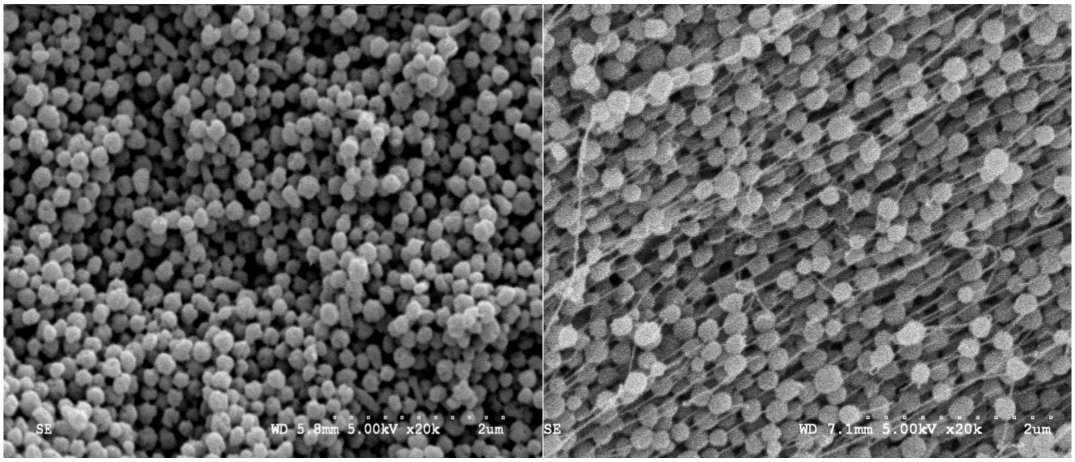

(a) (b)

Figure 6.1. *Typical SEM images of PTFE paste: (a) before extrusion, and (b) after extrusion using a capillary die having length-to-diameter ratio of L/D_a=19, reduction ratio (ratio of cross section of the barrel to that of die exit) RR=310, and contraction angle of $2\alpha = 45^o$ at $T = 55^oC$*

Modeling efforts to describe adequately the flow of paste through a typical cylindrical die including a contraction are hampered by a number of unknown important parameters. First, a lack of appropriate constitutive rheological relations, which is the case for most pastes (Bridgwater, 1989; Benbow et al., 1989; Benbow and Bridgwater, 1993; Ariawan et al., 2002b; Wilson and Rough, 2012). As PTFE paste flows through tapered dies, fibrillation is occurring continuously, and this changes the rheology of the paste increasing the flow complexity and making difficult the rheological characterization.

A simple approach is to use a rheological law that represents the PTFE paste average behaviour through the whole flow domain. In such cases, analytical expressions can be derived for the extrusion pressure (Snelling and Lontz, 1960; Benbow et al., 1989; Benbow and Bridgwater, 1993; Ariawan et al., 2002b; Cheyne et al., 2005; Patil et al., 2006b). Although these models give no information on the microstructure development of the material, nevertheless they are very helpful for scale-up purposes as they assess the physical mechanisms involved in the complex problem of PTFE paste flow. Another unknown significant parameter is slip at the wall. Since flow is lubricated, significant slip occurs at the wall and this should be taken into account.

Previous studies have shown that fibrillation occurs in the contraction zone of an extrusion die with characteristic dimensions of D_b (barrel diameter), D_a (die diameter), length-to-diameter or aspect ratio (L/D_a) and contraction angle (2α) (Ariawan et al., 2001). A mechanism for fibrillation has also been proposed and is shown schematically in Figure 6.2 (Ariawan et al., 2002b). The compacted resin particles entering the die contraction zone are highly compressed due to the reduction in the flow cross-sectional area. This results into the mechanical interlocking of particles. As connected particles experience an accelerated flow, this causes the mechanically locked crystallites to be consequently unwound, creating fibrils of submicron sizes. For more details see Ariawan et al. (2002a; 2002b).

The extent of fibrillation and the quality of the fibrils formed during paste extrusion are significantly affected by the resin properties, extrusion conditions, and the geometrical characteristics of the extrusion die. These variables consequently affect the final product properties, such as the mechanical strength of unsintered extrudates and calendered tapes, the dielectric breakdown property of wires, and the stretch void index of tubes and hoses (Ebnesajjad, 2000).

In this chapter, we study experimentally the flow behaviour of PTFE fine-powder resins in paste extrusion using three reservoirs of different diameters. This is done for the first time in the literature, and such data are extremely useful to check the suitability and capability of models for scale-up purposes. As it will be demonstrated here, the unique set of experimental data from three different reservoirs, have helped us to modify the model developed by Ariawan et al. (2002b). The resultant simple mathematical model is found to be consistent qualitatively and quantitatively with all experimental observations. Finally, this model is tested and found to be suitable to be used for scale-up of the process of PTFE paste extrusion. We also study the effects of die design and extrusion conditions on the mechanical properties of PTFE paste extrudates, and relate them to the quantity and quality of the fibrils formed during the extrusion. A new simple phenomenological model is also derived for the fibrillation, and its relation to mechanical properties (tensile strength) is studied in detail.

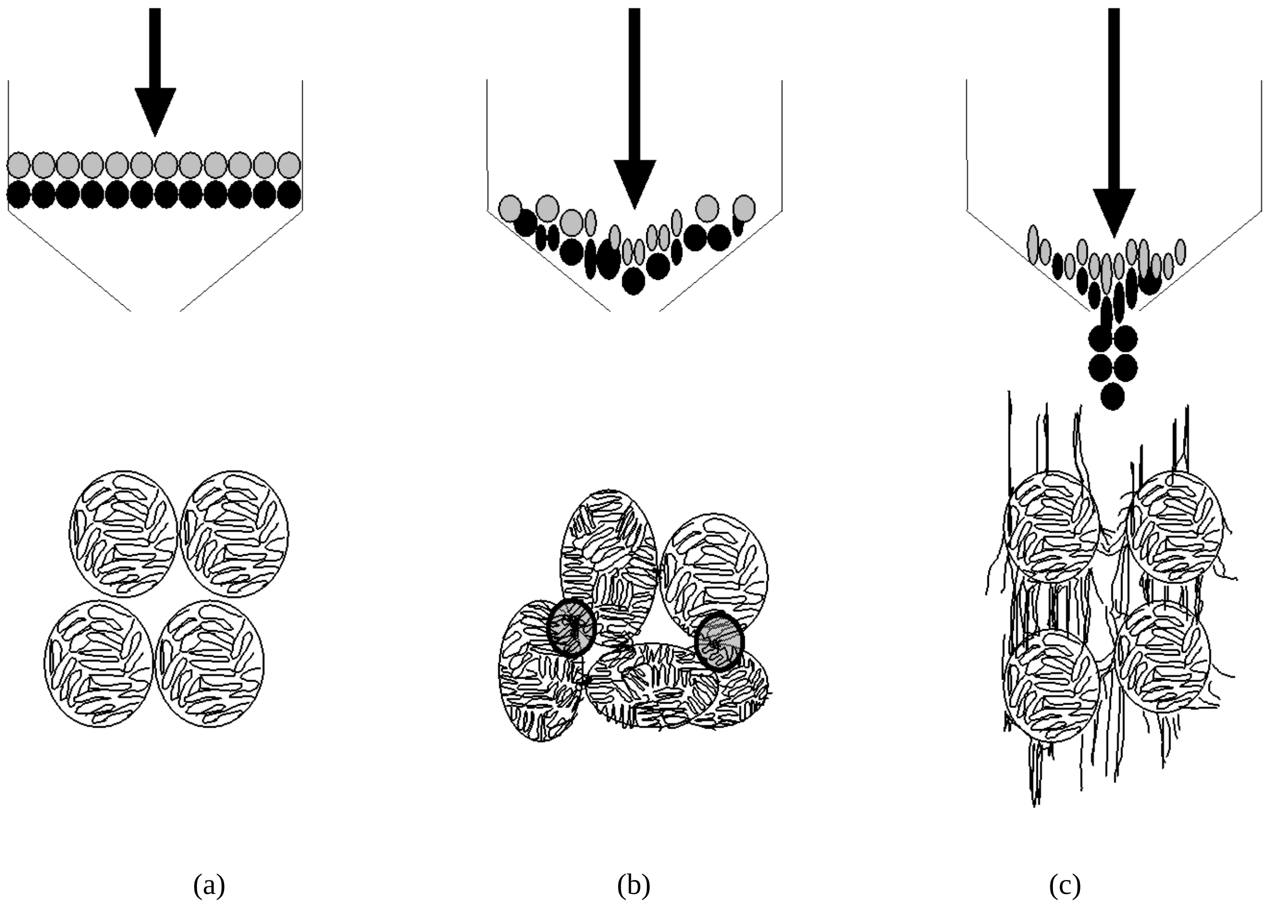

Figure 6.2*. Schematic diagram illustrating the proposed mechanism for fibrillation: (a) compacted resin particles enter the die conical zone, (b) resin particles are highly compressed and in contact with one another in the die conical zone, resulting in the mechanical locking of crystallites, (c) upon exiting the die, particles return to their original spherical shape, and entangled crystallites are unwound, creating fibrils that connect the particles*

6.2. Flow Model of PTFE Paste

Snelling and Lontz (1960) first derived an equation for PTFE paste flow to describe the effects of die design and extrusion speed based on the "radial flow" hypothesis (explained below in detail). However, this model does not take into account the frictional force, which becomes important when tapered dies of small entrance angle are used. Also, the analysis provided by these authors does not account for the pressure drop along the capillary length of the die that follows the entrance (contraction) region. Ariawan et al. (2002a) have proposed a viscoplastic model based on their previous experimental work (Ariawan et al., 2001; 2001a; 2001b) to predict the dependence of extrusion pressure on die geometrical parameters for rod extrusion. This approximate model captured the non-monotonic dependence of extrusion pressure on die entrance angle (critical testing of models for PTFE) and other geometrical characteristics of the cylindrical die. Similar to Snelling and Lontz (1960) model, its derivation is based on the "radial flow" hypothesis for flow through a tapered die (Figure 2.13), whose validity has been demonstrated experimentally (Ariawan et al., 2002a; 2002b) and numerically (Patil et al., 2006a).

Important die geometrical characteristics that play a significant role in the PTFE paste extrusion include: the die diameter, D_a, the reduction ratio, RR, defined as the ratio of initial to final cross sectional areas ($RR \equiv D_b^2 / D_a{}^2$), the contraction angle, 2α, and the length-to-diameter ratio, L/D_a (see Figure 6.3b). According to "radial flow" hypothesis all points located on virtual spherical surfaces of a constant radius r from the die apex have the same radial velocity (Binding, 1991). This also implies that PTFE paste slips massively on the die walls with a similar radial velocity. The mathematical form of the "radial flow" hypothesis for a cylindrical die (Figure 2.13a) can be written as:

$$\frac{dr}{dt} = -\frac{Q}{2\pi(1-\cos\alpha)r^2}, \tag{6.1}$$

where Q is the volumetric flow rate and r is the distance from the die apex. Based on this hypothesis, the kinematics of PTFE flow can be calculated independent of any rheological constitutive law at a given volumetric flow rate. Then assuming a simple constitutive rheological law, analytical models for the pressure drop can be derived.

Although these models (Snelling and Lontz, 1960; Ariawan et al., 2002b) do not explicitly predict micromechanical details of the extrudates (fibrillation), they explicitly predict the extrusion pressure very well and therefore are useful in die design, particularly the latest models proposed by Ariawan et al. (2002a) and Patil et al. (2006b). These models have considered an elasto-plastic and viscous contribution to stress, essentially a modified Kelvin stress-strain relation with an added power-law viscous term (Goh et al., 2004; Hoffman and Sachs, 1953; Ludwik, 1909). The stress expression can be written as:

$$\sigma = C\gamma^n + K\dot{\gamma}^m, \tag{6.2}$$

where σ is the shear stress, C is a consistency constant, γ is the shear strain, $\dot{\gamma}$ is the shear rate, K is the consistency index, and n and m are power-law exponents.

Ariawan et al. (2002b) assumed that slip on the die wall can be modeled by including a Coulombic friction coefficient. Based on Eq. (6.1) and the "radial flow" hypothesis, they derived the following equation for the extrusion pressure through a cylindrical die with geometric characteristics depicted in Figure 2.13:

$$P_{extrusion} = \sigma_{rb} = \sigma_{ra}(RR)^B + 2(1+B)\left\{ C\left(\frac{D_b}{2\sin\alpha}\right)^{2B} \int_{r_a=\frac{D_b}{2\sqrt{RR}\sin\alpha}}^{r_b=\frac{D_b}{2\sin\alpha}} \frac{\left(3\ln\left(r_b/r\right)\right)^n}{r^{2B+1}}\,dr + \right.$$

$$\left. \frac{K}{(3m+2B)}\left(\frac{12Q\sin^3\alpha}{\pi(1-\cos\alpha)D_b^3}\right)^m \left((RR)^{B+3m/2}-1\right)\right\}, \tag{6.3}$$

where

$$\sigma_{ra} = \sigma_{zo} = \sigma_{oa}\left(e^{-4f\,L/D_a}-1\right) + \sigma_{zL}e^{-4f\,L/D_a} \tag{6.4}$$

and

$$-\sigma_{oa} = C\left(\frac{3}{2}\ln\left(RR\right)\right)^{n} + K\left(\frac{12Q\sin^{3}\alpha(RR)^{3/2}}{\pi\left(1-\cos\alpha\right)D_{b}^{\;3}}\right)^{m}, \tag{6.5}$$

where f is a Coulombic friction coefficient, $B = f\sin\alpha/[2(1-\cos\alpha)]$ and σ_{zL} is the shear stress imposed at the die exit, which is negligible or zero. Consideration of friction on the wall allows this model to predict a minimum pressure at a specified contraction angle 2α at a given reduction ratio, die diameter, and apparent shear rate. This minimum seems to depend on the particular PTFE and can be from 15^{o} to 45^{o} (Ariawan et al., 2002b; Ochoa et al., 2005). Although this model captures the minimum angle for the pressure drop, it cannot predict correctly the rate of increase in the extrusion pressure with an increase of the contraction angle after the minimum.

An objective of the present work is to use a simple modification that overcomes this deficiency. Because the derivation of the model was performed in terms of spherical coordinates (in spite of the fact that the flow domain is cylindrical), integration of the force balance to calculate the extrusion does not include the spherical section at the exit of the die, and this is due to the consideration of spherical coordinates (Figure 2.13a). In other words, the pressure drop is calculated by summing the pressure drop in the die land of length *L* (Figure 2.13b) and in the conical part before the entrance to the die. Using the 'radial flow' hypothesis, the pressure drop in the conical zone can be evaluated between the two virtual surfaces (Figure 2.13a), which leaves a spherical section at the exit of the conical part out of the integration, which turns out to be significant.

Ariawan et al. (2002b) have set the virtual surface at the exit at a distance of ½$D_a$sin*a* from the die apex. As a result of this approximation, the area between this virtual surface and the flat die entry is left out from the pressure drop calculation. For low contraction angles, this area is small and it can be neglected. However, as the contraction angle increases, this area becomes larger and the approximation is not valid anymore. By changing the limits of integration this section can be taken into account approximately, other things remaining the same. The modified expression for the pressure drop in the conical part can be written as follows:

$$P_{extrusion} = \sigma_{rb} = \sigma_{ra}(RR)^{B} + 2\left(1+B\right)\left\{ C\left(\frac{D_b}{2\sin\alpha}\right)^{2B} \int_{r_a=\frac{D_b}{2\sqrt{RR}\tan\alpha}}^{r_b=\frac{D_b}{2\sin\alpha}} \frac{\left(3\ln\left(r_b/r\right)\right)^{n}}{r^{2B+1}}\,dr + \right.$$

$$\left. \frac{K}{\left(3m+2B\right)}\left(\frac{12Q\tan^{3}\alpha}{\pi\left(1-\cos\alpha\right)D_b^{3}}\right)^{m}\left((RR)^{B+3m/2}-1\right)\right\}, \tag{6.6}$$

The definitions of all parameters in Eq. (6.6) are the same as in Eqs. (6.3)-(6.5). The only difference between Eqs. (6.3) and (6.6) is in the lower limit of the integral, which essentially replaces $\sin\alpha$ with $\tan\alpha$. The error for small contraction angles is negligible as $\tan\alpha$ and $\sin\alpha$ become approximately equal. However, the error by neglecting a conical part at the exit is more significant at higher contraction angles. Although this modification does not correct the problem completely as it is another approximation itself, however it provides an expression that gives more consistent results over the previous proposed models (Ariawan et al., 2002b; Patil et al., 2006b) and it can be used for scale-up as will be shown in this work. Using the experimental data obtained from the reservoir having the smallest diameter, the parameters of the model (Eq. 6.6) were calculated to best describe the experimental data. Table 6.1 lists these values at different temperatures.

Table 6.1. *Model parameters for different temperatures*

Temperature (^{o}C)	*C* (Pa)	*n*	*K* (Pa·s^{m})	*m*	*f*
25	111.6	5.43	70049	0.56	0.015
35	101.7	5.43	73534	0.56	0.017
45	96.9	5.43	84937	0.56	0.013

Figure 6.3 illustrates the differences between the two models for one case. The present model and the Ariawan model (Ariawan et al., 2002b) give identical results at contraction angles up to about 20^{o}. The present model describes also very well the data for contraction angles greater than 20^{o}, while the Ariawan model does not exhibit the significant upturn of the experimental extrusion pressure with a further increase of the

contraction angle, which is a characteristic of PTFE paste flow behaviour due to significant fibrillation. Significantly, the paste model developed by Bridgwater (1989) exhibits a similar deficiency.

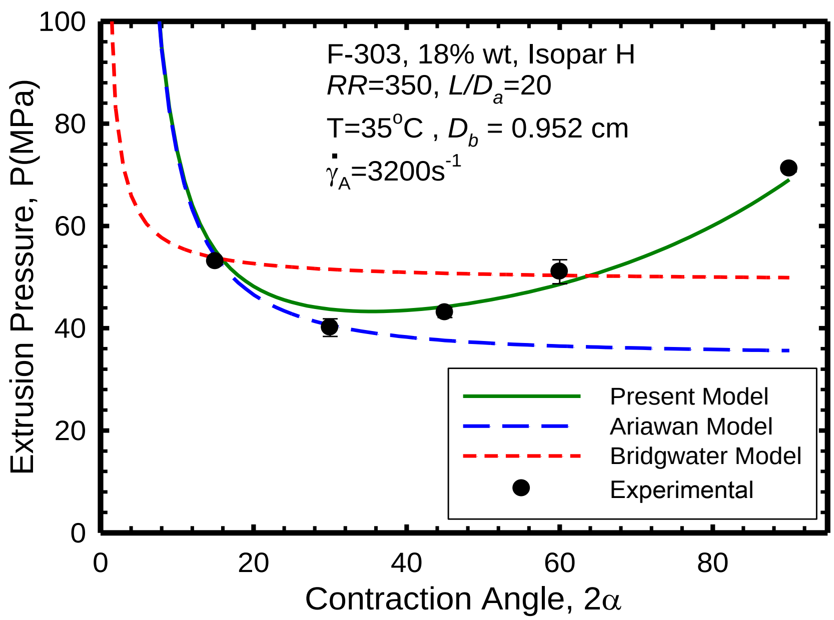

Figure 6.3. *Comparison of three paste models in predicting the extrusion pressure of PTFE paste as a function of contraction angle*

6.3. Fibrillation Model

Due to the fibril formation during the extrusion process, PTFE extrudates have solid-like properties. It has been reported that the tensile strength of the final product is a function of many parameters such as flow rate, die geometrical parameters of the die, temperature, lubricant concentration, among others (Ariawan et al., 2001; 2002a; 2002b; Ochoa and Hatzikiriakos, 2004; 2005). Certainly the tensile strength is related to the degree and quality of fibrils interconnecting the various particles (Figure 6.1). Therefore, a model predicting the degree of fibrillation can be used to correlate the predicted degree of fibrillation with the tensile strength of the extrudates. This is the main hypothesis and thus the main objective of the present work as discussed above.

Formation and destruction of the material structure due to flow in complex fluids has been studied extensively in the literature. In many cases, the structural build-up has been attributed to Brownian motion, which essentially results in weak structures (Coussot, 2005). Pinder (1964) and Coussot et al. (2002) suggested that the rate of structure build-up is always constant for various pasty materials. A few researchers also consider shear-induced structure build-up in suspensions and colloidal systems (Worral and Tuliani, 1964; Lee and Brodkey, 1971; Dullaert and Mewis, 2005). Patil et al. (2006a) suggested that the rate of fibril formation and breakage in PTFE paste flow can be described as a function of the deformation history exerted on the material.

In the present work due to the semi-solid behaviour of PTFE paste, it is assumed that the rate of fibril formation is proportional to the elastic energy, which is stored in the PTFE paste as it is being deformed during flow. It can be assumed that this elastic energy is a function of the Hencky strain, ε, an elongational quantity. As argued above, squeezing of the particles and subsequent acceleration can cause unwinding of mechanically interlocked crystallites to form fibrils. Therefore, a kinetic model that describes phenomenologically this structure formation can be written as:

$$\frac{d\xi}{dt} = A\varepsilon^{M}(1-\xi)\,, \tag{6.7}$$

where ξ is a structural parameter, which represents the percentage of PTFE particles interconnected with fibrils (degree of fibrillation), $0 \le \xi \le 1$, and A and M are constants.

Previous experimental reports have shown that PTFE flow through the conical part of the die is very similar to radial flow (Snelling and Lontz, 1960; Ariawan et al., 2002a). Based on the “radial-flow” hypothesis (Eq. 6.1), the flow parameters, such as strain and strain rate, can be calculated anywhere in the flow. In this case, the Hencky strain is the relevant quantity of interest and it can be expressed by:

$$\varepsilon = 3\ln\left(\frac{r_b}{r}\right), \tag{6.8}$$

where r_b is the distance at the die entrance from the die apex. Equation (6.8) shows the rate of change of the structural parameter in time. The time derivative of ξ can be written as:

$$\frac{d\xi}{dt} = \frac{d\xi}{dr}\frac{dr}{dt}. \tag{6.9}$$

having Eq. (6.1), we obtain:

$$\frac{dt}{dr} = -\frac{2\pi(1-\cos\alpha)r^2}{Q}. \tag{6.10}$$

Combining Eqs. (6.7) and (6.8), the following equation can be derived:

$$\frac{d\xi}{dr} = -\left[A\left\{3\ln\left(\frac{r_b}{r}\right)\right\}^M\right](1-\xi)\frac{2\pi(1-\cos\alpha)r^2}{Q}. \tag{6.11}$$

It can be assumed that the ultimate tensile strength should be related with the degree of fibrillation (Patil et al., 2005). Eq. (6.11) is solved by using MATLAB to calculate the degree of fibrillation as a function of the operating conditions and the geometrical characteristics of the capillary dies, and it is compared with corresponding experimental observations in terms of tensile strength. Eq. (6.11) is integrated in the domain $\left[r_b/\sin a,\ r_a/\tan a\right]$ or $\left[D_b/2\sin a,\ D_a/2\tan a\right]$, which defines the distance of the entry and exit from the die apex (Figure 6.3) .The value of ξ at the entry is taken equal to zero (no structure). Solving Eq. (6.11) the value of ξ is calculated as a function of the apparent shear rate (through Q) and the geometrical characteristics of the extrusion die (through r_b and α). The constants A and M are calculated such as to provide the best qualitative description of the tensile strength as a function of operating conditions and geometrical characteristics of the dies. As discussed above the degree of fibrillation and tensile strength are proportional to each other, and therefore exact fitting to experimental data is not possible. Best fitted values for those parameters are summarized in Table 6.2.

__Table 6.2.__ Model parameters for fibril formation

T (^oC)	$A(s^{-1})$	M
35	3.4×10^{-7}	15.35

6.4. Results and Discussion

All the reported extrusion pressure data refer to this steady state. Depending on the piston speed and die diameter, an apparent shear rate can be defined by $\dot{\gamma}_A \equiv 32Q/\pi D_a^3$, where Q is the volumetric flow rate defined as $Q \equiv \frac{1}{4} V_p(\pi D_b^2)$, where V_p is the piston velocity.

Experiments were performed by utilizing three different barrels of various diameters, D_b. For each barrel, tapered dies of various diameter, D_a, total tapered (contraction) angle, 2α, length to diameter ratio, L/D_a, and reduction or contraction ratio, $RR=(D_b/D_a)^2$, were used to determine the effects of die design on the extrusion pressure.

6.4.1. Effect of Apparent Shear Rate and Reduction Ratio

Figures 6.4a-c depict the steady-state extrusion pressure as a function of apparent shear rate for several reduction ratios at 25^{o}C, 35^{o}C, and 45^{o}C, respectively. The extrusion pressure generally increases with an increase in the apparent shear rate (volumetric flow rate), due to the increase in the viscous resistance of the paste. At low extrusion speeds, the residence time of the paste in the barrel and the die becomes sufficiently long to allow lubricant to redistribute itself non-uniformly in the paste matrix. Due to this non-uniformity, part of the lubricant is extruded early, and this results into a higher steady-state extrusion pressure. This explains the initial reduction in the extrusion pressure at low extrusion rates. In addition it can be seen that the extrusion pressure increases more and more (more nonlinearly and with a higher rate) with increasing reduction ratio. Similar results were obtained from the two other barrels of larger size (presented below).

As the temperature increases from $25^{o}C$ to $35^{o}C$ (the two transition temperatures are $19^{o}C$ and $30^{o}C$, which facilitate fibrillation), the extrusion pressure and the degree of fibrillation increase accordingly, which could have resulted in a higher extrusion pressure. However, at the same time better lubrication (lower lubricant viscosity) reduces the extrusion pressure. These two competing effects make the effect of temperature on the extrusion pressure negligible, although the extrusion pressure at high shear rates is increased slightly. A further increase of temperature to $45^{o}C$ shows again a mild increase in pressure due to an increase in fibrillation. Similar results have been reported by Ochoa et al. (2006).

It has been observed by previous authors (Ochoa et al., 2006; Patil et al., 2006a) that a decrease in the apparent shear rate results in an increase in the tensile strength of the PTFE extrudates. Extruding PTFE paste at lower shear rates allows more time for the PTFE particles to form fibrils, which are extended relatively slowly (thus avoiding breakage), and consequently this results into a higher tensile strength.

Figure 6.5 depicts the effects of the apparent shear rate on the extrusion pressure and tensile strength of the extrudates for three different dies having different contraction angles. The tensile strength shows a different trend and decreases with an increase in the apparent shear rate. The model predictions in terms of degree of fibrillation (Eq. 6.11) are consistent when compared with the experimental data in terms of tensile strength (as explained before, the tensile strength should be proportional to the degree of fibrillation).

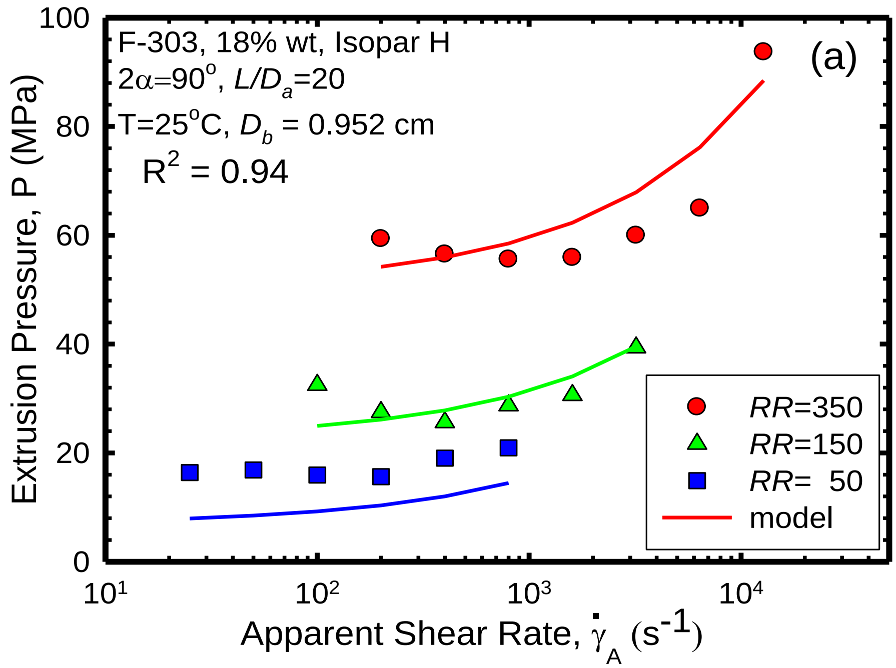
F-303, 18% wt, Isopar H
2α=90°, L/Da=20
T=25°C, Db = 0.952 cm
R2 = 0.94
(a)
RR=350
RR=150
RR= 50
model
Extrusion Pressure, P (MPa)
Apparent Shear Rate, γA (s-1)
0
20
40
60
80
100
101
102
103
104

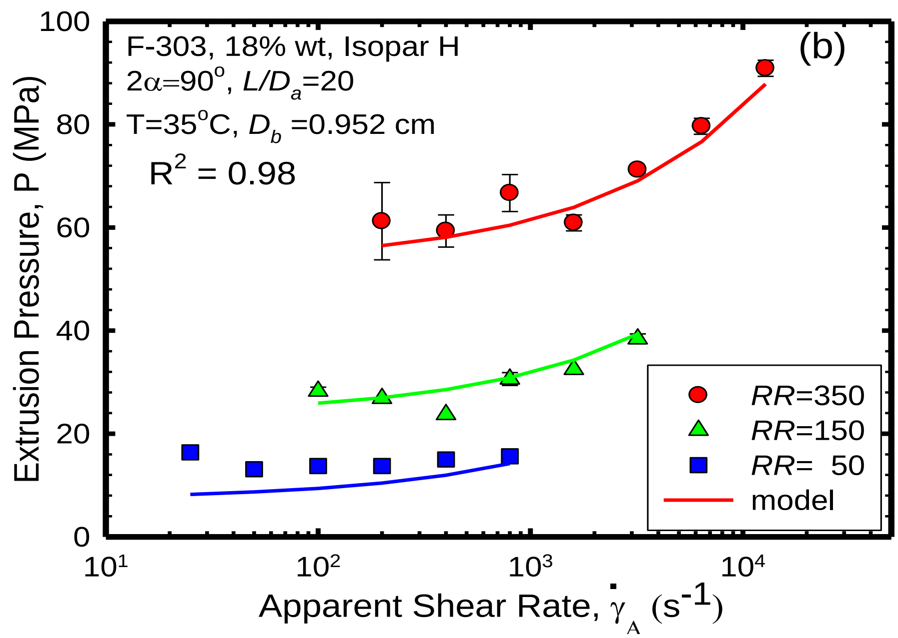
F-303, 18% wt, Isopar H
2α=90°, L/Da=20
T=35°C, Db =0.952 cm
R2 = 0.98
(b)
RR=350
RR=150
RR= 50
model
Extrusion Pressure, P (MPa)
Apparent Shear Rate, γA (s-1)
0
20
40
60
80
100
101
102
103
104

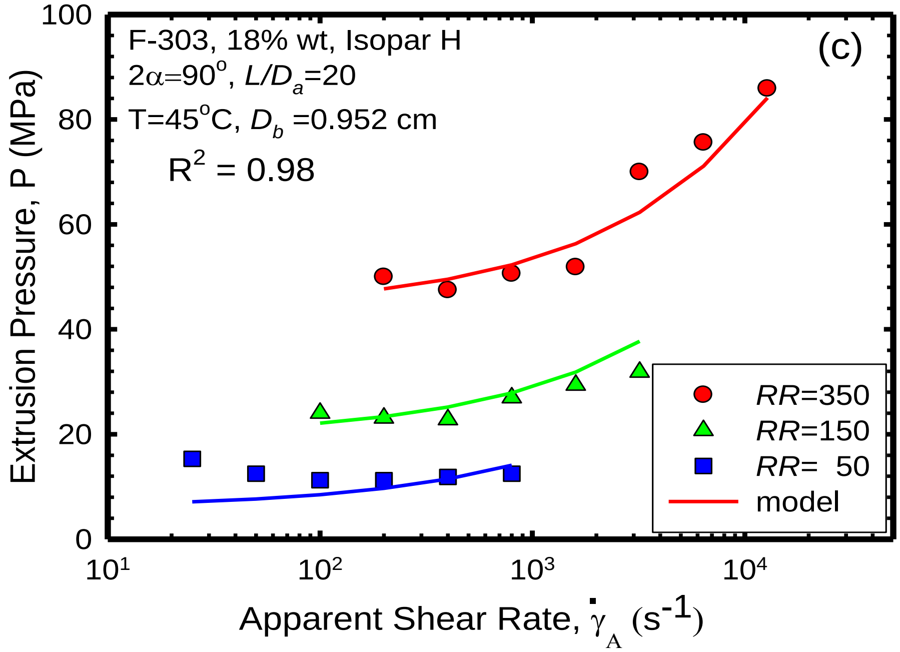

Figure 6.4. *The effect of apparent shear rate and reduction ratio on the steady-state extrusion pressure of PTFE paste: (a) at 25°C, (b) at 35°C, (c) at 45°C. Solid lines are model predictions (Eq. 6.6) with fitted parameters listed in Table 6.1*

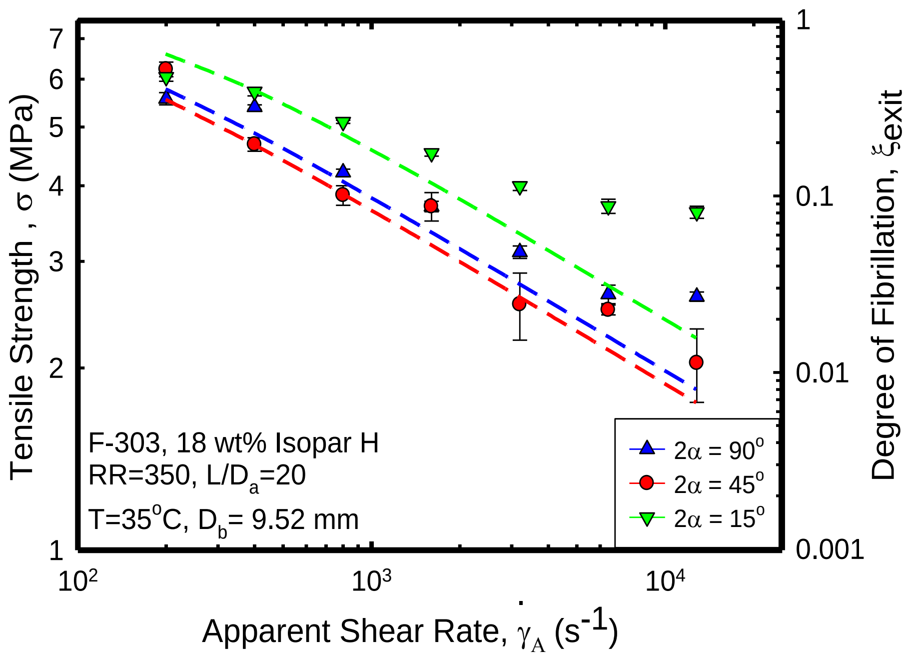

Figure 6.5*. The effect of apparent shear rate on tensile strength and fibrillation as predicted by Eq. (6.11) for a die with D_b=9.52 mm, D_a=0.508 mm, and L/D_a=20*

The extrusion pressure increases with an increase in reduction ratio in a nonlinear fashion (Ochoa et al., 2006, Patil et al., 2006b, Ardakani et al., 2012). A similar trend has been observed for the tensile strength of the PTFE paste extrudates. Figure 6.7 illustrates the effect of reduction ratio on the extrusion pressure and the mechanical properties of the PTFE extrudates for three different reduction ratios and different apparent shear rates.

Fibril formation during the process is a function of two main factors: extrusion time (residence time) and elastic deformation. At similar apparent shear rates, it takes a longer time for PTFE paste to be extruded through a die with a high reduction ratio. Furthermore, the deformation (average strain) of the paste is proportional to the logarithm of reduction ratio (see Eq. 6.8). Since the main source of the fibrillation is the stored elastic energy, a higher fibrillation occurs during extrusion at higher reduction ratios, which explains the trends found in Figure 6.6.

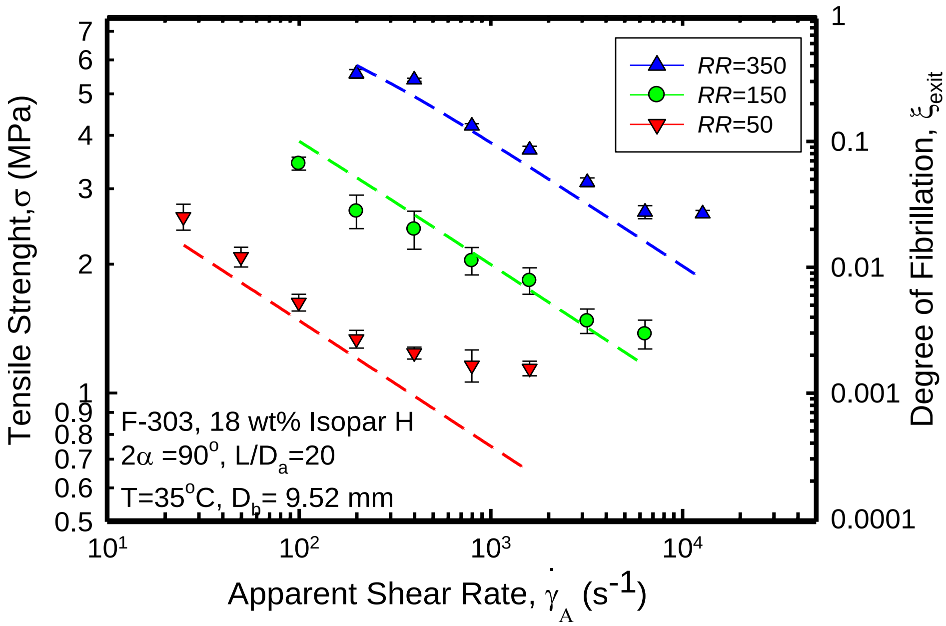

***Figure 6.6**. The effect of reduction ratio on tensile strength and fibrillation as predicted by Eq. (6.11) for a die with D_b=9.52 mm, 2α=90°, and L/D_a=20. Symbols represent experimental tensile strength data and the continuous lines represent the degree of fibrillation calculated by Eq. (6.11)*

Figure 6.7 shows SEM micrographs for three extrudates at similar apparent shear rates and different reduction ratios. At higher reduction ratios many fibrils have been formed, and most PTFE particles are connected to each other. On the other hand, at low reduction ratios only a few fibrils have been formed, and the arrangement of the PTFE particles is almost similar to their arrangement before extrusion.

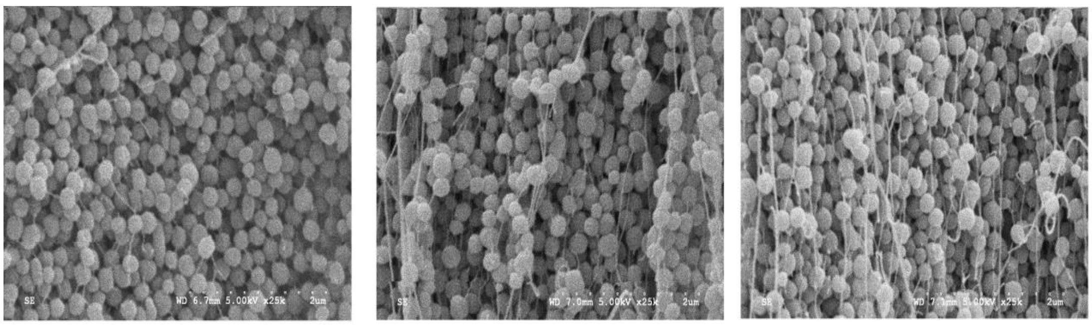

(a) ***(b)*** ***(c)***

Figure 6.7. *SEM images of PTFE paste: (a) RR=45, (b) RR=140, (c) RR=310. For all cases*

L/D_a=20, $\dot{\gamma}_A$ = 1600 s^{-1} and 2α= 90^o at T=35^oC

6.4.2. Effect of Die Entrance Angle

Figures 6.8a-c show the effect of contraction angle on the extrusion pressure at several apparent shear rates and temperatures, namely, 25^oC, 35^oC, and 45^oC, respectively. The extrusion pressure initially decreases, goes through a minimum and then increases, with increasing die entrance angle. The decrease in the extrusion pressure at small increasing entrance angle is similar to the trend predicted for polymer melts and other fluids using the lubrication approximation of Reynolds (Dealy and Wissbrun, 1990; Benbow and Bridgwater, 1993). When the die entrance angle is sufficiently small, paste flow in the die conical zone follows essentially a plug flow (Ariawan et al., 2002b), and the lubrication approximation is valid. However, the lubrication approximation predicts a monotonic decrease in the extrusion pressure with increasing die entrance angle, which is not consistent with the experimental results plotted in Figures 6.8a-c. Beyond a certain entrance angle the extrusion pressure increases with increasing angle 2α, as is commonly observed with the extrusion of elastic soft solids (Horrobin and Nedderman, 1998). The failure of the lubrication approximation is due to the assumed plug flow pattern in the die conical zone that becomes invalid when the entrance angle is large. As discussed before, this can be remedied by considering the "radial flow" hypothesis in the present model. Similar results were obtained from the two other barrels of larger size (presented below).

As temperature increases from 25^{o}C to 45^{o}C, the trend remains almost the same. However the extrusion pressure slightly decreases as also pointed out above. This can be explained by the lower viscosity and higher wettability of the lubricant at higher temperatures, which results in a better lubrication and therefore possibly in a higher degree of fibrillation (Ochoa et al., 2006).

Figure 6.9 shows the effect of contraction angle on the tensile strength for several apparent shear rates at 35^{o}C. Similar trends with extrusion pressure can be observed for the tensile strength of the PTFE extrudate. When the contraction angle is low, at the same apparent shear rate it takes a longer time for the PTFE paste to pass through the conical area. Based on the proposed kinetic equation for the fibril formation (Eq. 6.6), the rate of fibril formation is proportional to the strain. The total strain is almost the same, regardless of the die contraction angle. Therefore, the rate of fibril formation is similar for all the contraction angles. Considering the fact that the most of fibril formation occurs in the conical part of the die, when PTFE paste spends longer time in the conical area, this would increase the amount of fibril formation and at the same time decrease the possibility of fibril breakage that can be caused by fast movement of PTFE particles against each other. Therefore, better mechanical properties can be achieved by extruding PTFE paste through dies with relatively lower contraction angles. On the other hand, as the contraction angle increases, the rate of Hencky strain increases (the total strain remains the same), which possibly breaks some of the formed fibrils, and this consequently results in extrudates with a lower tensile strength.

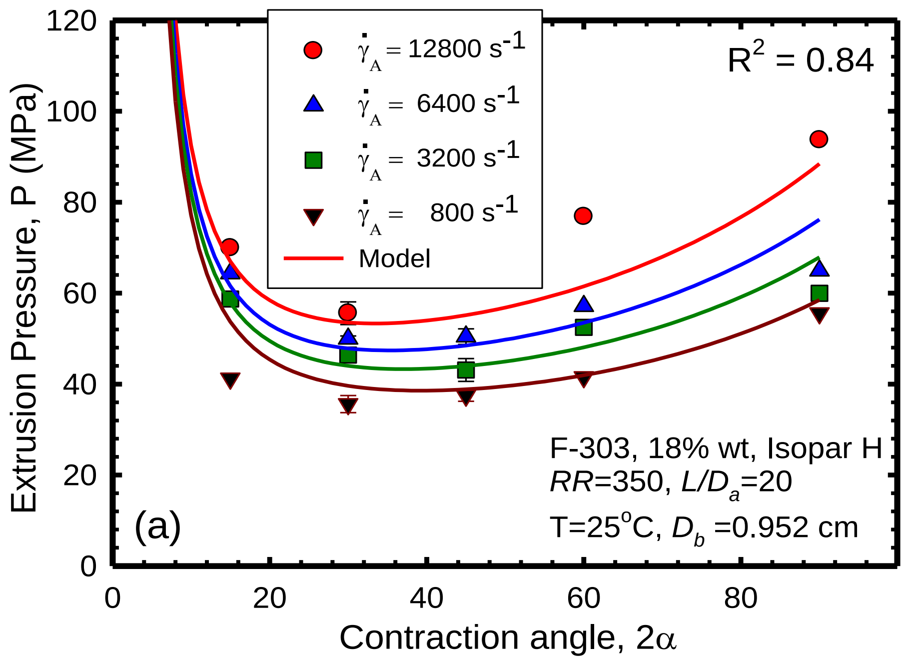

120
100
80
60
40
20
0
0
20
40
60
80
Extrusion Pressure, P (MPa)
Contraction angle, 2α
γ̇A = 12800 s-1
γ̇A = 6400 s-1
γ̇A = 3200 s-1
γ̇A = 800 s-1
Model
R2 = 0.84
F-303, 18% wt, Isopar H
RR=350, L/Da=20
T=25oC, Db =0.952 cm
(a)

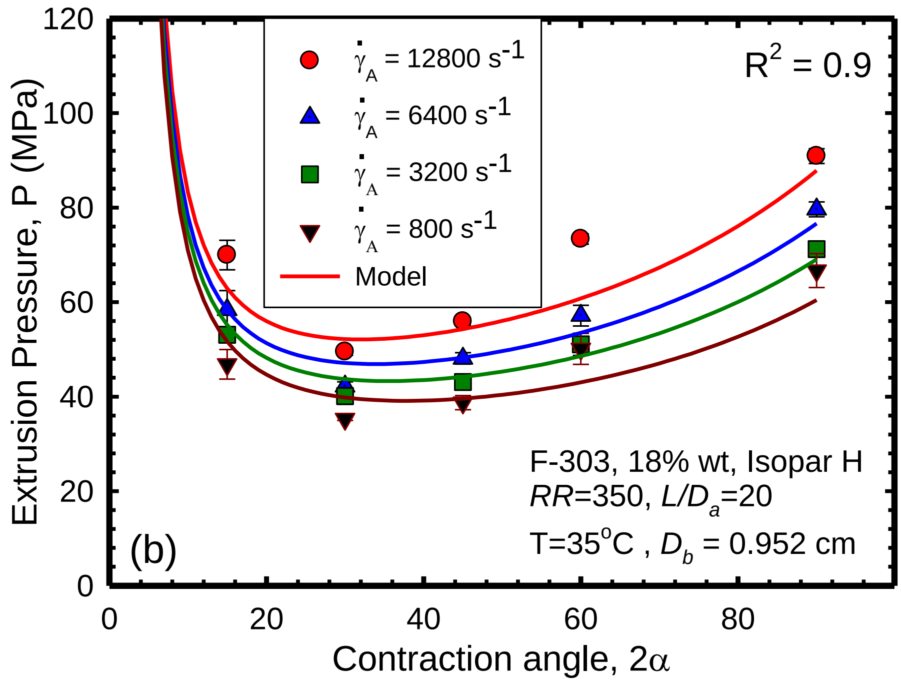

120
100
80
60
40
20
0
0
20
40
60
80
Extrusion Pressure, P (MPa)
Contraction angle, 2α
γ̇A = 12800 s-1
γ̇A = 6400 s-1
γ̇A = 3200 s-1
γ̇A = 800 s-1
Model
R2 = 0.9
F-303, 18% wt, Isopar H
RR=350, L/Da=20
T=35oC , Db = 0.952 cm
(b)

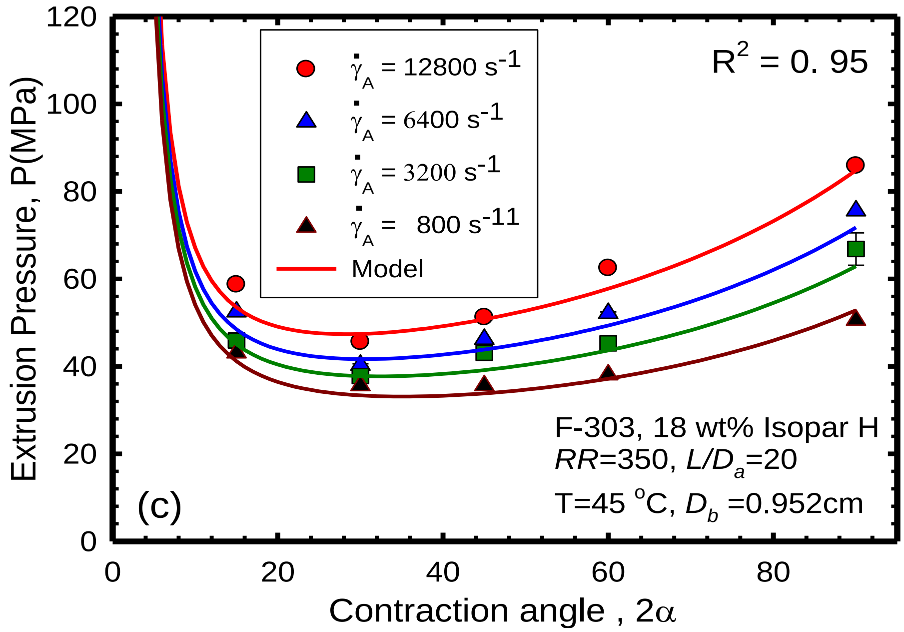

Figure 6.8. *The effect of entrance angle on the steady-state extrusion pressure of PTFE paste: (a) at 25^{o}C, (b) at 35^{o}C, (c) at 45^{o}C. Solid lines are model predictions (Eq. 6.6) with fitted parameters listed in Table 6.1*

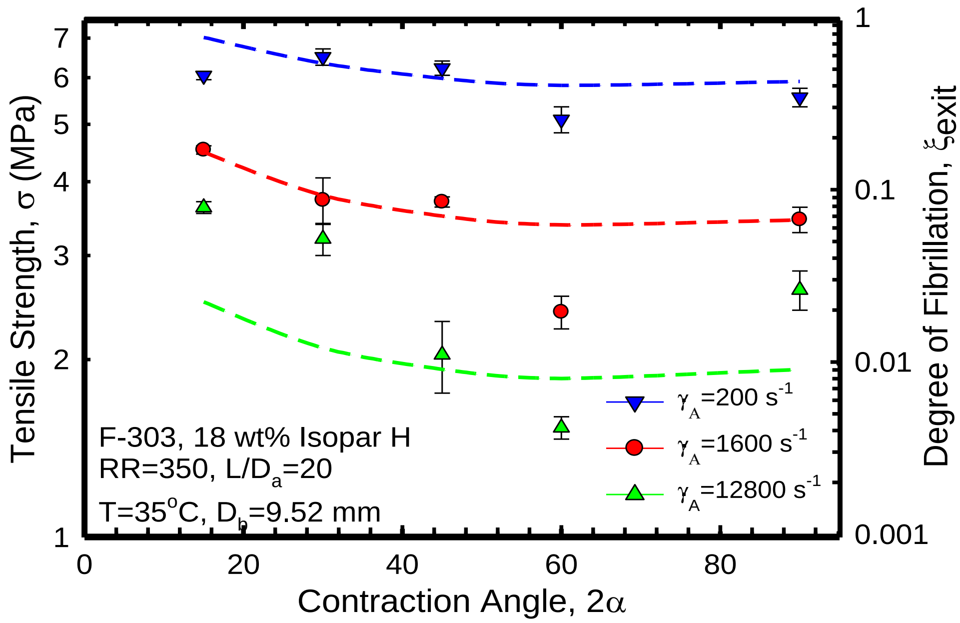

Figure 6.9. *The effect of contraction angle on tensile strength and fibrillation as predicted by Eq. (6.11) for a die with D_b=9.52 mm, D_a=0.508 mm, and L/D_a=20. Symbols represent experimental tensile strength data and the continuous lines represent the degree of fibrillation calculated by Eq. (6.11)*

Figure 6.10 depicts the effect of contraction angle on tensile strength. As discussed above, the tensile strength can be correlated with the degree of fibrillation. Meanwhile, the deformation before breakage is not only a function of the degree of fibrillation but also a function of the fibrils' initial direction. Figure 6.11 shows that as the contraction angle increases, the extrudates exhibit a higher extensibility before breakage. Application of a higher strain results into alignment of fibrils in the stretching direction (extrudates). A higher contraction angle implies a higher stretching rate, and this perhaps causes the breakage of some fibrils and thus the tensile strength drops.

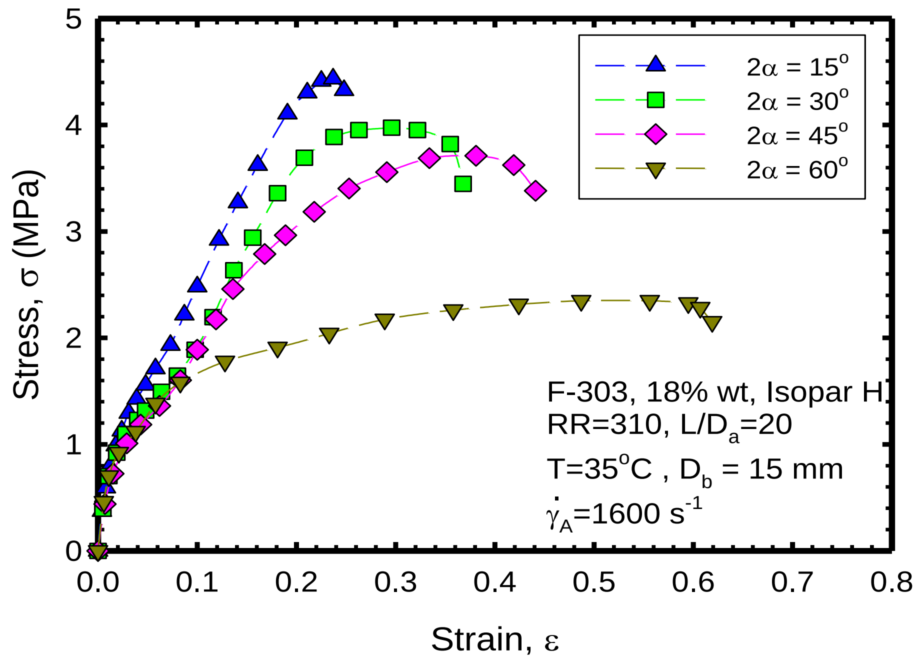

Figure 6.10. *The effect of contraction angle on tensile strength and maximum deformation in dies with D_b=15 mm, D_a=0.85 mm, and L/D_a=20*

6.4.3. Effect of Length-to-Diameter Ratio

Figure 6.11 illustrates the effect of the length-to-diameter ratio, L/D_a, on the extrusion pressure for dies having the same *RR*=350, *2a*=90°, *T*=35°C and various L/D_a.

Now the extrusion pressure increases with increasing L/D_a ratio. This is due to increased levels of frictional losses because more land area is available now for flow.

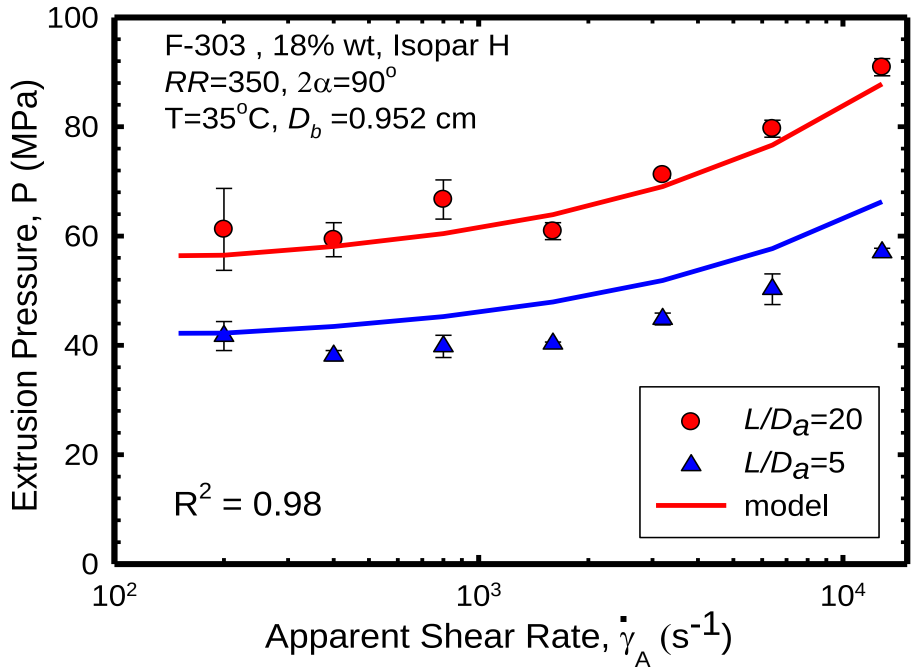

Figure 6.11. *The effect of L/D_a on the steady-state extrusion pressure of PTFE paste at 35°C. Solid lines are model predictions (Eq. 6.6) with fitted parameters listed in Table 6.1*

6.5. Model Predictions

Using the experimental data obtained from the reservoir having the smallest diameter, the parameters of the model (Eq. 6.6) were calculated to best describe the experimental data. Table 6.1 lists these values at different temperatures. The exponents *n* and *m* are the same, while the parameters *C*, *K* and *f* change accordingly with the overall effect to cause a small increase in the extrusion pressure. The model represents the data quite well as can be seen from the continuous lines in Figures 6.4a-c (effect of apparent shear rate and reduction ratio), Figures 6.9a-c (effect of contraction angle) and Figure 6.11 (effect of length-to-diameter ratio).

The values listed in Table 6.2 will now be used to predict the extrusion pressures obtained from the other two reservoirs. This will validate the model and show its consistency with the experimental results. Moreover it would show the capabilities of the model to be used for scale-up purposes. The scale-up is of the order of 7.2, that is the ratio of the areas of the large to smaller reservoir.

Figures 6.12a-b show the effect of different contraction angle on the extrusion pressure for the medium diameter barrel at 25^oC and 35^oC, respectively. The experimental data suggest that the contraction angle has a similar effect on the extrusion pressure as seen in the case of the smaller barrel. The model predictions are very good at 25^oC, while at 35^oC the model overpredicts the extrusion pressure up to about 30%.

Generally speaking, higher reduction ratios result in higher extrusion pressures as was seen in Figures 6.4a-c. The experimental data and the model predictions for different reduction ratios for two reservoirs having the medium and large diameters are illustrated in Figures 6.13 and 6.8 at 35^oC. In most cases the predictions are satisfactory.

Similar experiments were carried out by using barrels of various sizes to test the validity of the model for scale-up purposes. Figure 6.14 depicts the tensile strength of the extrudates for the larger barrel. The predicted level of fibrillation shows a good agreement with the measured tensile strength. There are three influential parameters in the process as discuss before: shear rate (flow rate), contraction angle, and reduction ratio. Based on the proposed model for scale-up purposes if those parameters remain the same in the process, the fibrillation and the mechanical properties of the PTFE extrudates will be the same independent of the barrel size. This hypothesis is shown to be consistent with the experimental findings (compare Figure 6.6 for a small barrel with results in Figure 6.14 for a larger barrel).

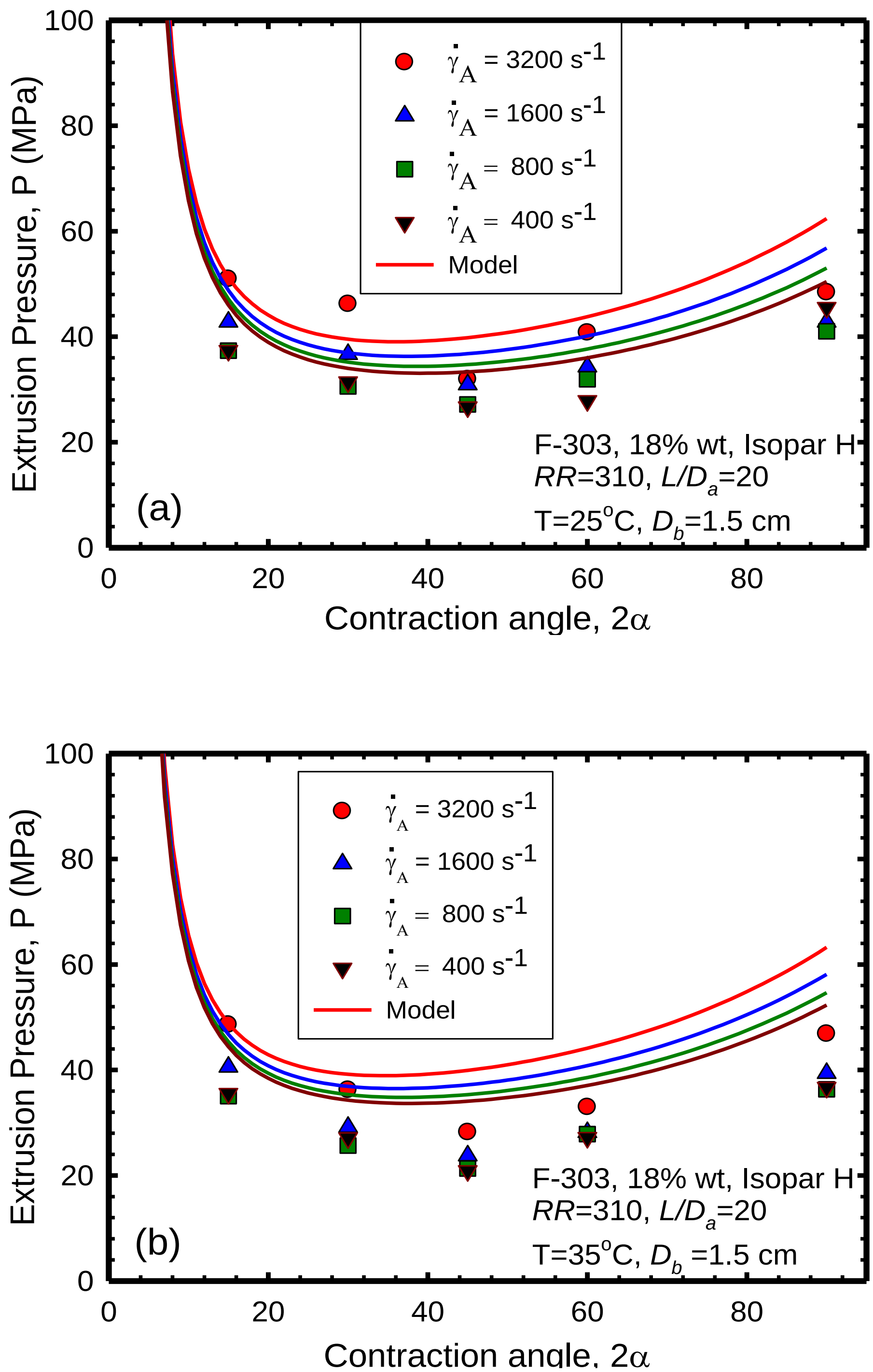

Figure 6.12. *The effect of entrance angle on the steady-state extrusion pressure of PTFE paste (a) at 25°C and (b) at 35°C. Solid lines are model predictions (Eq. 6.6) for the medium barrel with fitted parameters listed in Table 6.1*

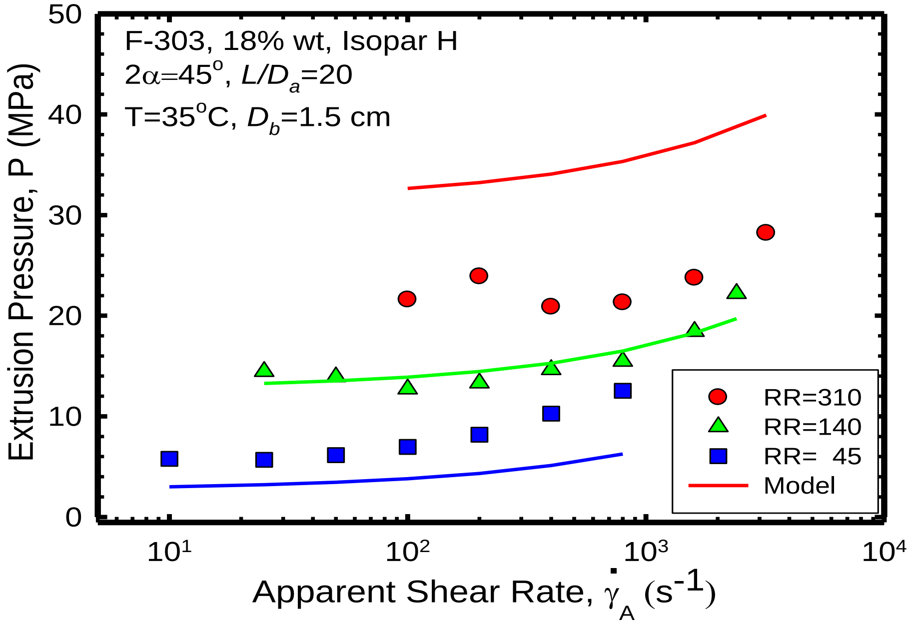

Figure 6.13. *The effect of apparent shear rate and reduction ratio on the steady-state extrusion pressure of PTFE paste at 35°C for the medium size reservoir (D_b=1.5 cm). Solid lines are model predictions (Eq. 6.6) with fitted parameters listed in Table 6.1*

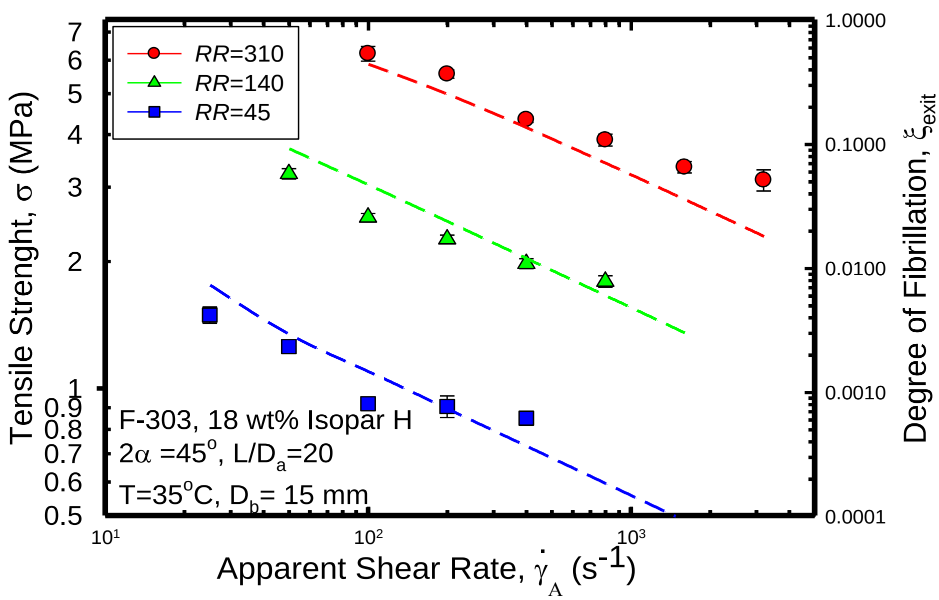

Figure 6.14. *The effect of reduction ratio on tensile strength and fibrillation as predicted by Eq. (6.11) for a die with D_b=15 mm, D_a=0.85 mm, and L/D_a=20. Symbols represent experimental tensile strength data and the continuous lines represent the degree of fibrillation calculated by Eq. (6.11)*

6.6. Summary

In this chapter, the flow behaviour of a PTFE paste was studied using simple capillary rheometry and three different sizes of the barrel to check consistency of the results as well as to test a modified model for PTFE flow for scale-up purposes. The model parameters were fitted using the experimental data from the smallest size reservoir and predictions were made for the rest of the data obtained from the larger reservoirs. A large number of dies were used and experiments were performed at two different temperatures to fully exploit and investigate the capabilities of the present model.

The model was found to be consistent with the experimental data and able to predict the steady-state extrusion pressure reasonably well. For this to occur it is necessary to obtain fitted parameters of the generalized Kelvin constitutive relation used to describe the rheological behaviour of the pastes. The present modified model, previously developed by Ariawan et al. (2002b), can be used for scale-up purposes effectively.

Fibril formation during PTFE paste extrusion and its relation to the mechanical properties of the PTFE extrudates were studied using capillary rheometry and three different sizes of the barrel. A new simple model has been proposed to predict the level of fibrillation during the extrusion process in conjunction with a model for the extrusion pressure. The elastic deformation (compression) in the presence of shear has been assumed to be the main source for causing fibrillation. A large number of dies were used and experiments were performed for different shear rates, contraction angles, and reduction ratios to fully exploit and investigate the capabilities of the developed model.

The model was found to be consistent with the experimental data and able to predict the fibrillation, which is in accordance with the mechanical properties (tensile strength) of the extrudates.

7. Capillary Flow of Chocolate

In this chapter, the rheological behaviour of a commercial milk chocolate is studied to understand its processing characteristics at different temperatures by using parallel-disk and capillary flow. Its rheological behaviour is distinctly different at temperatures below and above 30^{o}C. At temperatures below 30^{o}C it behaves as a soft solid. A previously developed phenomenological mathematical model for polytetrafluoroethylene (PTFE) paste flow is used to model its rheology and capillary extrusion. The predictive capability of this model is tested against capillary data for a variety of capillary dies having different length-to-diameter ratios (L/D_a) and contraction angles (2α). At temperatures above 30^{o}C, chocolate behaves as a visco-elasto-plastic liquid. Its behaviour is determined as a Herschel-Bulkley viscoplastic material with a small degree of thixotropy. The rheological data obtained from parallel-disk and bob-cup rheometers are used to formulate a thixotropic model using a structural parameter. The capillary data were found to be well described with the proposed models.

7.1. The Effect of Temperature

7.1.2. DSC Analysis

As mentioned before, six different polymorphic terms of cocoa butter can exist in semi-solid state (Loisel et al., 1998; Lovegren et al., 1976a; Lovegren et al., 1976b; Wille and Lutton, 1966). In general the thermal behaviour of chocolate is influenced by the existence and content of each of these forms in the final product. The main differences between these forms are the distance between fatty acids, angle of tilt, and the way that triglycerides are packed in crystallization (Talbot, 1999). The most stable form of chocolate has a melting point of around 37°C, while the less stable form has a melting point of 17°C (Talbot, 1999). Figure 7.1 depicts the thermograph of the sample studied in this work. Temperature increased from the low limit to high. The melt peak in this thermograph is equal to 30.8°C. Above 29°C, all four first unstable polymorphic forms of chocolate butter crystal melt down and only two stable forms remain in chocolate paste (Talbot, 1999).

7.1.2. The Effect of Temperature on Rheology

Processing temperature is a significant factor in chocolate extrusion pressure. At low temperatures below the melting point, chocolate behaves as semi-solid material (Chen and Mackley, 2006), and a much higher pressure is needed for extrusion. Increasing the extrusion temperature melts down the fat structure and reduces the chocolate solid fat content. The melting process of more stable fat structure starts below 20^{o}C, which was verified by DSC (Talbot, 1999). However, liquid fat content still remains below 50% for temperatures lower than 30^{o}C (Engmann and Mackley, 2006).

Simple temperature sweep oscillatory test was performed to study effects of temperature on chocolate rheology. Serrated parallel-disk geometry was used to minimize slip effects particularly at low temperatures. For all measurements the strain amplitude was held constant at 10^{-4} and the complex viscosity measured at three different frequencies as a function of temperature. Figure 7.2 summarizes the results, i.e., the effects of temperature on complex viscosity at different frequencies. There is a progressive drop in the complex viscosity before 30^{o}C which is followed by a sudden excessive drop in about 30^{o}C. The gradual decrease of chocolate complex can be explained by an increase of the liquid-fat content due to partial melting of cocoa butter. The excessive drop in 30^{o}C is related to the limit in which liquid phase dominates and the rheological behaviour of chocolate converts from solid-like material to liquid-like material. These findings are in agreement with the DSC results.

Capillary extrusion experiments were carried out at four different apparent shear rates over a broad temperature range to investigate the effects of temperature on the extrusion pressure. Figure 7.3 shows that at all investigated apparent shear rates, the extrusion pressure decreases rapidly with temperature at about 30^{o}C. These results are consistent with DSC analysis (Figure 7.1) and complex viscosity measurements (Figure 7.2). Different heating history for all rheological tests dramatically alters the results. Therefore, for all the experiments in this chapter solid chocolate is grinded and then heated to the desired temperature (similar to the DSC test).

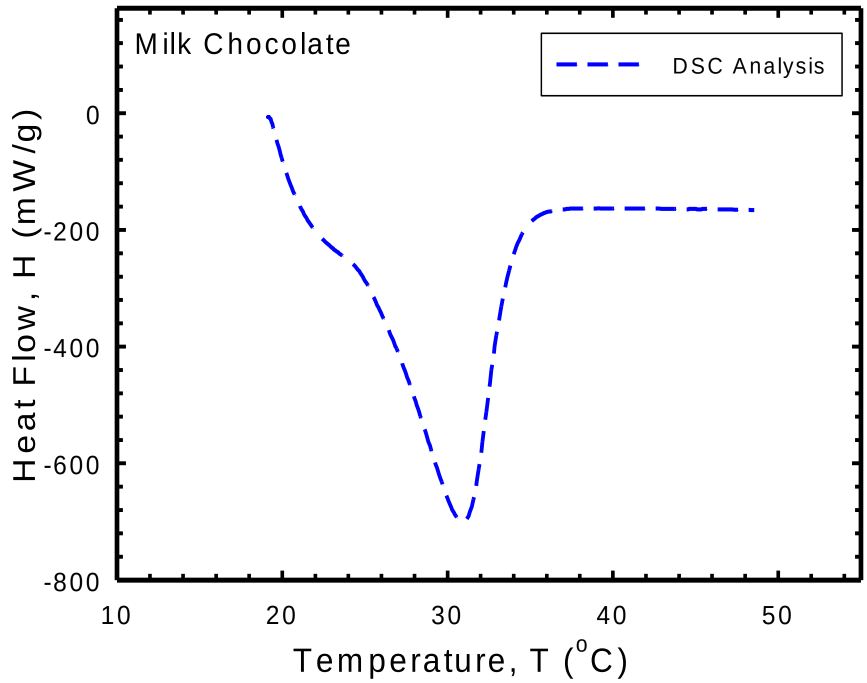

Figure 7.1. *DSC thermogram of the milk chocolate studied in this work. The melt peak appears at 30.8°C*

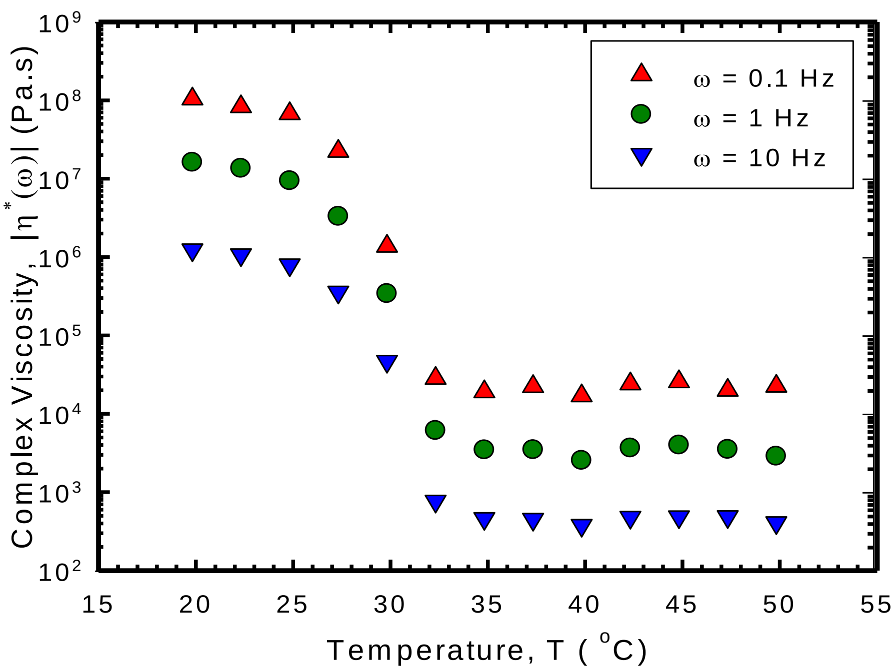

Figure 7.2. *The complex viscosity of the milk chocolate as a function of temperature at three frequencies. Note the sudden drop of complex modulus at about 30°C, which marks the transition from solid-like to liquid-like behaviour*

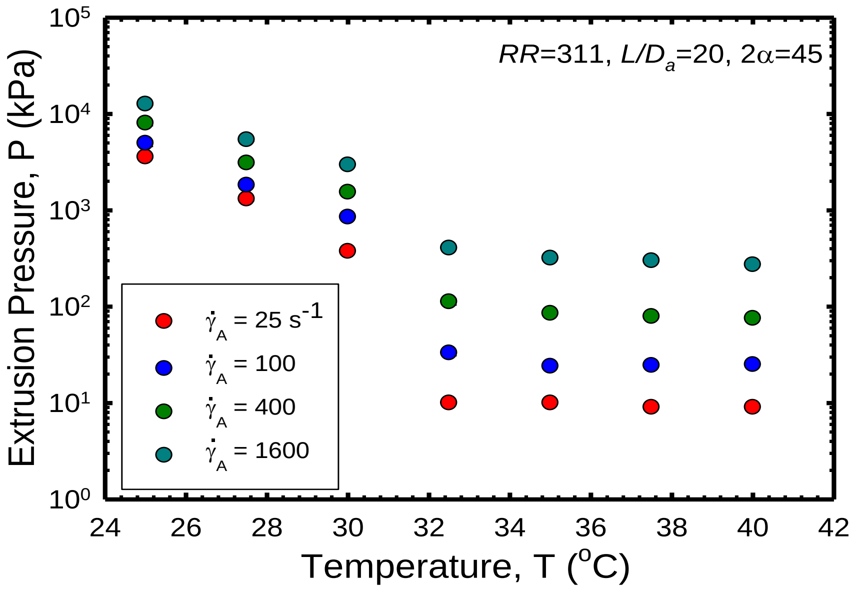

Figure 7.3. *The capillary extrusion pressure of the milk chocolate as a function of temperature at several values of the apparent shear rate using a capillary die having a length-to-diameter ratio of 20, reduction ratio (RR) of 311, and contraction angle of 45°. Note the sudden pressure drop at about 30°C corresponding to the sudden drop of complex viscosity at about 30°C*

7.2. Rheology of Semi-Solid Chocolate (T < 30°C)

Below 30°C chocolate behaves as solid as was discussed above based on the DSC thermogram. Therefore, rheological measurements of the apparent viscosity are not possible with the existing instruments, and thus a viscous constitutive model cannot be formulated. Instead, a semi-solid phenomenological constitutive model for paste extrusion can be used (Ariawan et al., 2001, Ariawan et al., 2002). In semi-solid paste extrusion the material slips on the wall (Coulombic friction). Phenomenological analytical flow models for calculating the extrusion pressure as a function of the operating conditions and geometrical characteristics of dies are based on the "radial-flow" hypothesis. This hypothesis assumes that the flow is along the radial direction in the die (assuming a spherical coordinate system as in Figure 2.13), and points located on virtual spherical surfaces of a constant radius *r* from the die apex have the same radial velocity.

The mathematical form of the "radial-flow" hypothesis for a cylindrical die (Figure 2.13) can be written as:

$$\frac{dr}{dt} = -\frac{Q}{2\pi(1-\cos\alpha)r^2} \; . \tag{7.1}$$

Based on this hypothesis, similar to the previous case (PTFE paste) the kinematics of semi-solid chocolate paste flow can be calculated independent of any rheological constitutive measurements at a given volumetric flow rate *Q*. The constitutive rheological behaviour of paste is modeled by elasto-plastic and viscous contribution to stress, essentially a modified Kelvin stress-strain relation with an added power-law viscous term.

Based on this hypothesis ("radial flow") and the given constitutive equation, an analytical expression for extrusion pressure was derived and can be written as follows:

$$P = \sigma_{ra}(RR)^B + 2(1+B)\left\{ C\left(\frac{D_b}{2\sin\alpha}\right)^{2B} \int_{r_a=\frac{D_b}{2\sqrt{RR}\tan\alpha}}^{r_b=\frac{D_b}{2\sin\alpha}} \frac{\left(3\ln\left(r_b/r\right)\right)^n}{r^{2B+1}} dr + \right.$$

$$\left. \frac{K}{(3m+2B)}\left(\frac{12Q\tan^3\alpha}{\pi(1-\cos\alpha)D_b^3}\right)^m \left((RR)^{B+3m/2} - 1\right) \right\}, \tag{7.2}$$

where

$$\sigma_{ra} = \sigma_{oa}\left(e^{-4f\,L/D_a} - 1\right) + \sigma_{zL} e^{-4f\,L/D_a} \tag{7.3}$$

and

$$-\sigma_{oa} = C\left(\frac{3}{2}\ln(RR)\right)^n + K\left(\frac{12Q\sin^3\alpha(RR)^{3/2}}{\pi(1-\cos\alpha)D_b^{\,3}}\right)^m , \tag{7.4}$$

where P is the extrusion pressure, *f* is a Coulombic friction coefficient, $B = f\sin\alpha/[2(1-\cos\alpha)]$, σ_{zL} is the shear stress imposed at the die exit, which is negligible or zero, and K and C are material constants, which can be evaluated by fitting extrusion pressure data. Table 7.1 lists the optimized values for this model that best fit the capillary experimental data presented below.

Table 7.1. *Fitted parameters for the semi-solid paste extrusion model (Eq. 7.2)*

C (Pa)	n	K (Pa·s^m)	m	f
139730	$4\text{x}10^{-10}$	312583	0.31	0.024

All the reported extrusion pressure data refer to steady-state values. Depending on the piston speed and die diameter, an apparent shear rate can be defined by $\dot{\gamma}_A \equiv 32Q/\pi D_a^3$, where Q is the volumetric flow rate defined as $Q \equiv \frac{1}{4}V_p(\pi D_b^2)$, where V_p is the piston velocity.

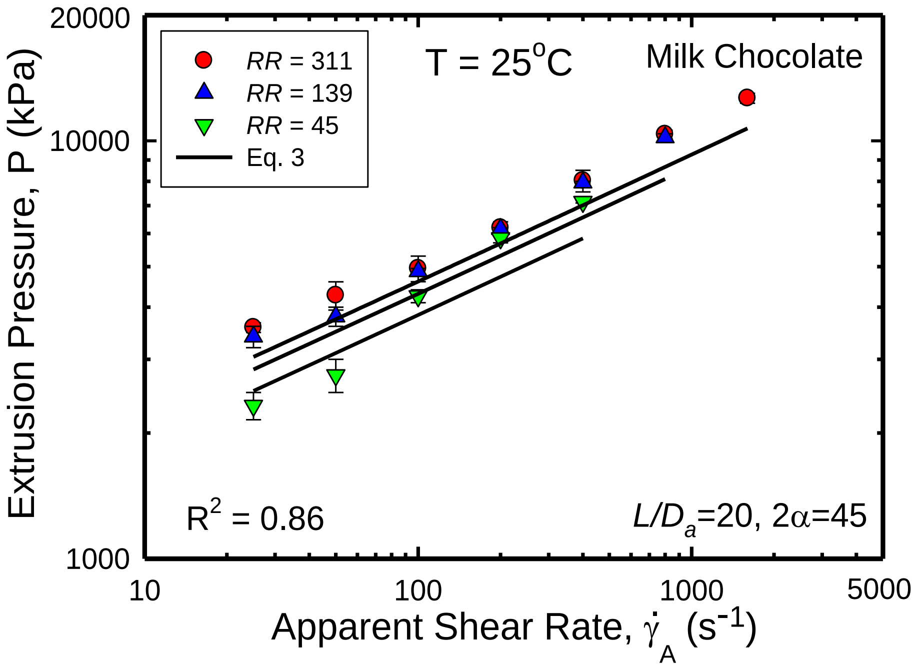

Figure 7.4. *The effect of apparent shear rate and reduction ratio on the steady-state extrusion pressure of chocolate at 25°C using capillary dies having length-to-diameter ratio of 20 and contraction angle of 45°. Solid lines are model predictions (Eq. 7.2) with fitted parameters listed in Table 7.1*

Figure 7.4 shows the effect of apparent shear rate and reduction ratio on the extrusion pressure. The extrusion pressure generally increases with an increase in the apparent shear rate (hence volumetric flow rate), due to the increase in the viscous resistance of the paste. In addition it can be seen that the extrusion pressure increases slightly with increasing reduction ratio. Due to elastic-plastic paste behaviour, a higher extrusion pressure is needed to yield chocolate through tapered dies with a higher reduction ratio.

Figure 7.5 summarizes the effect of contraction angle on the extrusion pressure at several apparent shear rates. The extrusion pressure initially decreases, goes through a minimum and then slightly increases, with increasing die entrance angle. The extrusion pressure is higher at low contraction angles as a result of Coulombic friction (larger area of die at smaller contraction angles).

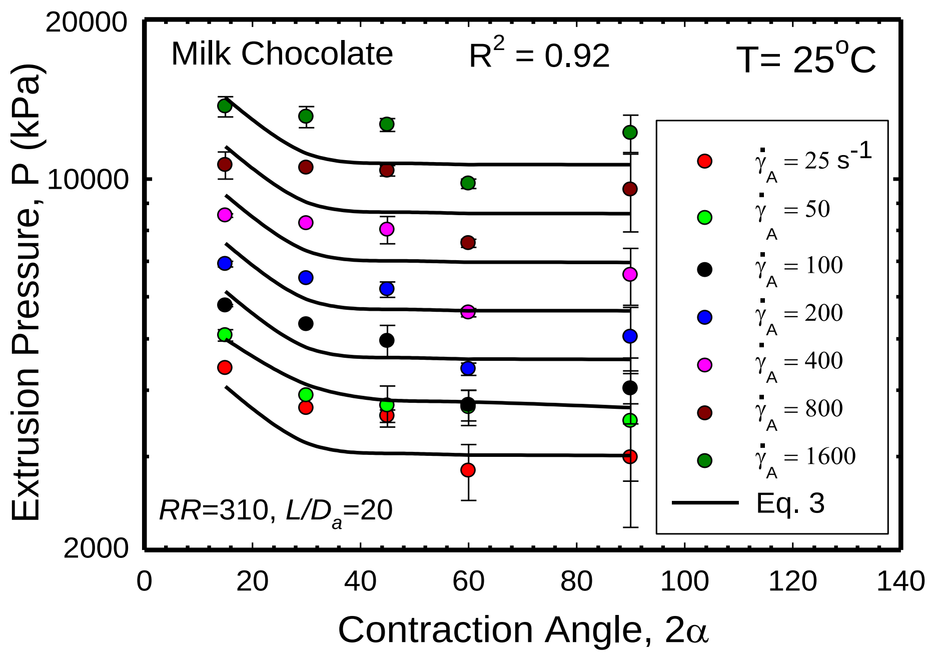

Figure 7.5. *The effect of entrance angle on the steady-state extrusion pressure of chocolate at 25°C using capillary dies having length-to-diameter ratio of 20 and reduction ratio (RR) of 311. Solid lines are model predictions (Eq. 7.2) with fitted parameters listed in Table 7.1*

The effect of L/D_a on the extrusion pressure is illustrated in Figure 7.6. Due to the solid-like behaviour of chocolate paste at 25°C, the pressure drop in the conical part of the die is considerable. It can be seen that at the lower shear rates, about half of pressure drop occurs in the conical part, i.e., comparing the data for L/D_a=0 with that for L/D_a=20.

Overall the model fit to the available experimental data has shown a good consistency. Optimized values for model parameters reveal an important understanding about the rheological properties of paste. The parameter n describes the significance of the strain hardening of material. When n is greater than 1, the material shows significant strain-hardening behaviour. If n is equal to zero, the material shows simple plastic deformation. Since in this case the value of n is very close to zero, it can be concluded that chocolate is a semi-solid paste with plastic deformation, which is consistent with previous findings (Beckett et al., 1994; Mulji et al., 2003; Chen and Mackley, 2006).

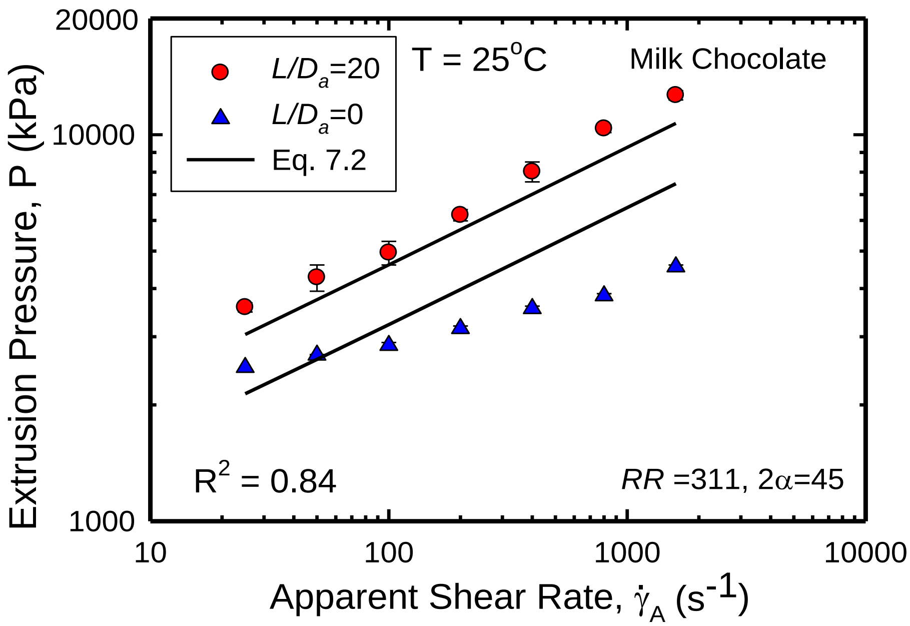

Figure 7.6. *The effect of L/D_a on the steady-state extrusion chocolate at 25°C using capillary dies having reduction ratio (RR) of 311 and contraction angle of 45°. Solid lines are model predictions (Eq. 7.2) with fitted parameters listed in Table 7.1*

7.3. Rheology of Melt Chocolate (T > 30^{o}C)

7.3.1. Equilibrium Flow Curve

Steady shear experiments were first performed using different gaps to examine possible effects of slip (Hatzikiriakos, 2012). Figure 7.7 plots the steady shear results for the cup-and-bob geometry using a small and large gap (in the small geometry the bob diameter is 14 mm and the cup diameter is 15.5 mm, while in the large geometry, the diameters are 25 mm and 27.5 mm, respectively) at 35°C. The results are independent of the gap. A small-gap dependence at small shear rates where yield stress effects prevail, although consistent with the assumption of slip, is within experimental error. Therefore, this set of data provides evidence that slip in the flow of chocolate is negligible.

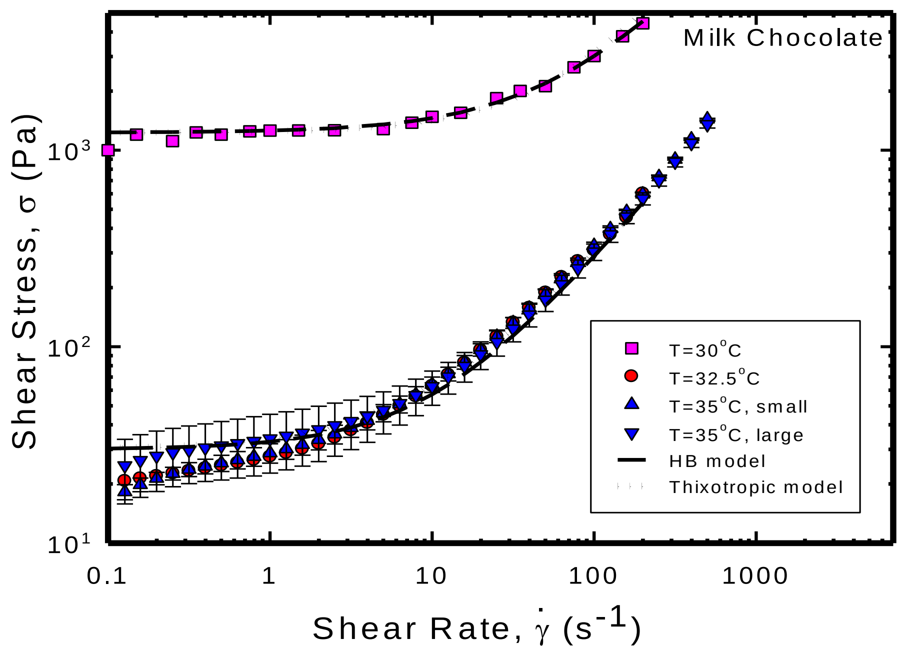

Figure 7.7. *The flow curve of chocolate using bob-and-cup geometries of various dimensions to check for slip effects. The flow curve of milk chocolate at 35°C is independent of gap size showing that the effects of slip are negligible. Continuous lines represent the fits to the data of various constitutive models (see text for additional explanations)*

Steady shear experiments were performed for chocolate sample at 30°C, 32.5°C and 35°C to determine the flow curve of this material as a basis for the development of an appropriate constitutive equation (Figure 7.7). As seen the temperature has a significant effect on the rheology of the material at temperatures close to 30°C where it dramatically drops. However, the rheological behaviour of chocolate melt at 32.5°C and 35°C is almost identical. These results are consistent with the previous results for complex viscosity measurements (Figure 7.2). They will be used to formulate a constitutive equation for the capillary simulations.

7.3.2. Time Dependency - Thixotropy

For a complete rheological characterization it is also necessary to identify the time-dependent effects, in particular the thixotropic behaviour of the chocolate (Sokmen and Gunes, 2006). Various start-up experiments were carried out. In each experiment, pre-shearing and rest to recover the structure as described above was first used. The shear rate is suddenly increased from zero to a certain value. As a result the shear stress increases from zero to a high value rapidly and subsequently gradually decreases with time until it reaches its steady value. Essentially a shear stress overshoot is obtained in each case, also indicating time dependency. This initial overshoot is related to the viscoelastic response of the material. After this viscoelastic response, thixotropic behaviour can be observed. Figures 7.8a and 7.8b show both viscoelastic and thixotropic effects. The viscoelastic effect can only be tracked at low shear rates where the thixotropic effect is limited. Therefore for model development, the elastic response is neglected, and the material is assumed to be purely thixotropic.

Figures 7.8a and 7.8b summarize the thixotropic results for milk chocolate at 30°C and 35°C. Thixotropic effects are more significant at 30°C as chocolate has a higher content of solid cocoa butter at a lower temperature (Talbot, 1999). During flow, shear forces cause a phase transition of cocoa butter and increase the overall liquid fat content of the material. Increase of the liquid fat content causes a drop in viscosity over time until it reaches a steady-state value. As can be seen the overall description of the changes are satisfactory. Deviations at short times are related to the viscoelastic nature of the material, which is not taken into account.

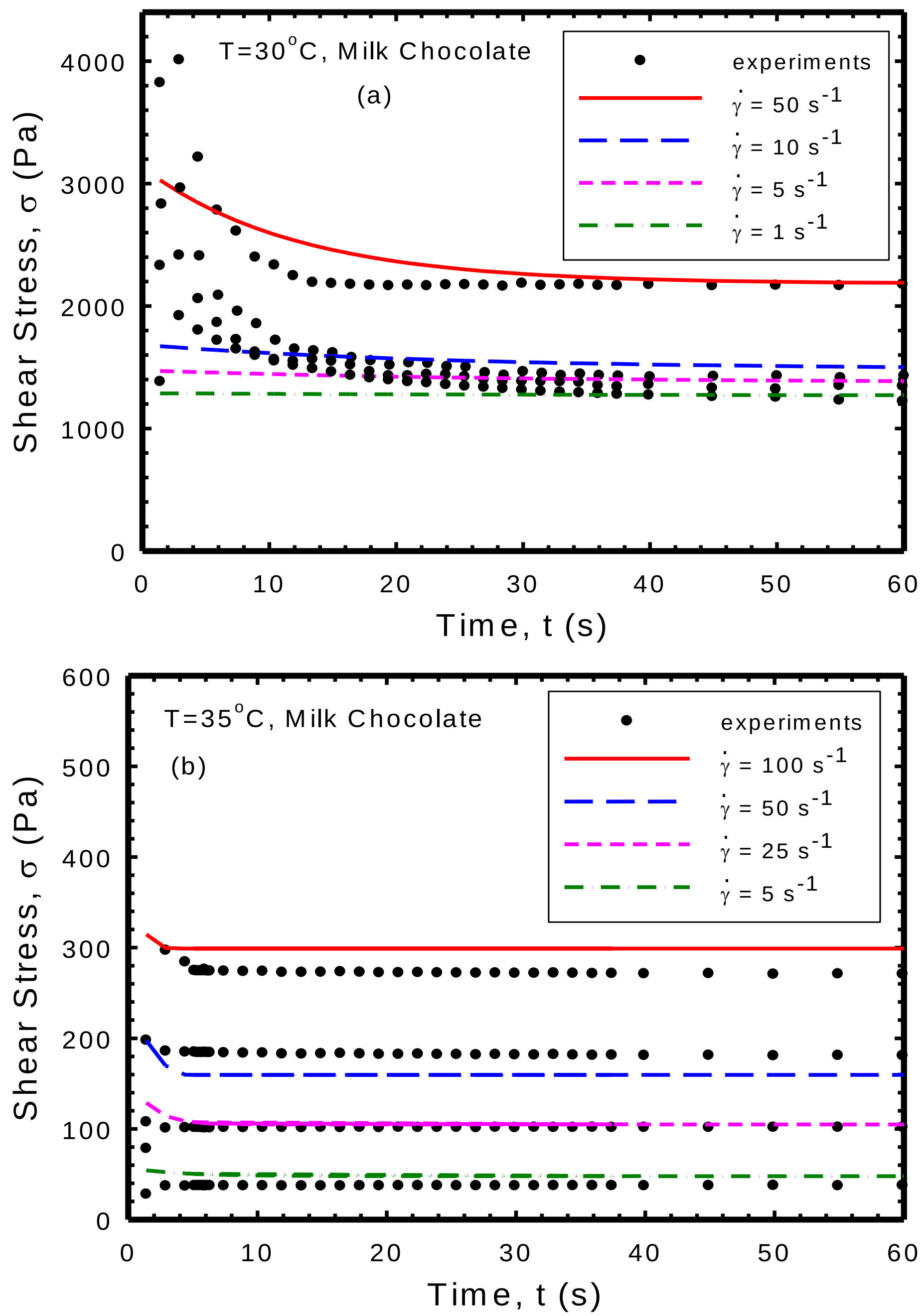

Figure 7.8. *Thixotropic behaviour of milk chocolate in three start-up tests at different shear rates: (a) T=30°C and (b) T=35°C. The continuous lines present predictions of the thixotropic model (Eq7.6) as explained in the text*

7.3.3. Constitutive Modeling of Melt Chocolate

As discussed above and based on the experimental data, chocolate behaves as a viscoplastic melt at temperatures greater than 30°C. The rheological data obtained by using the rotational rheometer (Figure 7.7) can be used to model fluid behaviour. The Herschel-Bulkley model has been widely used to model the rheological behaviour of pastes, suspensions, and emulsions, in which the material shows power-law behaviour after yielding. Therefore the stress can be written as

$$\tau = \tau_y + k\dot{\gamma}^n \tag{7.5}$$

where τ_y is the yield stress, k is the consistency index, and n is the power-law index. The equilibrium flow curve data was used to determine the parameters of the model at 30°C and 35°C. Table 7.2 shows the optimized values for the Herschel-Bulkley model, and predictions are illustrated as dashed lines in Figure 7.7.

Table 7.2. *Herschel-Bulkley model parameters (Eq. 7.5)*

Temperature (°C)	τ_y (Pa)	k (Pa·s^n)	n
30	1230	29.25	0.89
35	30	2.84	0.98

Although the Herschel-Bulkley model predicts equilibrium data well, this model is not able to capture thixotropic behaviour as observed above (Figures 7.8a and 7.8b). A constitutive model for a typical paste should possess at least two elements. First, a yield stress which is the stress below which no flow is observed. Then, thixotropy should be included through an appropriate kinetic equation involving a structural parameter (Teng and Zhang, 2013). It has been claimed by many authors that the existence of yield stress indicates the existence of structure that requires initial energy to decay and let the material flow, which implies that flow might alter the structure and thus thixotropy is expected (Mewis and Wagner, 2009; Krieger, 1990).

To represent chocolate rheology, the proposed model includes two terms and can be written as follows:

$$\tau = (1+\xi)\tau_{y,th} + (1+\xi)\eta_{\infty}\dot{\gamma}^{n} . \qquad (7.6)$$

The first term represents the yield stress behaviour of the material. It is often assumed that the yield stress is related to the structure of the material through a structural parameter, ξ (Teng and Zhang, 2013; Carleton et al., 1974). The second term includes the viscous part of the response, and it is a function of the structural parameter, ξ, which can be described by a kinetic equation. The rate of change in structure can be described by (Derksen, 2009):

$$\frac{d\xi}{dt} = -k_1\dot{\gamma}\xi + k_2(1-\xi) . \qquad (7.7)$$

This way the structural parameter ξ is a normalized quantity that varies between 0 and 1 and indicates the integrity of the network (ξ = 0: no network or structure; ξ = 1: fully developed network or structure). The first term on the RHS of Eq. (7.7) indicates breakdown of the network due to material deformation; the second term is responsible for build-up of the network with a time constant $1/k_2$ associated to it.

Structure formation occurs due to Brownian motion and is partially due to imposition of shear rate (Mewis and Wagner, 2009). According to the above Eq. (7.7), the shear contribution in structure build-up is neglected, and the rate of formation is set proportional to $(1-\xi)$ (Mujumdar et al., 2002). It has been assumed that the shear rate may break down structure. The rate of structural break-down is proportional to the shear rate and also to the degree of structure.

According to this kinetic equation, the structural parameter approaches a steady-state value, ξ_{eq}, at a given value of shear rate, $\dot{\gamma}$, that is:

$$\xi_{eq} = \frac{k_2}{k_1\dot{\gamma} + k_2} . \qquad (7.8)$$

Therefore the equilibrium flow curve is given by:

$$\tau_{eq} = (1+\xi_{eq})\tau_{y,th} + (1+\xi_{eq})\eta_\infty \dot{\gamma}^n . \quad (7.9)$$

Then the equilibrium apparent viscosity η_{eq} is given by:

$$\eta_{eq} = \frac{(1+\xi_{eq})\tau_{y,th}}{\dot{\gamma}} + (1+\xi_{eq})\eta_\infty \dot{\gamma}^{(n-1)} . \quad (7.10)$$

The η_∞ and n were set equal to consistency index and power-law index in the Herschel-Bulkley model for the sake of convenience. At high shear rates, the structural parameter (ξ_{eq}) approaches asymptotically zero (Eq. 7.8). Therefore, both models result in the same apparent viscosity. At low shear rates, the structural parameter (ξ_{eq}) approaches the value of 1 (Eq. 7.8) and for consistency the thixotropic yield stress ($\tau_{y,th}$) has been set half of the yield stress in the Herschel-Bulkley model. Thus, both models predict the same value for yield stress in the lower shear rates. The ratio k_1/k_2 was calculated by fitting Eq. (7.10) to the data of Figure 7.7 by writing $\xi_{eq} = 1/[1+(k_1/k_2)\dot{\gamma}]$ from Eq. (7.8). Subsequently, using the data of Figures 7.8a and 7.8b, the individual values of k_1 and k_2 were calculated. Optimized values for the proposed models are summarized in Table 7.3, and the model predictions for the equilibrium flow curves are illustrated as dotted lines in Figure 7.7.

Table 7.3. *Fitted parameters for the structural model*

Temperature(°C)	$\tau_{y,th}$ (Pa)	η_∞ (Pa·s)	n	k_1	k_2 (s^{-1})
30	615	29.25	0.89	0.001	0.03247
35	15	2.84	0.98	0.018	0.18

7.3.4. Capillary Melt Flow Simulations

Similar with the toothpaste case, we consider the conservation equations of mass and momentum for incompressible fluids under isothermal, creeping, steady flow conditions. These are written as (Tanner, 2000):

$$\nabla \cdot \bar{u} = 0 , \quad (7.11)$$

$$0 = -\nabla p + \nabla \cdot \overline{\overline{\tau}}\,, \qquad (7.12)$$

where $\overline{u}$ is the velocity vector, p is the pressure and $\overline{\overline{\tau}}$ is the extra stress tensor.

The viscous stresses are given for inelastic incompressible fluids by the relation (Tanner, 2000):

$$\overline{\overline{\tau}} = \eta\left(|\dot{\gamma}|\right)\overline{\overline{\dot{\gamma}}}\,, \qquad (7.13)$$

where $\eta\left(|\dot{\gamma}|\right)$ is the apparent viscosity of Eq. (7.5), in which the shear rate $\dot{\gamma}$ is replaced by the magnitude $|\dot{\gamma}|$ of the rate-of-strain tensor $\overline{\overline{\dot{\gamma}}} = \nabla\overline{u} + \nabla\overline{u}^T$, which is given by:

$$|\dot{\gamma}| = \sqrt{\frac{1}{2} II_{\dot{\gamma}}} = \left(\frac{1}{2}\left(\overline{\overline{\dot{\gamma}}} : \overline{\overline{\dot{\gamma}}}\right)\right)^{1/2}, \qquad (7.14)$$

where $II_{\dot{\gamma}}$ is the second invariant of $\overline{\overline{\dot{\gamma}}}$

$$II_{\dot{\gamma}} = \left(\overline{\overline{\dot{\gamma}}} : \overline{\overline{\dot{\gamma}}}\right) = \sum_i \sum_j \dot{\gamma}_{ij}\dot{\gamma}_{ij}\,, \qquad (7.15)$$

Thus, the apparent viscosity is written as:

$$\eta\left(|\dot{\gamma}|, \xi\right) = \frac{(1+\xi)\tau_{y,th}}{|\dot{\gamma}|} + (1+\xi)\eta_\infty \dot{\gamma}^{(n-1)}. \qquad (7.16)$$

In the above, the apparent viscosity is a function of ξ, which obeys the kinetic Eq. (7.7). In general flows, Eq. (7.7) becomes the convective-transport equation (Mitsoulis and Hatzikiriakos, 2009a; Mitsoulis and Hatzikiriakos, 2009b):

$$\frac{\partial \xi}{\partial t} + \overline{u} \cdot \nabla \xi = -k_1 |\dot{\gamma}| \xi + k_2 \left(1 - \xi\right). \qquad (7.17)$$

For steady-state conditions, $\partial \xi / \partial t = 0$.

The above rheological model (Eqs. 7.13 and 7.16) is introduced into the conservation of momentum (Eq. 7.12) and closes the system of equations. The boundary conditions applied, the solution domain, as well as the method used to solve the equations, have been explained in chapter five.

7.3.5. Extrusion Experiments

7.3.5.1 Effect of Apparent Shear Rate

Figures 7.9a,b depict the steady-state extrusion pressure as a function of apparent shear rate for several reduction ratios at 30°C and 35°C, respectively. The extrusion pressure generally increases with an increase in the apparent shear rate (hence volumetric flow rate), due to the increase in the viscous resistance of the paste.

At 35°C almost all of cocoa fat butter is converted into liquid. It is expected that chocolate has the lowest crystallized structure and solid content at 35°C. Figure 7.9a shows that at 35°C both the Herschel-Bulkley and the thixotropic model capture the extrusion pressure well and result in very similar values. The temperature of 30°C is very close to melting and therefore a higher level of structure is expected. In this case, the thixotropic effects become very important. In other words, the apparent viscosity of chocolate paste during the process is higher than that predicted for the equilibrium flow curve. It takes a longer time for structure to break down. Thus, the Herschel-Bulkley model underpredicts the extrusion pressure.

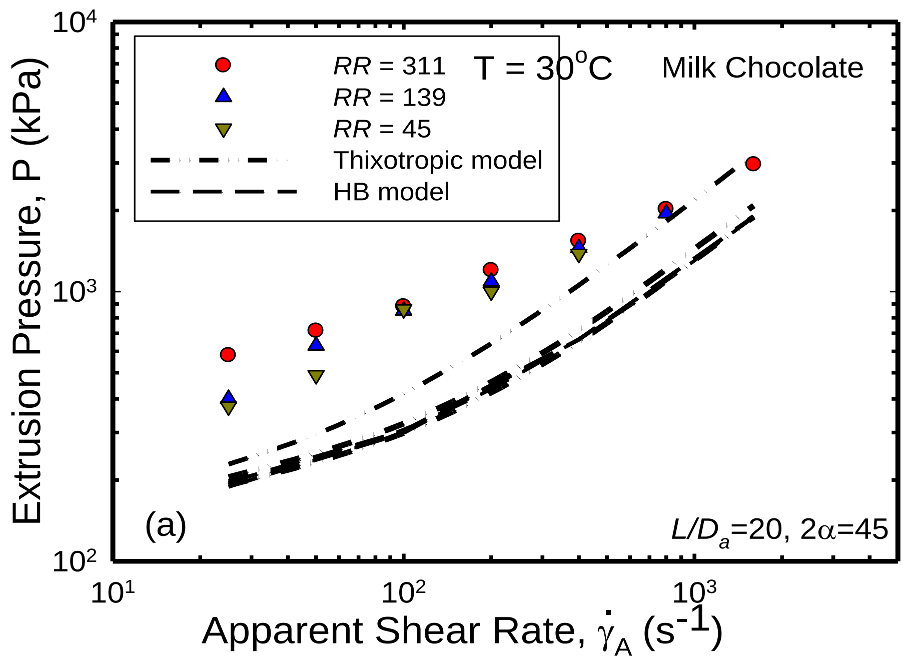

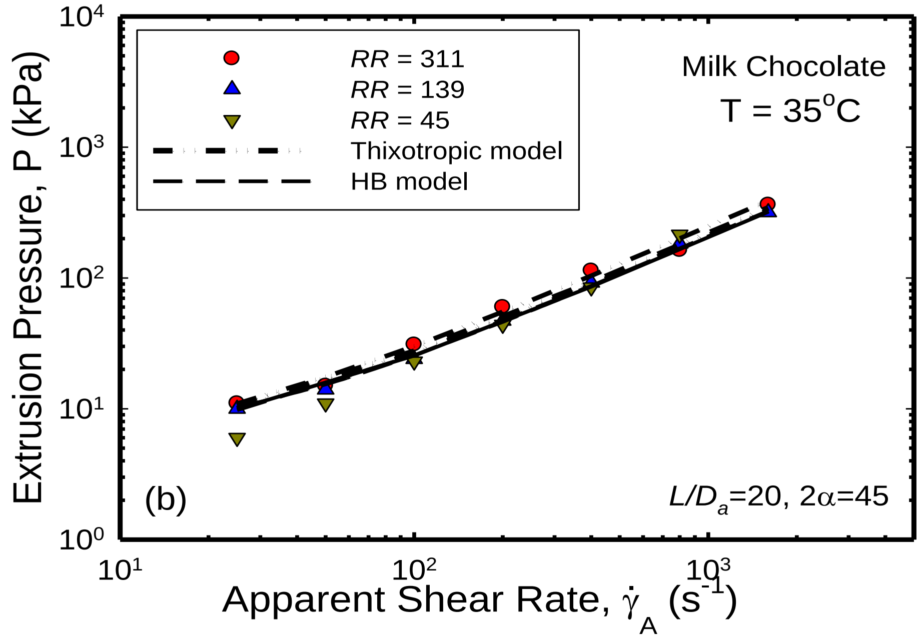

Figure 7.9. *The effect of apparent shear rate and reduction ratio on the steady-state extrusion pressure of chocolate paste using capillary dies having length-to-diameter ratio of 20, and contraction angle of 45°: (a) T=30°C, (b) T=35°C. Continuous lines are the model predictions*

7.3.5.2. Effect of Die Entrance Angle

Figures 7.10a,b depict the effect of contraction angle on the extrusion pressure at several apparent shear rates and temperatures, namely 30°C and 35°C, respectively. The effects of contraction angle on extrusion pressure are negligible in both cases. It is worth mentioning that most of the pressure drop occurs in the die land region, and therefore the effect of die entry design on the extrusion pressure is much less compared to the case of semi-solid chocolate. At 30°C, a significant portion of the pressure drop occurs in the conical part of the die.

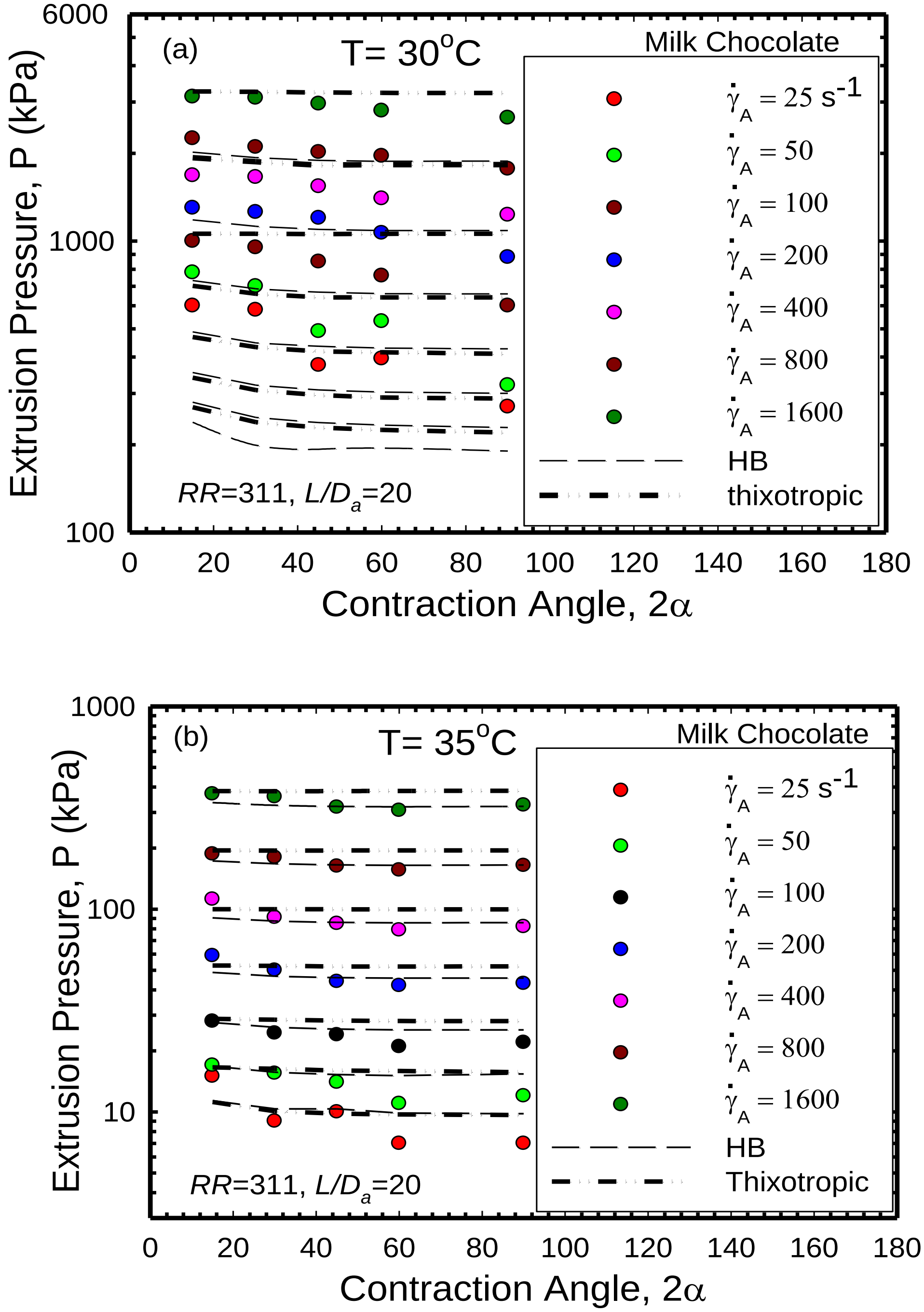

Figure 7.10. *The effect of contraction angle on the steady-state extrusion pressure of chocolate paste using capillary dies having length-to-diameter ratio of 20 and reduction ratio (RR) of 311: (a) T=30°C, (b) T=35°C. The continuous lines represent the model predictions*

7.3.5.3. Effect of Length-to-Diameter Ratio

The effect of L/D_a ratio on the extrusion pressure at different temperatures is shown in Figures 7.11a,b. Again, it can be seen that at the lower temperature, the Herschel-Bulkley model underpredicts the extrusion pressure. Close to 30°C, the flow curve of chocolate changes more non-linearly. The extrusion pressure for L/D_a=0 is underpredicted as viscoelastic effects might be important here and are not taken into account in the modelling.

7.4. Summary

Rheological experiments and simulations in capillary flow were performed for a commercially manufactured chocolate. It was found that its rheological behaviour is distinctly different at temperatures below and above 30^{o}C. At temperatures below 30^{o}C chocolate behaves as a soft solid. A previously developed phenomenological mathematical model for polytetrafluoroethylene (PTFE) paste flow was used to model its rheology and capillary extrusion. The model takes into account the elastic-plastic (strain hardening) and viscous nature of the material in its non-melt state. The predictive capability of this model is tested against capillary data for a variety of capillary dies having different length-to-diameter ratios (L/D_a) and contraction angles (2α). It was found that it can represent its behaviour in capillary flow very well.

At temperatures above 30^{o}C, chocolate behaves as a visco-elasto-plastic liquid. Its behaviour has been determined as a Herschel-Bulkley viscoplastic material with a small degree of thixotropy. The rheological data obtained from parallel-disk and bob-cup rheometers were used to formulate a thixotropic model using a structural parameter. The capillary data were found to be well described with the proposed model.

Comparing the capillary flow of semi-solid and liquid-chocolate, it can be seen that in the semi-solid regime 35-70% of pressure drop occurs in the conical part of the die. Meanwhile, this reduces to only 15% for the liquid chocolate. This shows the magnified importance of the die design in the case of semi-solid paste extrusion.

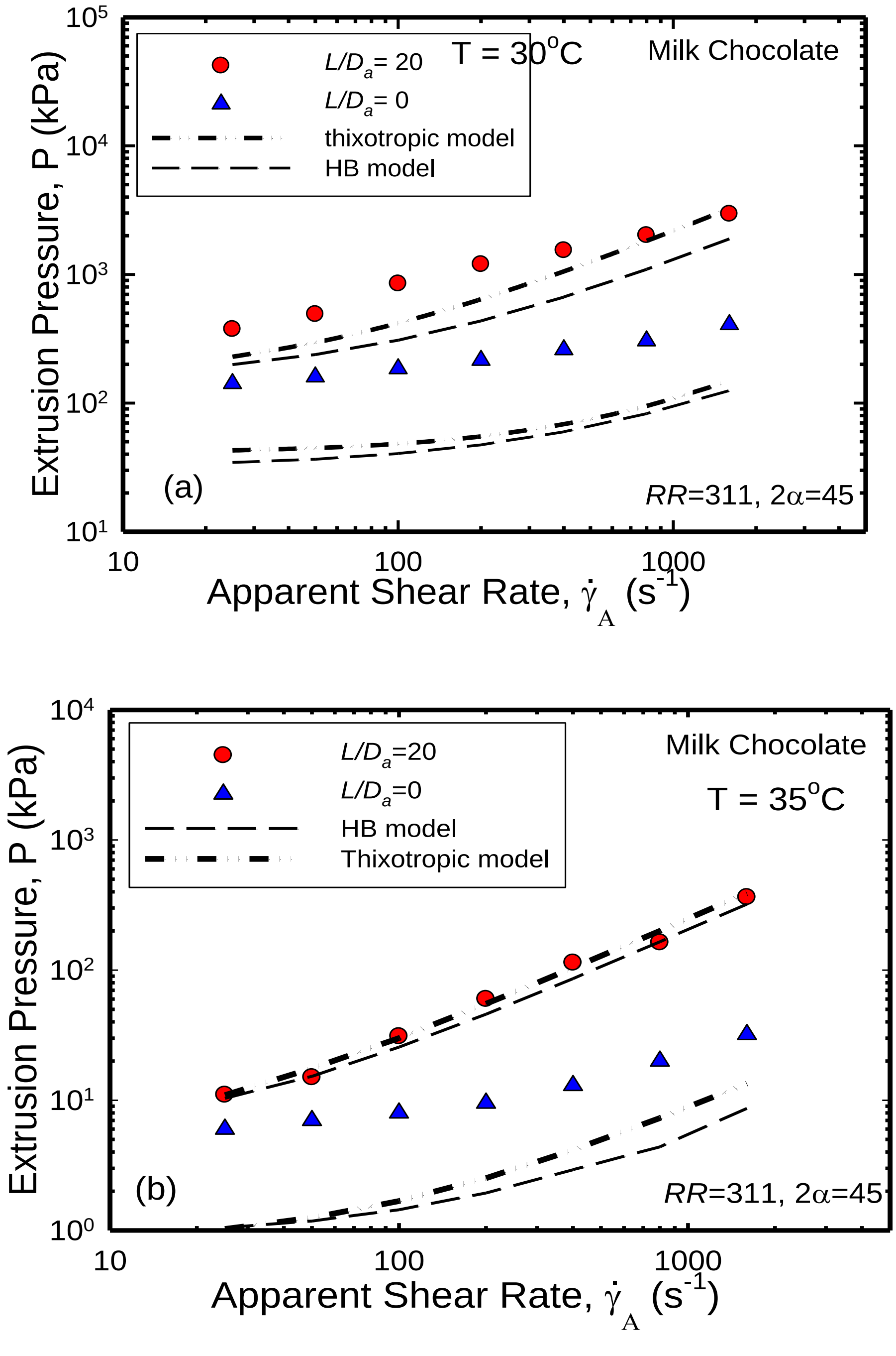

Figure 7.11. *The effect of L/D_a on the steady-state extrusion pressure of chocolate paste using capillary dies having reduction ratio (RR) of 311 and contraction angle of 45°: (a) T=30°C, (b) T=35°C. The continuous lines represent the model predictions*

8. Conclusions, Contribution to Knowledge and Recommendations

8.1. Conclusions

The rheological behaviour of three different pastes was investigated by a number of rheological techniques. First the rheological behaviour of a commercial toothpaste was investigated and described by a thixotropic model. The equilibrium flow curve and several thixotropic start-up tests were carried out and compared with the model predictions. The time dependent (thixotropic) behaviour of toothpaste was described by a structural parameter that was part of a kinetic equation describing the structure formation. Based on the proposed kinetic equation, the shear forces result in the structural breakdown of toothpaste. The apparent viscosity at each instant of time and point in space is a function of the structural parameter. The equations of conservation of mass, conservation of momentum, coupled with the rheological constitutive equation, and the kinetic equations were solved for capillary flow using appropriate boundary conditions including slip at the wall. The predictions were found to be in good agreement with capillary data obtained using a variety of dies having different length-to-diameter ratios (L/D_a), contraction angles (2α), and reduction ratios $(D_b/D_a)^2$. The good agreement pointed to the validity of the thixotropic model developed for the rheology of toothpaste.

The rheology of polytetrafluoroethylene (PTFE) paste was also studied. Unlike toothpaste, the PTFE paste exhibits more solid-like behaviour with visco-elastic characteristics. A simple phenomenological model based on “radial-flow” hypothesis (RFH) and a visco-elastic behaviour (generalized Kelvin constitutive equation) was developed to predict the extrusion pressure in capillary flow. This model is a proper modification of a previous model (Ariawan et al., 2002b), and it has been shown suitable for scale-up purposes. The model predictions were tested against the extrusion measurements using three different barrel sizes and dies having different length-to-diameter ratios (L/D_a), contraction angles (2α), and reduction ratios $(D_b/D_a)^2$. These experiments were carried out at three different temperatures and were shown to be in good agreement with the model predictions.

Fibril formation during the PTFE extrusion process has been shown to play an essential role in the quality of the final product. Therefore, effects of die design and extrusion condition were comprehensively studied to understand the physics of this phenomenon. It was found that the apparent shear rate (process speed) is a critical parameter for the amount of fibril formation. Generally, extrusion at a lower apparent shear rate results in a higher degree of fibrillation, and therefore, in a higher tensile strength. The geometrical parameters of the die also have a significant impact on the fibrillation process. Higher reduction ratios $(D_b/D_a)^2$ result in a higher degree of fibrillation due to higher amounts of extensional deformation during the process of extrusion. To describe and predict the degree of fibrillation, a new model has been proposed. Based on this model, the degree of fibrillation is proportional to extensional strain. Combining the proposed model with the "radial-flow" hypothesis (RFH), the degree of fibrillation for the final extrudates can be calculated. The results were compared qualitatively with tensile strength measurements and were shown to be in good agreement.

Finally, a commercial milk chocolate was studied as a model paste system to understand its processing characteristics at different temperatures. At temperatures below 30^oC, the chocolate was found to behave as a solid-like material. Therefore, the proposed model for PTFE paste extrusion was used to model the capillary extrusion process of chocolate. The rheological behaviour of chocolate paste changes as temperature in increased beyond 30^oC from a solid-like to a liquid viscoelastic behaviour. The rheological data obtained from parallel-disk and bob-cup rheometers were used to formulate a thixotropic model based on the Herschel-Bulkley model for chocolate rheology above 30^oC. The simple Herschel-Bulkley model without thixotropy was also used. Flow simulations were performed for both models and compared with capillary data at 30^oC and 35^oC. At higher temperatures chocolate exhibits a lower degree of thixotropy. Therefore, as it is expected, at 35^oC both models gave similar results.

8.2. Contribution to Knowledge

The present work has provided the following new contributions to knowledge:

1. A thixotropic model was developed to describe the rheology of toothpaste, which was used to simulate its capillary flow. The good agreement between experimental results and model predictions pointed to the suitability of the developed model.
2. An existing model for the rheology of PTFE paste in capillary extrusion was properly modified and significantly increased its capabilities in describing this process. Moreover, this model was proven also capable for scale-up purposes, as it was successfully tested against capillary data from three capillary rheometers having different barrel sizes.
3. A new model for PTFE fibril formation was proposed. The model predictions for the degree of fibrillation were compared with experimental measurements for tensile strength and were found qualitatively consistent.
4. An extensive study of chocolate capillary flow was performed and an appropriate model was developed for its flow at below 30^{o}C, where chocolate behaves as an elastic solid, and above 30^{o}C where chocolate behaves more like a viscous liquid.

8.3. Recommendations for Future Work

1. Slip is a critical parameter in the paste extrusion process. Surface roughness and hydrophobicity are two important factors that may play a significant role in controlling slip. A study of the effects of these properties on the slip phenomenon of PTFE and toothpaste can be examined, which might lead into fabrication of more efficient extrusion dies.
2. The proposed modified model for PTFE paste extrusion is derived for capillary dies. Use of this model can be extended by some modification to other useful geometries, such as flat and annular dies.
3. A comprehensive simulation was performed for toothpaste and chocolate capillary flow based on the conservation of mass and momentum. The same simulation can

be performed for PTFE paste extrusion, although some difficulty is expected to result from the explicit appearance of the extensional Hencky strain in the proposed constitutive equation.

4. PTFE membranes have been shown to have a positive Poisson ratio. This is due to existing network of fibrils that has been formed during the extrusion. Further study in this field could result in a better constitutive equation, which can represent more accurately the rheological behaviour of PTFE paste.
5. During the process of chocolate cold extrusion, part of cocoa butter melts down due to application of shear forces. The effect of this phenomenon on the quality and taste of the final product can be investigated.

Bibliography

E.O. Afoakwa, A. Paterson, M. Fowler, Factors influencing rheological and textural qualities in chocolate—a review, Trends Food Sci. Tech. **18** (2007) 290–298.

E.O. Afoakwa, A. Paterson, M. Fowler, J. Vieira, Comparison of rheological models for determining dark chocolate viscosity, Int. J. Food Sci. Tech. **44** (2009) 162-167.

A.B. Ariawan, S. Ebnesajjad, S.G. Hatzikiriakos, Preforming Behavior of Polytetrafluoroethylene Paste, Powder Technology **121** (2001)249-258.

A.B. Ariawan, S. Ebnesajjad, S.G. Hatzikiriakos, Properties of Polytetrafluoroethylene (PTFE) Paste Extrudates, Polym.Eng.Sci. **42 (**2002a**)** 1247-1259.

A.B. Ariawan, S. Ebnesajjad, S.G. Hatzikiriakos, Paste Extrusion of Polytetrafluoroethylene (PTFE) Fine Powder Resins, Can. J. Chem. Eng. **80 (**2002b) 1153-1165.

P.K. Awua, Cocoa processing and chocolate manufacture in Ghana, David Jamieson and Associates Press Inc, Essex, UK, 2002.

H.A. Barnes, J.F. Hutton, K. Walters, An introduction to rheology, Vol. 3., Elsevier, 1989.

H.A. Barnes, The myth of yield stress fluids, Progress and Trends in Rheology, Vol. V, (1998) 201-202.

H.A. Barnes, The yield stress - a review or 'ta panta rei' - everything flows?, J. Non-Newtonian Fluid Mech. **81** (1999) 133-178.

H.A. Barnes, A Handbook of Elementary Rheology, University of Wales Institute of Non-Newtonian Fluid Mechanics, Aberystwyth, Wales, 2000.

S.T. Beckett, M.A. Craig, R.I. Gurney, B.S. Ingleby, M.R. Mackley, T.C.L. Parsons, The cold extrusion of chocolate, Trans. I. Chem. E. Part C **72** (1994) 47–52.

S.T. Beckett, Industrial chocolate manufacture and use (3rd Ed.), pp. 153-181, 201-230, 405-428, 460-465, Blackwell Science, Oxford, 1999.

S.T. Beckett, The science of chocolate, Royal Society of Chemistry Paperbacks, 2000.

J.J. Benbow, J. Bridgwater, Paste Flow and Extrusion, Oxford University Press, Oxford, 1993.

JJ. Benbow, T.A. Lawson, E.W. Oxley, and J. Bridgwater, Prediction of Paste Extrusion Pressure, Ceramic Bulletin **68** (1989) 1821-1824.

D.M. Binding, Further Considerations of Axisymmetric Contraction Flows, J. Non-Newtonian Fluid Mech **41** (1991) 27-42.

E.C. Bingham, Plasticity and Elasticity, J. Franklin Institute **197** (1924) 99-115.

T.A. Blanchet, Polytetrafluoroethylene, in Handbook of Thermoplastics. Marcel Dekker, New York, 1997.

A.W. Blair, A.L. Prince, Influence of organic matter on crop yield and on carbon-nitrogen ratio and nitrate formation in the soil, Soil Science **35** (1933) 209-219.

J. Bridgwater, Paste Extrusion – an Overview, in Recent Advances in Chemical Engineering. Tata McGraw-Hill, New Delhi, 1989.

A.J. Carleton, D. Cheng, W. Whittaker, Determination of the rheological properties and start-up pipiline [sic] flow characteristics of waxy crude and fuel oils, Institute of Petroleum, London, 1974.

Y.W. Chen, M.R. Mackley, Flexible chocolate, Soft Matter **2** (2006) 304–309.

J. Chevalley, Chocolate flow properties, in S.T. Beckett (Ed.), Industrial Chocolate Manufacture and Use, 3rd Ed., Blackwell Science, Oxford, 1999.

A. Cheyne, J. Barnes, and D.I. Wilson, Extrusion Behavior of Cohesive Potato Starch Pastes: I. Rheological Characterization, J. Food Eng. **66** (2005) 1-12.

P. Coussot, Q.D. Nguyen, H.T. Huynh, D. Bonn, Viscosity bifurcation in thixotropic yielding fluids, J. Rheol. **46** (2002) 573-589.

P. Coussot, Rheometry of pastes, suspensions, and granular materials: applications in industry and environment, Wiley, New York, 2005.

P. Coussot, L. Tocquer, C. Lanos, G. Ovarlez, Macroscopic vs. local rheology of yield stress fluids, J. Non-Newtonian Fluid Mech. **158** (2009) 85-90.

J.M. Dealy, K.F. Wissbrun, Melt Rheology and its Role in Plastics Processing – Theory and Applications, Van Nostrand Reinhold, New York, 1990.

J.M. Dealy, J. Wang, *Melt Rheology and its Applicaitons in the Plastics Industry* , Springer, Munich, 2013.

J.J. Derksen, Prashant, Simulations of complex flow of thixotropic liquids, J. Non-Newtonian Fluid Mech. **160** (2009) 65-75.

H. Domininghaus, Plastics for engineers, Hanser publishers, 1993.

K. Dullaert, J. Mewis, A model system for thixotropy studies, Rheol. Acta **45** (2005) 23-32.

S. Ebnesajjad, Fluoroplastics Vol. 1: Non-Melt ProcessibleFluoroplastics, Plastics Design Library. William Andrew Corp., New York, 2000.

J. Engmann, M.R. Mackley, Semi-solid processing of chocolate and cocoa butter. The experimental correlation of process rheology with microstructure, Food Bioprod. Proces. **84** (2006) 95-101.

H. Freundlich, F. Juliusburger, Thixotropy, influenced by the orientation of anisometric particles in sols and suspensions, Trans. Faraday Soc. **31** (1935) 920-921.

S.V. Gangal, Polytetrafluoroethylene, in Encyclopedia of Chemical Technology, John Wiley & Sons, 621-644 (1994).

S.M. Goh, M.N. Charalambides, J.G. Williams, Determination of the Constitutive Constants of Non-Linear Viscoelastic Materials, Mech. Time-Dependent Materials **8** (2004) 255–268.

C.F Goodeve, A general theory of thixotropy and viscosity, Trans. Faraday Soc. **35** (1939) 342-357.

S.G. Hatzikiriakos, J.M. Dealy, Wall Slip of Molten High Density Polyethylenes II. Capillary Rheometer Studies, J. Rheol. **26** (1992) 703-741.

S.G. Hatzikiriakos, Rheology and Processing of PTFE Paste, Applied Polymer Rheology.Kontopoulou M. (Ed.), Wiley, New York, 2012.

W.H. Herschel, R. Bulkley, Measurement of consistency as applied to rubber benzene solutions, Proc. Am. Soc. Test. Mat. **26** (1926) 621-633.

O. Hoffman, G. Sachs, Introduction to the Theory of Plasticity for Engineers, McGraw-Hill, New York, 1953.

D.J. Horrobin, R.M. Nedderman, Die Entry Pressure Drops in Paste Extrusion, Chem. Eng. Sci. **53** (1998) 3215-3225.

K. Jackson, Recipes, in S.T. Beckett (Ed.), Industrial Chocolate Manufacture and Use (3rd Ed.), pp. 323-346, Blackwell Science, Oxford, 1999.

I.M. Krieger, The role of instrument inertia in controlled-stress rheometers, J. Rheol. **34** (1990) 471-483.

R.G. Larson, The structure and rheology of complex fluids. New York: Oxford University Press, 1999.

K.H. Lee, R.S. Brodkey, Time-dependent polymer rheology under constant stress and under constant shear, Trans. Soc. Rheol. **15** (1971) 627-646.

C. Loisel, G. Keller, G. Lecq, C. Bourgaux, M. Ollivon, Phase transitions and polymorphism of cocoa butter, J. Amer. Oil Chem. Soc. **75** (1998) 425–439.

N.V. Lovegren, M.S. Gray, R.O. Feuge, Polymorphic changes in mixtures of confectionery fats, J. Amer. Oil Chem. Soc. **53** (1976) 83–88.

N.V. Lovegren, M.S. Gray, R.O. Feuge, Effect of liquid fat on melting point and polymorphic behaviour of cocoa butter and a cocoa butter fraction, J. Amer. Oil Chem. Soc. **53** (1976) 108–112.

P. Ludwik, Elemente der Technologischen Mechanik, Springer Verlag, Berlin,1909.

S. Mazur, 1995, Paste Extrusion of Poly(tetrafluoroethylene) Fine Powders, Polymer Powder Technology, Wiley, New York, 1995.

J. Mewis, Thixotropy - General-Review, J. Non-Newtonian Fluid Mech. **6** (1979) 1-20.

J. Mewis, N.J. Wagner, Thixotropy, in Advances in Colloid and Interface Science, **48** (2009) 147-148, 214-227.

E. Mitsoulis, S.G. Hatzikiriakos, Bagley correction: the effect of contraction angle and its prediction, Rheo. Acta. 42, 4 (2003) 309-320.

E. Mitsoulis, S.G. Hatzikiriakos, Steady Flow Simulations of Compressible PTFE Paste Extrusion under Severe Wall Slip, J. Non-Newtonian Fluid Mech. **157** (2009a) 26-33.

E. Mitsoulis, S.G. Hatzikiriakos, Modelling PTFE Extrusion: The Effect of an Objective Flow Type Parameter, J. Non-Newtonian Fluid Mech. **159** (2009b) 41-49.

C. Macosko, Rheology principles, measurements and applications, New York, Wiley-VCH, 1994.

G. Mongia, G.R. Ziegler, The role of PSD of suspended solids in defining the flow properties of milk chocolate, Int. J. Food Proc. **3** (2000) 137–147.

M. Mooney, Explicit relations for slip, J. Rheol. **2** (1931) 210-221.

M. Mooney, A viscometer for measurements during thixotropic recovery; results with a compounded latex, J. Colloid Sci. **1** (1946) 195-208.

A. Mujumdar, A.N. Beris, A.B. Metzner, Transient phenomena in thixotropic systems, J. Non-Newtonian Fluid Mech. **102** (2002) 157-178.

N.C. Mulji, M.E. Miquel, L.D. Hall, M.R. Mackley, Microstructure and mechanical property changes in cold extruded chocolate, Trans. I. Chem. E. Part C **81** (2003) 97–105.

Q.D. Nguyen, D.V. Boger, Thixotropic behaviour of concentrated bauxite residue suspensions, Rheol. Acta **24** (1985) 427-437.

I. Ochoa, S.G. Hatzikiriakos, PTFE Paste Preforming: Viscosity and Surface Tension Effects, Powder Technology **146** (2004) 73-83.

I. Ochoa, S.G. Hatzikiriakos, Paste Extrusion of PTFE: Viscosity and Surface Tension Effects, Powder Technology **153** (2005) 108-118.

I. Ochoa, S.G. Hatzikiriakos, E. Mitsoulis, Paste Extrusion of Polytetrafluoroethylene (PTFE): Temperature, Blending and Processing Aid Effects, Intern. Polym. Proc. **21 (**2006) 497-503.

H. Ovaici, M.R. Mackley, G.H. McKinley, S.J. Crook, The experimental observation and modelling of an “Ovaici” necklace and stick-spurt instability arising during the cold extrusion of chocolate, J. Rheol. **42** (1998) 125–157.

T.C. Papanastasiou, Flows of materials with yield, J. Rheol. **31** (1987) 385–404.

P.D. Patil, J.J. Feng, S.G. Hatzikiriakos, Constitutive modeling and flow simulation of polytetrafluoroethylene (PTFE) paste extrusion, J. Non-Newtonian Fluid Mech. **139** (2006a) 44-53.

P.D. Patil, J. Feng, S.G. Hatzikiriakos, An Approximate Analytical Flow Model of PTFE Paste through Annular Dies. J. AIChE **52** (2006b) 4028-4038.

F. Pignon, A. Magnin, J.M. Piau, Thixotropic colloidal suspensions and flow curves with minimum: Identification of flow regimes and rheometric consequences, J. Rheol. **40** (1996) 573-587.

K.L. Pinder, Time-dependent rheology of the tetrahydrofuran-hydrogen sulphide gas hydrate slurry, Can. J. Chem. Eng. **132** (1964) 234-245.

A. Potanin, 3D simulations of the flow of thixotropic fluids, in large-gap Couette and vane-cup geometries, J. Non-Newtonian Fluid Mech. **165** (2010) 299-312.

J. Pryce-Jones, Thixotropy , J. Oil Col. Chem. Assoc., 1934.

B. Schantz, H. Rohm, Influence of lecithin-PGPR blends on the rheological properties of chocolate, LWT-Food Sci. Tech. **38** (2005) 41–45.

G.R. Snelling, J.F. Lontz, Mechanism of Lubricant-Extrusion of Teflon® TFE-Tetrafluoroethylene Resins, J. Appl. Polym. Sci. **3** (1960) 257-265.

A. Sokmen, G. Gunes, Influence of some bulk sweeteners on rheological properties of chocolate, LWT- Food Sci. Tech. **39** (2006) 1053–1058.

C.A. Sperati, Physical Constants of Fluoropolymers, in Polymer Handbook, Wiley, New York, 1989.

G. Talbot, Chocolate temper, in S.T. Beckett (Ed.), Industrial chocolate manufacture and use (3rd Ed.), (pp. 218-230), Blackwell Science, Oxford, 1999.

R.I. Tanner, Engineering Rheology, 2nd Ed., Oxford University Press, Oxford, 2000.

J.E. Taylor, I. Van Damme, M.L. Johns, A.F. Routh, D.I. Wilson, Shear rheology of molten crumb chocolate, J. Food Sci. **74** (2009) E55–E61.

H. Teng, J. Zhang, A new thixotropic model for waxy crude, Rheol. Acta **52** (2013) 903-911.

C. Tiu, D.V. Boger, Complete rheological characterization of time-dependent food products, J. Texture Stud. **5** (1971) 328-338.

E.A. Toorman, Modelling the thixotropic behaviour of dense cohesive sediment suspensions, Rheol. Acta **36** (1997) 56-65.

H.D. Tscheuschner, D. Wunsche, Rheological properties of chocolate masses and the influence of some factors, in P. Sherman (Ed.), Food Texture and Rheology (pp. 355–368), Academic Press, New York, 1979.

A.V. Ramamurthy, Wall slip in viscous fluids and influence of materials of construction, J. Rheol. **30** (1986) 337-357.

A.N. Vavreck, Flow of molten milk chocolate from an efflux viscometer under vibration at various frequencies and displacements, Int. J. Food Sci. Tech. **39** (2004) 465–468.

R. Whitefield, Making chocolates in the factory, Kennedy's Publications Ltd, London, UK, 2005.

R.L. Wille, E.S. Lutton, Polymorphism of cocoa butter, J. Amer. Oil Chem. Soc. **43** (1966) 491–496.

D.I. Wilson, S.L. Rough, 2012, Paste Engineering: Multi-Phase Materials and Multi-Phase Flows, Can. J. Chem. Eng. **70** (2012) 277-289.

W.E. Worrall, S. Tuliani, Viscosity changes during the ageing of clay-water suspensions, Trans. Brit. Ceramic Soc. **63** (1964) 167-185.

F. Yziquel, P.J. Carreau, M. Moan, P.A. Tanguy, Rheological modelling of concentrated colloidal suspensions , J. Non-Newtonian Fluid Mech. **86** (1999) 133-155.